Final Report

Modeling Atmospheric Mercury Chemistry and Deposition with CAMx for a 2002 Annual Simulation

Prepared for:

Wisconsin Department of Natural Resources
101 S. Webster St.
Madison, WI 53703

Prepared by:

Greg Yarwood
Steven Lau
Yiqin Jia
ENVIRON International Corporation
101 Rowland Way, Suite 220
Novato, California 94945

and

Prakash Karamchandani
Krish Vijayaraghavan
Atmospheric and Environmental Research, Inc.
2682 Bishop Dr., Suite 120
San Ramon, CA 94583

November 13, 2003

TABLE OF CONTENTS

TABLES

FIGURES

1. INTRODUCTION

The Wisconsin Department of Natural Resources (WDNR) has been actively studying the environmental impacts of mercury (Hg) pollution since the 1970s. Atmospheric mercury can cause adverse health effects when it is deposited to the earth's surface and enters the food chain. Consequently, the WDNR issues an annual fish consumption advisory covering all inland Wisconsin waters. The WDNR is developing strategies to reduce the amount of mercury emitted by coal-burning power plants and other major emitters (WDNR, 2003). The WDNR needs the ability to model atmospheric mercury and its deposition to support the development of the most effective and cost-effective mercury emissions reduction strategies. Modeling atmospheric mercury deposition is complex because it involves the emissions, transport, dispersion, chemistry and deposition of mercury over spatial scales ranging from local to global. The WDNR already uses the Comprehensive Air Quality model with extensions (CAMx) for air quality planning as part of the Midwest Regional Planning Organization (MRPO). The MRPO recently completed a mercury "scoping study" to provide scientific background for mercury modeling and planning in the upper Midwest (Seigneur et al., 2003).

The objectives of this study were to modify CAMx (ENVIRON, 2003) to treat atmospheric processes for mercury and test the model for an application suitable for investigating mercury deposition in Wisconsin. The mercury chemistry module implemented in CAMx was developed by Atmospheric & Environmental Research, Inc. (AER) and has been previously tested and evaluated (Seigneur et al., 2001a; 2003b). The mercury chemistry module treats chemical conversions between elemental mercury, Hg(0), and oxidized mercury, Hg(II). The oxidized form of mercury is sometimes referred to as reactive gaseous mercury (RGM). The model also treats primary particulate mercury, Hg(p), as a chemically inert species. Section 2 of this report describes how mercury chemistry was included in the CAMx model. An annual 2002 modeling database was developed to test and evaluate the CAMx mercury model. The modeling domain was the 36 km resolution "National RPO grid" covering the entire continental United States and parts of Canada and Mexico. The development of the modeling database is described in Section 3 and the model testing and evaluation is described in Section 4. The study conclusions and recommendations are presented in Section 5.

2. MODEL DEVELOPMENT

The starting point for model development was the publicly released version 4.02 of the Comprehensive Air quality Model with extensions (CAMx4) which is described in ENVIRON (2003). The major modification to CAMx was the addition of a new chemistry module to treat the gas and aqueous-phase chemistry of Hg species. Other modifications included improvements to the dry deposition module to better resolve differences between seasons and the effects of snow cover. The effect of snow-cover on photolysis rates also was accounted for.

MERCURY CHEMISTRY

Mercury exists in the atmosphere as elemental mercury, Hg(0), and oxidized mercury, Hg(II) (Schroeder and Munthe, 1998). Hg(II) can be inorganic (e.g., mercuric chloride, $HgCl_2$) or organic (e.g., methyl mercury, MeHg). It can also be present as particulate mercury (e.g., mercuric oxide, HgO, or mercury sulfide, HgS). In the global atmosphere, Hg(0) is the dominant form. Hg(II) typically constitutes a few percent of total mercury and is predominantly in the gas phase. MeHg concentrations in the atmosphere are negligible, about a factor of 10 to 30 lower than Hg(II) concentrations, based on analysis of precipitation samples conducted by Frontier Geosciences, Inc. (e.g., Seigneur et al., 1998). However, Hg(II) becomes methylated in water bodies, where it can bioaccumulate in the food chain. Hg(0) is sparingly soluble and is not removed significantly by wet deposition; its dry deposition velocity is also believed to be low. As a result, Hg(0) has a long atmospheric lifetime, on the order of several months, that is governed by its oxidation to Hg(II). On the other hand, Hg(II) is quite soluble; it is consequently removed rapidly by wet and dry deposition processes. Particulate mercury, Hg(p), is mostly present in the fine fraction of particulate matter ($PM_{2.5}$), although some Hg(p) may be present in coarse PM (e.g., Landis and Keeler, 2002).

Known transformations among inorganic mercury species include the gas-phase oxidation of Hg(0) to Hg(II), the aqueous-phase oxidation of Hg(0) to Hg(II), the aqueous-phase reduction of Hg(II) to Hg(0), various aqueous-phase equilibria of Hg(II) species and the aqueous-phase adsorption of Hg(II) to PM. The inorganic mercury chemistry modules implemented in CAMx for this study are based on our current knowledge of these transformations. However, it should be noted that our knowledge of mercury chemistry continues to evolve as new laboratory data become available, and the Hg chemical kinetic mechanisms in CAMx and other models that treat the atmospheric fate of mercury will need to be revised accordingly.

Below, we provide additional details on the gas- and aqueous-phase mercury chemistry mechanisms implemented in CAMx, and the implementation approach.

Gas-Phase Chemistry

The gas-phase transformations include the oxidation of Hg(0) to Hg(II) by ozone (O_3) (Hall, 1995), hydrogen chloride (HCl) (Hall and Bloom, 1993), hydrogen peroxide (H_2O_2) (Tokos et

al., 1998), molecular chlorine (Cl_2) (Ariya et al., 2002), and hydroxyl radicals (OH) (Sommar et al., 2001):

$Hg(0)\,(g) + O_3\,(g) \rightarrow Hg(II)\,(g)$, $k = 3 \times 10^{-20}$ cm^3 $molec^{-1}s^{-1}$
$Hg(0)\,(g) + HCl\,(g) \rightarrow HgCl_2\,(g)$, $k = 1 \times 10^{-19}$ cm^3 $molec^{-1}s^{-1}$
$Hg(0)\,(g) + H_2O_2\,(g) \rightarrow Hg(OH)_2\,(g)$, $k = 8.5 \times 10^{-19}$ cm^3 $molec^{-1}s^{-1}$
$Hg(0)\,(g) + Cl_2\,(g) \rightarrow HgCl_2\,(g)$, $k = 2.6 \times 10^{-18}$ cm^3 $molec^{-1}s^{-1}$
$Hg(0)\,(g) + OH\,(g) \rightarrow Hg(OH)_2\,(g)$, $k = 8 \times 10^{-14}$ cm^3 $molec^{-1}s^{-1}$

The reaction rate constants provided above are for temperatures in the range of 20 to 25°C; no temperature dependence information is available.

Aqueous-Phase Chemistry

The aqueous-phase chemistry includes the reduction of Hg(II) to Hg(0) via reaction with hydroperoxy radicals (HO_2) and by the formation of the sulfite complexes (at low HCl concentrations), $HgSO_3$ and $Hg(SO_3)_2^{2-}$, as well as the oxidation of Hg(0) to Hg(II) by dissolved O_3, OH, and Cl_2. Adsorption of Hg(II) species on atmospheric particulate matter (PM) is simulated using an adsorption coefficient ($K = 34$ L g^{-1}) recommended by Seigneur et al. (1998). The relevant reactions are listed below. Note that the gas-liquid equilibria and ionic equilibria of the non-mercury species (e.g., SO_2, O_3) involved in the mercury aqueous-phase chemistry are not shown here, since they are identical to those in the base CAMx.

Gas-liquid Equilibria

$Hg(0)\,(g) \Leftrightarrow Hg(0)\,(aq)$, $K = 0.11$ M atm^{-1}, Sanemasa, 1975; Clever et al., 1985
$HgCl_2\,(g) \Leftrightarrow HgCl_2\,(aq)$, $K = 1.4 \times 10^6$ M atm^{-1}, Lindqvist and Rodhe, 1985
$Hg(OH)_2\,(g) \Leftrightarrow Hg(OH)_2\,(aq)$, $K = 1.2 \times 10^4$ M atm^{-1}, Lindqvist and Rodhe, 1985

The Henry's Law constants listed above are for temperatures in the range of 20 to 25°C. Temperature dependence information is available for the Hg(0) Henry's Law constant but the validity of this information for temperatures below 0°C is not established.

Aqueous-phase Equilibria

$HgCl_2\,(aq) \Leftrightarrow Hg^{2+} + 2Cl^-$, $K = 10^{-14}$ M^2, Sillen and Martel, 1964
$Hg(OH)_2\,(aq) \Leftrightarrow Hg^{2+} + 2OH^-$, $K = 10^{-22}$ M^2, Sillen and Martel, 1964
$Hg^{2+} + SO_3^{2-} \Leftrightarrow HgSO_3$, $K = 2.1 \times 10^{13}$ M^{-1}, van Loon et al., 2001
$HgSO_3 + SO_3^{2-} \Leftrightarrow Hg(SO_3)_2^{2-}$, $K = 1 \times 10^{10}$ M^{-1}, van Loon et al., 2001

Adsorption of Hg(II) on PM

$Hg(II)\ (aq) \Leftrightarrow H(II)\ (p),\ K = 34\ L\ g^{-1}$, Seigneur et al., 1998

Aqueous-phase Kinetics

$Hg(0)\ (aq) + O_3\ (aq) \rightarrow Hg^{2+},\ k = 4.7 \times 10^7\ M^{-1}s^{-1}$, Munthe, 1992
$Hg(0)\ (aq) + OH\ (aq) \rightarrow Hg^{2+},\ k = 2 \times 10^9\ M^{-1}s^{-1}$, Lin and Pehkonen, 1997
$HgSO_3\ (aq) \rightarrow Hg(0)\ (aq),\ k = 0.0106\ s^{-1}$, van Loon et al., 2000
$Hg(II)\ (aq) + HO_2\ (aq) \rightarrow Hg(0)\ (aq),\ k = 1.7 \times 10^4\ M^{-1}s^{-1}$, Pehkonen and Lin, 1998
$Hg(0)\ (aq) + HOCl\ (aq) \rightarrow Hg^{2+},\ k = 2.09 \times 10^6\ M^{-1}s^{-1}$, Lin and Pehkonen, 1998
$Hg(0)\ (aq) + OCl^- \rightarrow Hg^{2+},\ k = 1.99 \times 10^6\ M^{-1}s^{-1}$, Lin and Pehkonen, 1998

In the last two reactions listed above, HOCl and OCl^- come from the dissolution and subsequent dissociation of molecular chlorine (Cl_2). Note that Hg(II) (aq) refers to all divalent Hg species in solution (i.e., Hg^{2+} + $HgCl_2(aq)$ + $Hg(OH)_2(aq)$ + $HgSO_3$ + $Hg(SO_3)_2^{2-}$).

The rate constants listed for the aqueous-phase kinetics are for temperatures in the range of 20 to 25°C. Temperature dependence information is available for the $HgSO_3$ reduction reaction.

As mentioned previously, the gas- and aqueous-phase Hg transformations presented above represent the current state of the science (Ryaboshapko et al., 2002; Seigneur et al., 2001a, 2003b), but our knowledge of mercury chemistry continues to evolve. For example, Gardfeldt and Johnson (2003) have recently challenged the aqueous-phase reduction of Hg(II) to Hg(0) by dissolved HO_2, suggesting that this pathway is unimportant. There also seems to be some circumstantial evidence of reduction of Hg(II) to Hg(0) in power plant plumes from various experimental studies that is not accounted for in current treatments of Hg chemistry (e.g., Edgerton et al., 2001; Seigneur et al., 2001b). Additional details are provided in a recent scoping study for mercury deposition conducted for the Midwest Regional Planning Organization by Seigneur et al. (2003d).

Implementation Approach

The approach used to implement the mercury transformation pathways, discussed above, into CAMx is based on the assumption that the mercury species concentrations are much smaller than those of the species with which they react. Thus, the concentrations of the non-mercury species can be assumed to be constant during the mercury chemistry calculations and analytical solutions are available for both the gas-phase and aqueous-phase conversions.

The mercury chemistry discussed in the previous sections requires the concentrations of the following non-mercury species: O_3, H_2O_2, OH, SO_2, HO_2, Cl_2, HCl, and atmospheric particulate matter (PM). The concentrations of most of these species are available from CAMx. However, Cl_2 and HCl are not explicitly simulated because the emissions data required to model these species are generally inadequate and were not available for this study.

Thus, we specify typical vertical profiles of HCl and Cl_2 concentrations. The Cl_2 concentrations are prescribed to be non-zero over oceans and zero elsewhere. Also, daytime Cl_2 concentrations are lower than nighttime values to account for the fact that Cl_2 is photolyzed during the day. The zenith angle (available from CAMx) is used for the determination of night/day. A 2-D array of integer values (1 if ocean, 0 if not) is used to determine if the grid column is predominantly over ocean. This array is initialized at the beginning of the simulation from an input file and is specific for the modeling domain and grid.

The mercury aqueous-phase chemistry module also requires the specification of cloud liquid water content (LWC) and cloudwater pH. Both these variables are available from CAMx – the mercury aqueous-phase chemistry module is invoked after the base CAMx aqueous-phase chemistry calculations are performed, so the cloudwater pH has already been calculated. Note that the base CAMx aqueous-phase module (based on the RADM aqueous-phase chemistry module that is also used in Models-3/CMAQ) does not explicitly simulate the cloud chemistry of OH and HO_2 radicals. The concentrations of these radicals can be reduced by their heterogeneous chemistry within clouds (e.g., Jacob, 2000; Jaegle et al., 2001). In the CAMx implementation, we account for this by reducing the concentrations of OH and HO_2 radicals by factors of 2 and 10, respectively.

CHEMISTRY PARAMETERS FOR MERCURY

The chemistry parameters input file for CAMx specifies:

- What chemical mechanism is being used
- What species are being simulated
- Certain physical properties of the species
- Reaction rates for the gas-phase chemistry

The mercury chemistry module requires total PM concentrations so mercury can only be modeled in conjunction with PM chemistry. In CAMx version 4.02 PM chemistry is modeled using optional mechanism number 4 (M4). The CAMx M4 treatment uses the CB4 gas-phase mechanism, the RADM aqueous-phase chemistry mechanism, the ISORROPIA module for thermodynamic equilibrium of inorganic species and the SOAP module for semi-volatile secondary organic aerosols (ENVIRON, 2003).

Mercury chemistry is selected in the modified CAMx by selecting M4 and including mercury species among the list of modeled species. The CAMx mercury species names are:

HG0 – elemental gaseous mercury, or Hg(0)
HG2 – reactive gaseous mercury, or Hg(II)
HGP – primary particulate mercury, or Hg(P)

CAMx requires that all three or none of these species be included in an M4 simulation. Therefore, mercury chemistry is not required for PM modeling with M4, but if mercury chemistry is selected then all three mercury species must be modeled.

All of the rate constants and equilibrium constants for the mercury chemistry module are hard-coded and so no mercury reaction rate data are included in the chemistry parameters input file. This is similar to the RADM aqueous chemistry and ISORROPIA inorganic aerosol equilibrium modules.

Several physical properties of the mercury species must be specified on the chemistry parameters file. These values are shown in the correct input file format in Figure 2-1.

Species Records

	Gas Spec	lower bnd	H-law	T-fact	Diffrat	Reactvty	Rscale
1	NO	1.00E-15	1.90e-03	-1480.	1.29	0.0	1.
2	NO2	1.00E-09	1.00e-02	-2516.	1.60	0.1	1.
3	O3	1.00E-09	1.10e-02	-2415.	1.63	1.0	1.
4	PAN	1.00E-09	3.60e+00	-5910.	2.59	0.1	1.
5	NXOY	1.00E-12	3.20e+04	-8706.	2.45	0.1	0.
6	OLE	1.00E-09	5.00e-03	0.	1.80	0.0	1.
7	PAR	1.00E-04	1.00e-03	0.	2.00	0.0	1.
8	TOL	1.00E-09	1.20e+00	0.	2.26	0.0	1.
9	XYL	1.00E-09	1.40e+00	0.	2.43	0.0	1.
10	FORM	1.00E-09	6.30e+03	-6492.	1.29	0.0	1.
11	ALD2	1.00E-09	6.30e+03	-6492.	1.56	0.0	1.
12	ETH	1.00E-09	1.00e-02	0.	1.25	0.0	1.
13	CRES	1.00E-09	2.70e+03	-6492.	2.45	0.0	1.
14	MGLY	1.00E-09	2.70e+03	-6492.	2.00	0.0	1.
15	OPEN	1.00E-12	2.70e+03	-6492.	2.47	0.0	1.
16	PNA	1.00E-09	2.00e+04	-5910.	2.09	0.0	1.
17	CO	1.00E-04	1.00e-10	0.	1.25	0.0	1.
18	HONO	1.00E-09	5.90e+01	-4781.	1.62	0.1	1.
19	H2O2	1.00E-09	7.40e+04	-6643.	1.37	1.0	1.
20	HNO3	1.00E-09	2.00e+05	-8707.	1.87	0.0	0.
21	ISOP	1.00E-09	1.00e-02	0.	1.94	0.0	1.
22	MEOH	1.00E-09	2.20e+02	-4932.	1.33	0.0	1.
23	ETOH	1.00E-09	2.20e+02	-4932.	1.60	0.0	1.
24	ISPD	1.00E-09	6.30e+03	-6492.	1.97	0.0	1.
25	NTR	1.00E-09	9.40e+03	-8706.	2.72	0.0	1.
26	SO2	1.00E-09	1.00e+05	-3156.	1.89	0.0	1.
27	SULF	1.00E-12	1.00e+10	0.	1.00	0.0	0.
28	NH3	1.00E-09	2.00e+04	-3400.	0.97	0.0	1.
29	HCL	1.00E-12	1.00e+05	0.	1.42	0.0	0.
30	OLE2	1.00E-12	5.00e-03	0.	1.80	0.0	1.
31	CG1	1.00E-12	2.70e+03	-6492.	2.50	0.0	1.
32	CG2	1.00E-12	2.70e+03	-6492.	2.50	0.0	1.
33	CG3	1.00E-12	2.70e+03	-6492.	2.50	0.0	1.
34	CG4	1.00E-12	2.70e+03	-6492.	2.50	0.0	1.
35	HG0	1.00E-12	1.00e-10	0.	3.34	0.0	1.
36	HG2	1.00E-12	2.00e+05	0.	3.76	0.0	1.

	Aero Spec	lower bnd	Density	Low cut	Upper cut
1	PNO3	1.00E-09	1.5	0.04	2.50
2	PSO4	1.00E-09	1.5	0.04	2.50
3	PNH4	1.00E-09	1.5	0.04	2.50
4	POA	1.00E-09	1.0	0.04	2.50
5	SOA1	1.00E-09	1.0	0.04	2.50
6	SOA2	1.00E-09	1.0	0.04	2.50
7	SOA3	1.00E-09	1.0	0.04	2.50
8	SOA4	1.00E-09	1.0	0.04	2.50
9	PEC	1.00E-09	2.0	0.04	2.50
10	FPRM	1.00E-09	3.0	0.04	2.50
11	FCRS	1.00E-09	3.0	0.10	10.00
12	CPRM	1.00E-09	3.0	4.30	10.00
13	CCRS	1.00E-09	3.0	4.30	10.00
14	NA	1.00E-09	2.0	0.04	2.50
15	PCL	1.00E-09	2.0	0.04	2.50
16	HGP	1.00E-12	2.0	0.04	2.50

Figure 2-1. CAMx chemistry parameters file species records for mechanism 4 (M4) including the mercury species HG0, HG2 and HGP.

The physical properties specified for the gas species (Henry's Law, molecular diffusivity, surface reactivity) influence the deposition characteristics. The Henry constant for HG2 is assumed to be similar to that of HNO_3 because these two gases have similar solubility. The HG2 species represents $HgCl_2$ and $Hg(OH)_2$. The Henry constant for the former is 1.4E+06 M atm-1 and for the latter it is 1.2E+04 M atm^{-1}. The Henry constant used for HNO_3 is 2.0E+05 M atm^{-1} and is within this range. No temperature dependence is assumed for the HG2 Henry constant because there is no information available to determine this. The molecular diffusivity ratio for HG2 was calculated as the average for $HgCl_2$ and $Hg(OH)_2$. The surface reactivity parameter is set to zero for strong acids, such as HNO_3, that have a strong tendency to stick to surfaces. Setting the surface reactivity to zero overrides the surface resistance calculated in the Wesely (1989) deposition algorithm and forces the surface resistance to zero. The reactivity parameter for HG2 is set to 1 so that surface resistance will be calculated based on the Henry constant using Wesely's algorithm.

The dry deposition of HG0 was set to zero by choosing a very low Henry constant (similar to CO). This is based on the assumption that background emissions and dry deposition of HG0 balance each other over the modeling domain. This assumption is justified by the fact that the atmospheric lifetime of HG0 (about 1 year) greatly exceeds its residence time (days to weeks) within a regional modeling domain. Since background emissions of HG0 are not included in the mercury emissions inventory, this means that the dry deposition of HG0 should be ignored. In CAMx, setting a Henry constant of smaller the 1.0E-08 M atm^{-1} results in zero dry and wet deposition for the species. The HG0 Henry constant is set to 1.0E-10 M atm^{-1}.

The physical properties specified for the PM species (size and density) influence the deposition characteristics. The physical properties of HGP were selected to represent typical fine particles that the HGP may be associated with.

SEASONAL VARIATIONS IN DRY DEPOSITION

The CAMx dry deposition algorithm is based on the scheme developed for the Regional Acid Deposition Model (RADM) by Wesely (1989). The dry deposition velocity v_d is calculated from three primary resistances r (s/m) in series:

$$V_d = \frac{1}{r_a + r_b + r_s}$$

The aerodynamic resistance r_a represents bulk transport through the lowest model layer by turbulent diffusion, and operates equivalently for all gases and small particles. The quasi-laminar sublayer (or boundary) resistance r_b represents molecular diffusion through the thin layer of air directly in contact with the particular surface to which material is being deposited.

The surface resistance r_s depends upon the properties of the surface and the depositing species. For example, over land Wesely's model includes stomatal and mesophyllic resistance terms for active plants, an upper canopy resistance, a lower canopy resistance and a ground surface resistance. Many of these resistances are season- and landuse-dependent and Wesely's model includes data to describe these dependencies. Two improvements to the dry deposition model

were completed in this project to improve the representation of dry deposition in annual simulations for a continental scale domain:

1. Improved the description of seasonal dependencies based on geographic location and time of year. The existing season map in CAMx 4.02 is representative for the continental US.

2. Added a mechanism for directly specifying when surfaces are snow-covered and modified the dry deposition rates accordingly.

Improved "Season Map" for Dry Deposition

The Wesely (1989) deposition algorithm has resistances by land cover type for five seasons:

Spring
Summer
Fall
Winter
Winter with snow-cover

A season map was defined to determine the season by month and latitude in five latitude bands in each hemisphere:

Tropical	< 20°
Sub-tropical	20° to 35°
Temperate	35° to 50°
Cool	50° to 75°
Polar	> 75°

The CAMx season map is shown in Table 2-1. The seasons in the Northern and Southern hemispheres are offset by six months. This offset does not cause any discontinuity at the equator because all 12 months are defined as summer in the tropical band at the equator. This season map is generalized and may not be ideal for all locations. The season map is coded into data statements in the "CHMDAT" subroutine and could be changed to better suit a specific region (e.g., parts of Europe influenced by the gulf stream that have a milder climate than other regions at the same latitude).

Table 2-1. Relationships between season and month/latitude used in the CAMx dry deposition algorithm.

Month		Latitude Band				
Northern Hemisphere	Southern Hemisphere	< 20°	20° - 35°	35° - 50°	50° - 75°	> 75°
		Tropical	Sub-tropical	Temperate	Cool	Polar
Jan	Jul	summer	winter	winter	winter	winter
Feb	Aug	summer	spring	winter	winter	winter
Mar	Sep	summer	spring	spring	winter	winter
Apr	Oct	summer	spring	spring	spring	winter
May	Nov	summer	summer	spring	spring	winter
Jun	Dec	summer	summer	summer	summer	spring
Jul	Jan	summer	summer	summer	summer	summer

Month		Latitude Band				
Northern Hemisphere	Southern Hemisphere	< 20°	20° - 35°	35° - 50°	50° - 75°	> 75°
		Tropical	Sub-tropical	Temperate	Cool	Polar
Aug	Feb	summer	summer	summer	summer	fall
Sep	Mar	summer	summer	fall	fall	winter
Oct	Apr	summer	fall	fall	fall	winter
Nov	May	summer	fall	fall	winter	winter
Dec	Jun	summer	fall	winter	winter	winter

Specifying Snow-Cover

The season map shown in Table 2-1 does not specify any snow-cover because snow-cover is variable from year-to-year except near the poles or at very high elevations. Instead, CAMx was modified to provide a way of explicitly specifying which grid cells are snow-covered during the simulation. An optional snow-cover data field was added to the albedo-haze-ozone column (AHO) file. This allows the snow-cover to vary spatially and temporally during a simulation. The new snow-cover field uses a similar format to the existing ozone column and haze data fields on the AHO file. The snow-cover input is a binary value where 1 signifies that the grid cell is snow-covered. Snow-covered grid cells are assigned the Wesely (1989) surface resistances for winter with snow-cover.

Snow-cover data could be developed in several ways:

- Spatially interpolated observed snow-cover.
- Analyses of snow-cover data included in existing metrological data sets, such as the NCEP ETA Data Assimilation System (EDAS) data.
- Analyses of climatological snow-cover such as that reported Herman and Celarier (1997) based on surface reflectivity data from the Total Ozone mapping Spectrometer (TOMS).

For this study, we used 3-hourly gridded snow-cover fields that also were input to the MM5 meteorological model and were based on EDAS data for 2002. Grid cells were defined as snow-covered if the EDAS snow-cover fraction for the grid cell was greater than 0.5.

SNOW-COVER EFFECT ON PHOTOLYSIS REACTIONS

The rates of atmospheric photolysis reactions depend upon solar irradiance and therefore are sensitive to the amount of solar radiation reflected from the earth's surface (albedo). Snow is much more reflective than other types of surfaces and so snow-cover will enhance the rates of photolysis reactions. Since most photolysis reactions depend upon ultra-violet radiation it is important to characterize the effect of snow-cover on UV-albedo. Measurements of the UV-albedo for Antarctic snow report values of 0.96 to 0.98 over a wide range of snow grain sizes and solar zenith angles. However, these high values should be considered an upper limit to the reflectivity of snow-covered surfaces at the scale of grid cells because snow may not cover all surface features (e.g., in forests and urban areas) and because the snow my be dirty.

The CAMx albedo-haze-ozone column (AHO) input file specifies the UV-albedo for each grid cell. Five albedo ranges are specified in the header of the AHO file and then each grid cell is classified to one of these five ranges. The albedo ranges used in the AHO file must be identical to the albedo ranges used in the photolysis rate input file. The UV-albedo generally is calculated from land cover data using characteristic values by land cover type shown in Table 2-2 (ENVIRON, 2003). This approach results in UV-albedo's that fall in the range 0.04 to 0.08 and are constant in time, because the land cover data are constant in time. Analyses of reflected UV radiation recorded in TOMS satellite data (Herman and Celarier, 1997) report similar UV-albedo values in the range 0.02-0.08 for surfaces not covered by snow. For areas with snow-cover, the TOMS climatology shows surface albedos spanning a wide range of values from 0.2 to nearly 1.0. Potential reasons for this wide range of values include coarse resolution (1° latitude by 1.25° longitude) such that snow-covered and snow-free surfaces are combined, differences between rough and smooth land cover types (e.g., forest vs. open range land), and differences between clean and dirty snow.

Table 2-2. UV-albedo values for CAMx land cover categories.

Category Number	Land Cover Category	UV-Albedo
1	Urban	0.08
2	Agricultural	0.05
3	Rangeland	0.05
4	Deciduous forest	0.05
5	Coniferous forest including wetland	0.05
6	Mixed forest	0.05
7	Water	0.04
8	Barren land	0.08
9	Non-forested wetlands	0.05
10	Mixed agricultural and range	0.05
11	Rocky (with low shrubs)	0.05

The CAMx code was modified so that snow-covered grid cells are assigned the highest albedo value included in the AHO and photolysis rate input files. As described above, the AHO and photolysis rate input files classify grid cells to one of five albedo ranges. When providing snow-cover data to CAMx, the fifth (highest) albedo range should be assigned a value representative of snow and the lower four albedo ranges should represent surfaces without snow-cover. We used a UV-albedo of 0.5 for snow-covered surfaces because this is in the middle of the range reported by Herman and Celarier (1997) and because grid cells were defined as snow-covered if the fractional snow-cover was greater than 0.5

3. MODELING DATABASE FOR 2002

An annual 2002 modeling database was developed to test and evaluate the CAMx mercury model. The modeling domain was the 36 km resolution "National RPO grid" covering the entire continental United States and parts of Canada and Mexico (Figure 3-1). The Regional Planning Organizations (RPOs) developed this modeling grid to promote consistency in regional particulate matter (PM) and visibility modeling.

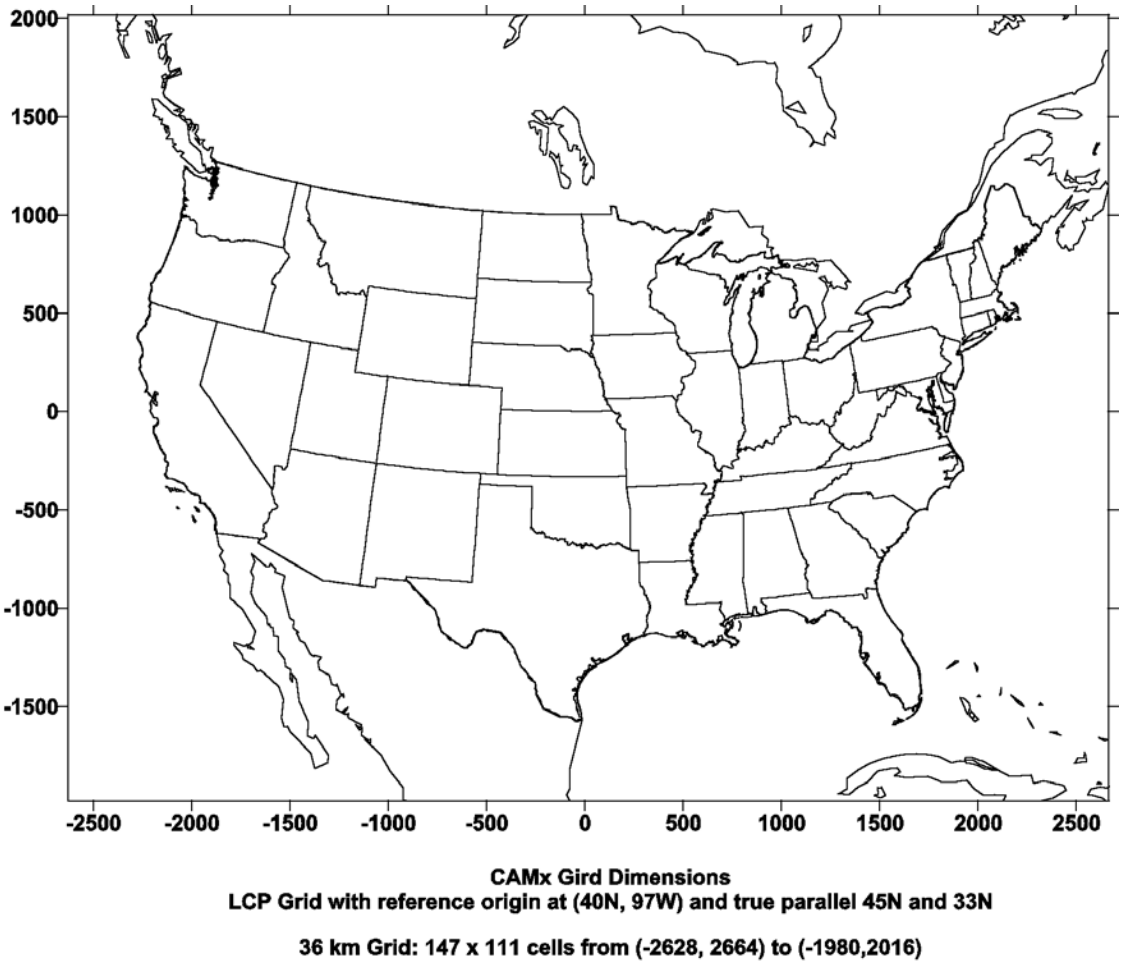

Figure 3-1. The CAMx "National RPO" modeling domain with 36 km grid resolution.

Modeling an entire year is important to capture seasonal cycles in mercury deposition and modeling a continental-scale domain is preferable to maximize the influence of mercury emissions over boundary conditions. However, even with a continental-scale modeling domain the lateral boundary conditions are more important for mercury than for other pollutants (e.g., PM or ozone) because the long atmospheric lifetime of Hg(0) leads to global scale mercury transport. To account for the global mercury background, this study followed the multiscale approach of Seigneur et al. (2001a) of specifying the continental scale boundary conditions for Hg species from a global model. Study participants developed the model inputs for the annual 2002 CAMx simulation as follows. The Wisconsin Department of Natural

Resources (WDNR) conducted annual meteorological modeling to develop the 2002 meteorology. The WDNR also developed the mercury emissions inventory. The Lake Michigan Air Directors Consortium developed the emission inventory for non-mercury species for Midwest RPO modeling studies. AER developed the mercury boundary conditions from global model simulations. ENVIRON developed other model inputs including the boundary conditions for non-mercury species. The model simulations were performed by ENVIRON.

EMISSION INVENTORY

Emissions Inventory for Non-Mercury Species

The emissions inventory for all non-mercury species were based on the Midwest Regional Planning Organization (MRPO) "BaseD" emissions inventories. The Lake Michigan Air Directors Consortium (LADCO) prepared the BaseD inventory using the EMS2002 emissions modeling system as described in LADCO (2003). The main emissions data sources were:

- EPA's 1999 NEI in the NET Input Format (NIF) version 2.0 with several corrections listed by LADCO (2003)
- On-road mobile source emissions based on MOBILE6
- Off-road mobile source emissions based on NONROAD2002
- US Electric Generating Units (EGUs) based on EPA's Acid Rain Database
- Ammonia emissions based on the Carnegie-Mellon University (CMU) ammonia model
- 1995 Canadian point source inventory based on data provided by US EPA
- Biogenic emissions from BIOME3 which is based on the BEIS3 model

BaseD emission inventories were available for winter and summer episode periods:

- January 2, 2000 to January 31, 2000
- July 1, 2001 to July 31, 2001

During each episode the biogenic emissions were day specific (for the temperature and solar radiation conditions of each day) but the anthropogenic emissions were for a weekday (nominally Friday), Saturday or Sunday.

The LADCO BaseD emissions inventories were analyzed to develop representative seasonal emission inventories for summer, winter and spring/fall as follows:

1. Average the day-specific biogenic emissions for each episode period to obtain single day representative winter and summer biogenic emissions.

2. Merge the biogenic emissions with the summer/winter day of week anthropogenic emissions to obtain summer and winter emissions for a weekday, Saturday and Sunday.

3. Average the summer and winter emissions for each day of week to obtain spring/fall emissions for a weekday, Saturday and Sunday.

The total surface and elevated point source emissions for nine different emission inventory scenarios are reported in Tables 3-1 and 3-2. These tables list emission totals by the species in the CAMx chemical mechanism and then sub-totals for major species groups. Tables 3-1 and 3-2 were prepared directly from the CAMx emissions input files.

Table 3-1. Summary of surface emission totals (tons/day).

	Winter			Summer			Fall/Spring		
Species	**Friday**	**Saturday**	**Sunday**	**Friday**	**Saturday**	**Sunday**	**Friday**	**Saturday**	**Sunday**
ALD2	4732	4880	4870	23173	23324	23258	13953	14102	14065
CCRS	18376	13921	13565	17123	16806	14018	17749	15363	13791
CO	436993	375874	371003	393575	365878	342142	415288	370880	356576
CPRM	2042	1547	1507	1903	1867	1558	1972	1707	1532
ETH	2182	2288	2267	3746	3769	3646	2964	3028	2956
ETOH	936	465	459	715	599	582	825	532	520
FCRS	4405	3895	3864	3831	3762	3714	4118	3829	3789
FORM	539	428	419	445	399	374	492	413	397
FPRM	777	687	682	676	664	655	727	676	669
HG0	0.165	0.151	0.145	0.171	0.151	0.145	0.168	0.151	0.145
HG2	0.031	0.029	0.028	0.029	0.027	0.026	0.030	0.028	0.027
HGP	0.013	0.013	0.013	0.011	0.011	0.011	0.012	0.012	0.012
ISOP	9116	9108	9108	171497	171474	171461	90306	90291	90285
MEOH	554	521	518	772	708	689	663	614	604
NH3	8951	8654	8673	9872	9695	9609	9411	9174	9141
NO	45269	40226	40621	94532	88737	86748	69904	64487	63690
NO2	6832	5973	6040	12402	11415	11076	9618	8695	8559
NR	23016	22018	21232	26666	26888	25937	24843	24455	23585
OLE	2489	2132	2090	2408	2203	2056	2448	2167	2073
PAR	55090	44836	44215	135793	130308	128957	95439	87572	86585
PEC	1126	982	995	1591	1227	1182	1358	1104	1089
PNO3	29	24	24	11	11	11	20	17	17
POA	2794	2707	2697	3075	3090	3044	2935	2898	2870
PSO4	376	233	229	245	209	195	310	221	212
SO2	32320	8670	7095	7783	7074	6687	20051	7872	6891
SULF	411	97	72	68	67	62	240	82	67
TOL	7438	5318	5078	7535	6637	6371	7486	5977	5725
XYL	11899	10590	10204	6748	7031	6775	9324	8811	8490
Sub-Totals									
VOC	117990	102584	100461	379498	373337	370107	248744	237962	235285
CO	436993	375874	371003	393575	365878	342142	415288	370880	356576
NOx	52101	46199	46661	106934	100152	97825	79523	73182	72249
SOx	32731	8767	7166	7851	7141	6749	20291	7954	6958
NH3	8951	8654	8673	9872	9695	9609	9411	9174	9141
PM	29925	23995	23563	28454	27636	24377	29190	25816	23970
HG	0.209	0.193	0.186	0.212	0.189	0.182	0.211	0.191	0.184

Table 3-2. Summary of elevated point source emission totals (tons/day).

	Winter			Summer			Fall/Spring		
Species	**Friday**	**Saturday**	**Sunday**	**Friday**	**Saturday**	**Sunday**	**Friday**	**Saturday**	**Sunday**
ALD2	45	36	34	39	35	31	42	36	33
CCRS	603	561	536	640	570	525	621	564	530
CO	11246	10808	10544	12259	11734	11131	11724	11247	10815
CPRM	67	62	60	71	63	58	69	63	59
ETH	122	114	111	119	102	97	121	108	104
ETOH	43	40	35	31	28	26	37	34	31
FCRS	577	527	510	601	524	498	588	525	503
FORM	137	131	129	136	125	121	136	128	125
FPRM	577	527	510	601	524	498	588	525	503
HG0	0.152	0.149	0.148	0.156	0.153	0.151	0.154	0.151	0.149
HG2	0.128	0.126	0.125	0.130	0.128	0.127	0.129	0.127	0.126
HGP	0.016	0.016	0.015	0.016	0.016	0.016	0.016	0.016	0.015
ISOP	0.267	0.253	0.251	0.226	0.215	0.210	0.246	0.234	0.231
MEOH	6	5	5	7	5	5	6	5	5
NH3	350	347	344	347	342	337	349	344	340
NO	12946	12429	12099	14092	13631	13031	13486	13002	12540
NO2	2207	2119	2063	2401	2322	2220	2297	2215	2137
NR	1617	1552	1513	1461	1374	1318	1537	1461	1414
OLE	124	116	111	121	113	102	122	114	107
PAR	1289	1139	1090	1289	1114	1037	1286	1125	1062
PEC	90	82	77	112	94	87	101	88	82
PNO3	9	8	8	9	8	8	9	8	8
POA	361	333	321	396	344	327	378	338	324
PSO4	262	244	238	281	249	242	271	246	240
SO2	44456	42963	41333	47315	46067	43832	45856	44490	42561
SULF	838	809	776	892	869	825	865	839	800
TOL	156	112	98	147	105	87	151	108	92
XYL	156	121	104	147	113	91	152	117	98
Sub-Totals									
VOC	3696	3365	3229	3498	3112	2916	3592	3235	3070
CO	11246	10808	10544	12259	11734	11131	11724	11247	10815
NOx	15153	14547	14162	16493	15954	15251	15783	15218	14676
SOx	45294	43772	42109	48207	46935	44657	46722	45329	43361
NH3	350	347	344	347	342	337	349	344	340
PM	2547	2344	2261	2710	2376	2243	2625	2357	2249
HG	0.296	0.291	0.288	0.302	0.297	0.294	0.299	0.294	0.291

Mercury Emissions Inventory

The mercury emissions inventory was developed by the WDNR using the following data sources:

- National Air Toxics Assessment National Emission Inventory (NATA/NEI) version 3, draft for 1999
- Data provided by the Electric Power Research Institute (EPRI) for US EGUs
- Great Lakes States data for 1999 for Minnesota, Illinois, Michigan and Wisconsin
- Canadian National emission inventory for 1995 from Environment Canada (EC)
- Ontario emission inventory for 1999 from the Ontario Ministry of the Environment (OME)

When reviewing the Canadian emissions inventory data, the following limitations should be considered. The Canadian emissions inventory is based on incomplete emissions inventories for 1995 and 1999. 1999 Canadian data outside of Ontario were unavailable. In part, these limitations are a consequence of the voluntary nature of the emissions inventory and of point source confidentiality granted to a significant fraction of point sources.

The WDNR processed the mercury emissions using EMS2002 and developed surface and elevated point source files for a typical weekday, Saturday and Sunday in summer and winter. The speciated mercury emissions included in the model ready surface and elevated point mercury emissions are summarized by season and day-of-week in Tables 3-1 and 3-2, above. Table 3-3 shows the annual mercury emissions by State and major source category.

Table 3-3. Summary of US mercury emissions by State and major source category (tons/year).

State	On-Road Mobile	Off-road Mobile	Area	Point	Total
Alabama	0.426	0.095	0.063	4.053	4.636
Arizona	0.385	0.092	0.060	1.099	1.636
Arkansas	0.285	0.115	0.034	1.585	2.019
California	0.177	0.884	7.094	4.086	12.241
Colorado	0.310	0.112	0.048	0.826	1.296
Connecticut	0.228	0.044	0.152	0.358	0.782
Delaware	0.073	0.019	0.015	0.761	0.868
District of Columbia	0.022	0.007	0.004	0.002	0.035
Florida	1.093	0.262	0.278	3.996	5.629
Georgia	0.851	0.155	0.137	2.931	4.075
Idaho	0.136	0.056	0.084	0.818	1.093
Illinois	0.811	0.356	0.359	8.298	9.824
Indiana	0.633	0.204	0.087	6.550	7.474
Iowa	0.283	0.233	0.052	1.110	1.678
Kansas	0.251	0.205	0.037	1.313	1.806
Kentucky	0.448	0.121	0.058	3.127	3.752
Louisiana	0.381	0.214	0.047	2.382	3.023
Maine	0.091	0.025	3.834	0.181	4.130
Maryland	0.392	0.077	0.106	3.366	3.942
Massachusetts	0.381	0.143	0.235	0.691	1.450
Michigan	0.800	0.188	0.149	4.739	5.876
Minnesota	0.457	0.223	0.186	1.958	2.824

State	On-Road Mobile	Off-road Mobile	Area	Point	Total
Mississippi	0.394	0.100	0.030	1.172	1.696
Missouri	0.581	0.199	0.075	1.977	2.832
Montana	0.102	0.105	0.013	0.568	0.789
Nebraska	0.172	0.182	0.021	0.976	1.351
Nevada	0.142	0.051	0.025	11.537	11.755
New Hampshire	0.113	0.016	0.079	0.423	0.631
New Jersey	0.481	0.107	0.287	1.227	2.102
New Mexico	0.216	0.049	0.022	1.136	1.423
New York	0.992	0.261	0.654	2.439	4.345
North Carolina	0.785	0.152	0.117	5.277	6.331
North Dakota	0.074	0.168	0.016	2.941	3.200
Ohio	0.886	0.280	0.170	4.671	6.008
Oklahoma	0.382	0.116	0.043	3.039	3.579
Oregon	0.317	0.093	0.053	0.527	0.991
Pennsylvania	0.887	0.193	0.309	9.221	10.609
Rhode Island	0.058	0.011	0.039	0.143	0.250
South Carolina	0.427	0.074	0.060	1.800	2.362
South Dakota	0.085	0.114	0.013	0.061	0.274
Tennessee	0.563	0.134	0.071	2.331	3.099
Texas	1.703	0.428	0.240	11.733	14.104
Utah	0.168	0.084	0.029	0.514	0.795
Vermont	0.068	0.010	0.026	0.001	0.105
Virginia	0.632	0.140	0.127	2.659	3.559
Washington	0.422	0.148	0.067	1.097	1.734
West Virginia	0.193	0.047	0.028	2.687	2.955
Wisconsin	0.523	0.147	0.128	3.863	4.662
Wyoming	0.080	0.040	0.008	1.784	1.912
Total	20.365	7.279	15.869	130.032	173.544

METEOROLOGY

MM5 Modeling

The WDNR completed an annual simulation from January 1, 2002 to December 31, 2002 using the PSU/NCAR Mesoscale Model, version 5 (MM5). The MM5 grid is the National Regional Planning Organization 36km grid covering most of the North America (Figure 3-2.). The domain had 165 by 129 grid points and 34 vertical layers. The grid is defined in a Lambert Conformal Projection (LCP) with the origin at 97.0 W 40.0 N and true parallels at 33.0 N and 45.0 N.

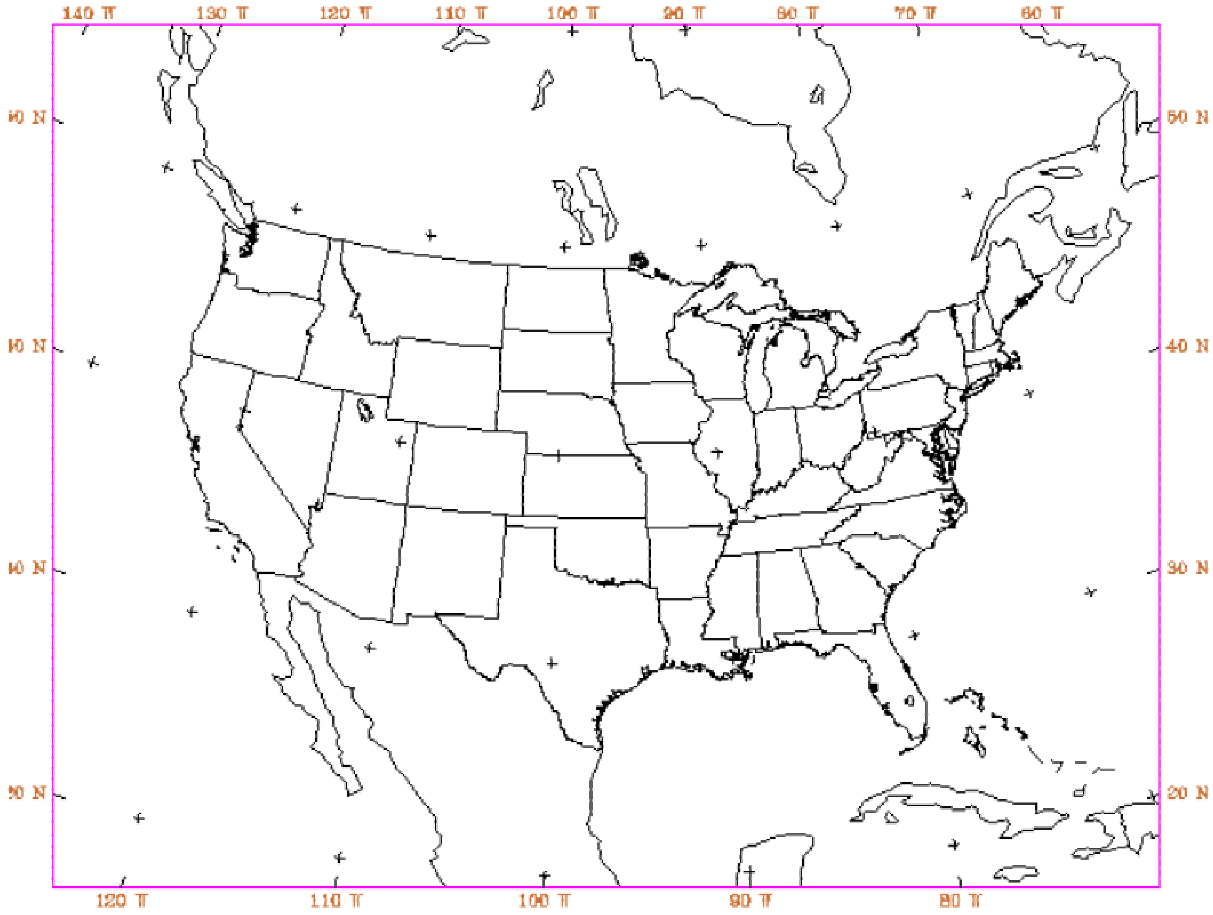

Figure 3-2. The MM5 36 km grid based on the National RPO grid.

The annual MM5 simulation used atmospheric input data from the National Center for Environmental Prediction (NCEP) for initialization, boundary conditions and 4 dimensional data assimilation (4DDA). The NCEP data used were:

- NCEP GDAS analysis
- NCEP Eta model output
- NCEP surface and upper air data

The MM5 was configured with the following options:

- Simple ice for the moisture scheme
- Kain-Fritcsh cumulus parameterization
- Pleim-Xiu PBL scheme and soil model
- RRTM radiation scheme
- 4DDA analysis nudging outside the PBL

The WDNR evaluated MM5 model performance by comparing modeled to observed wind speed, wind direction, temperature, and humidity using the METSTAT program. WDNR concluded that the MM5 produced reasonable meteorology fields that were suitable for annual

air-quality modeling. The Iowa DNR completed essentially the same model simulation and performance evaluation as described in IDNR (2003).

CAMx Meteorological Input Data

CAMx requires meteorological input data for the parameters described in Table 3-4.

Table 3-4. CAMx version 4 meteorological input data requirements.

CAMx Input Parameter	Description
Layer interface height (m)	3-D gridded time-varying layer heights for the start and end of each hour
Winds (m/s)	3-D gridded wind vectors (u,v) for the start and end of each hour
Temperature (K)	3-D gridded temperature and 2-D gridded surface temperature for the start and end of each hour
Pressure (mb)	3-D gridded pressure for the start and end of each hour
Vertical Diffusivity (m^2/s)	3-D gridded vertical exchange coefficients for each hour
Water Vapor (ppm)	3-D gridded water vapor mixing ratio for each hour
Cloud Water (g/m^3)	3-D gridded cloud water content for each hour
Precipitation Water (g/m^3)	3-D gridded precipitation content for each hour

MM5 output fields were translated to CAMx-ready inputs using ENVIRON's MM5CAMx translation software. This program performs several functions:

1. Extracts wind, temperature, pressure, humidity, cloud, and rain fields from each MM5 grid that matches the corresponding CAMx grid.
2. Performs mass-weighted vertical aggregation of data for CAMx layers that span multiple MM5 layers.
3. Diagnoses fields of vertical diffusion coefficient (Kv), which are not directly output by MM5.
4. Outputs the meteorological data into CAMx-ready input files.

Vertical Layers

The correspondence between the MM5 and CAMx layer structures is shown in Figure 3-3. MM5 was configured with 34 vertical layers up to a height of about 15 km (100 mb pressure), which is above the tropopause. CAMx was configured with fewer vertical layers to improve model run times and had 14 vertical layers and a model top at about 7 km. As discussed below, based on this study we recommend that the CAMx model top should be higher than 7 km for mercury modeling.

MM5 Layer	Sigma Level	Pressure (mb)	Depth (m)	Height (m)	CAMx Layer
34	0.000	100	1841	14661	
33	0.050	145	1466	12820	
32	0.100	190	1228	11354	
31	0.150	235	1062	10126	
30	0.200	280	939	9064	
29	0.250	325	843	8125	
28	0.300	370	767	7282	--14---
27	0.350	415	704	6515	
26	0.400	460	652	5811	
25	0.450	505	607	5159	
24	0.500	550	569	4552	--13---
23	0.550	595	536	3983	
22	0.600	640	506	3447	
21	0.650	685	480	2941	--12---
20	0.700	730	367	2461	--11---
19	0.740	766	266	2094	
18	0.770	793	259	1828	--10---
17	0.800	820	169	1569	
16	0.820	838	166	1400	---9---
15	0.840	856	163	1234	
14	0.860	874	160	1071	---8---
13	0.880	892	158	911	
12	0.900	910	78	753	---7---
11	0.910	919	77	675	
10	0.920	928	77	598	
9	0.930	937	76	521	---6---
8	0.940	946	76	445	
7	0.950	955	75	369	
6	0.960	964	74	294	---5---
5	0.970	973	74	220	
4	0.980	982	37	146	---4---
3	0.985	987	37	109	---3---
2	0.990	991	36	72	---2---
1	0.995	996	36	36	---1---
0	1.000	1000	0	=======Surface====	

Figure 3-3. MM5 and CAMx vertical grid structures based on 34 sigma-p levels.

Modeling Domain

The CAMx modeling domain was exactly matched to the MM5 horizontal coordinate system but was slightly smaller than the MM5 grid to eliminate any numerical noise close to the MM5 boundaries. The CAMx domain had 147 by 111 36 km grid cells with a grid origin at –2628 km W and –1980 km N. The CAMx domain is shown in Figure 3-1, above.

Vertical Diffusivities

Vertical diffusivities are an important input to the CAMx simulation since they determine the rate and depth of mixing in the planetary boundary layer (PBL) and above. Vertical

diffusivities (Kv) are preferably calculated from output fields of turbulent kinetic energy (TKE) predicted by the MM5. However, not all of the PBL schemes in MM5 use TKE and the Pleim-Xiu PBL scheme used for this study does not output TKE. MM5CAMx has several alternative methods for diagnosing Kv including several local gradient approaches and an approach that uses the MM5 output PBL depth. For this study, the MM5CAMx "OB70" method was used which preserves the MM5 output PBL depth and prescribes a profile of Kv within each grid column below the PBL top that depends on surface layer stability and the underlying surface characteristics. The methodology follows from O'Brien (1970).

The strength and extent of near-surface vertical mixing at night can be under-stated by the MM5 and/or the method used to diagnose Kvs. Minimum values for Kv were set according to land-use type for layer interfaces below 100 m as shown in Table 3-5.

Table 3-5. Minimum values for vertical diffusivity (m^2/s) were set according to land-use category for layer interfaces below 100 m.

Land-use Category	Minimum Kv below 100 m
Urban	1.0
Agricultural	0.1
Range	0.1
Deciduous forest	0.5
Coniferous forest	0.5
Mixed forest	0.5
Water	0.1
Barren land	0.1
Non-forest wetlands	0.1
Mixed agriculture and range	0.1
Rocky/low shrubs	0.1

BOUNDARY CONDITIONS

The mercury boundary conditions used for the CAMx annual simulation were derived from Hg concentrations simulated over North America by a global mercury chemistry transport model (CTM). This CTM has been evaluated extensively and used successfully to provide boundary conditions for several prior studies that investigated Hg deposition over North America (Shia et al. 1999, Seigneur et al. 2001a; 2003a; 2003c, Vijayaraghavan et al., 2003). The global model simulates mercury in its elemental [Hg(0)], gaseous divalent [Hg(II)], and particulate [Hg(p)] valence state forms. Annual simulations of the global atmospheric fate and transport of mercury are performed repeatedly until steady state is achieved.

The CAMx modeling domain used in this study has a horizontal resolution of 36 km x 36 km while the global model provides a horizontal resolution of 8 degrees latitude and 10 degrees longitude. The mapping between each CAMx boundary grid cell and the nearest global grid cell was determined by converting the Lambert Conformal projection used in CAMx to the true global geographic coordinates (in latitude/longitude). A mapping was also constructed between the CAMx vertical levels and the global model layers. The CAMx grid has 14 layers ranging from the surface to an altitude of about 7 km while the global CTM has nine layers extending to the lower stratosphere. Seven of these layers are in the troposphere (between the

surface and ~12 km altitude). The average height of each CAMx layer was used to determine the corresponding global layer.

Monthly average 3-D concentrations of the three Hg species were obtained from the global model for January, April, July and October (representing winter, spring, summer and fall respectively). The global Hg concentrations were available in units of $\mu g/m^3$. The CAMx boundary conditions for the gaseous Hg species (Hg(0) and Hg(II)) are specified in ppmV and those for Hg(p) in $\mu g/m^3$. The temporally-resolved and spatially-distributed CAMx meteorological fields at the domain boundaries were processed to determine a representative temperature and pressure in each model layer and boundary for each season. These temperature and pressure fields were used to convert Hg(0) and Hg(II) concentrations from mass units to ppmV. No conversion of units was required for the Hg(p) values. The Hg concentrations across all global grid cells corresponding to each CAMx boundary were then averaged to determine the seasonally varying Hg boundary conditions for each layer. A modified version of the CAMx preprocessor "icbcprep" was used to create the final binary boundary condition files. The boundary conditions at the top of the modeling domain were determined by calculating the average of the topmost layer concentrations at the four boundaries. The range of Hg boundary conditions over all layers for each season is shown in Table 3-6. The two values shown are the minimum and maximum across all layers.

Table 3-6. Range of CAMx Hg boundary conditions over all layers.

	West	East	South	North
Winter				
HG0 (ppmV)	1.5e-07 to 2.0e-07	1.6e-07 to 2.1e-07	1.5e-07 to 2.0e-07	1.6e-07 to 1.9e-07
HG2 (ppmV)	2.5e-09 to 1.1e-08	4.0e-09 to 1.1e-08	2.0e-09 to 1.1e-08	3.0e-09 to 1.2e-08
HGP ($\mu g/m^3$)	3.8e-06 to 5.5e-06	2.7e-06 to 5.7e-06	2.5e-06 to 4.6e-06	3.3e-06 to 5.0e-06
Spring				
HG0 (ppmV)	1.6e-07 to 2.0e-07	1.6e-07 to 2.1e-07	1.5e-07 to 2.0e-07	1.6e-07 to 1.9e-07
HG2 (ppmV)	3.3e-09 to 1.4e-08	3.3e-09 to 1.8e-08	1.8e-09 to 1.5e-08	3.9e-09 to 1.8e-08
HGP ($\mu g/m^3$)	4.1e-06 to 4.9e-06	3.7e-06 to 4.8e-06	2.2e-06 to 5.3e-06	3.1e-06 to 4.4e-06
Summer				
HG0 (ppmV)	1.4e-07 to 2.1e-07	1.5e-07 to 2.0e-07	1.5e-07 to 2.1e-07	1.5e-07 to 2.0e-07
HG2 (ppmV)	2.4e-09 to 2.5e-08	2.1e-09 to 1.9e-08	2.5e-09 to 1.7e-08	1.8e-09 to 2.5e-08
HGP ($\mu g/m^3$)	3.7e-06 to 5.0e-06	2.4e-06 to 3.7e-06	3.1e-06 to 8.6e-06	3.5e-06 to 4.0e-06
Fall				
HG0 (ppmV)	1.5e-07 to 2.0e-07	1.5e-07 to 2.0e-07	1.5e-07 to 2.0e-07	1.5e-07 to 1.9e-07
HG2 (ppmV)	2.0e-09 to 1.7e-08	2.1e-09 to 1.6e-08	1.5e-09 to 1.3e-08	2.9e-09 to 1.9e-08
HGP ($\mu g/m^3$)	4.1e-06 to 5.3e-06	2.9e-06 to 4.0e-06	2.0e-06 to 4.8e-06	3.3e-06 to 4.7e-06

Boundary Conditions for Non-Mercury Species

The boundary conditions for non-mercury species were set to clean values based on the MRPO modeling for the January 2000 and July 2001 episode periods. These clean values were used for all lateral and top boundaries as well as the initial conditions as shown in Table 3-7.

Table 3-7. Boundary conditions for non-mercury species.

Species	Boundary Condition
Gasses (ppmV)	
NO	0.00005
NO2	0.00015
O3	0.04
PAR	0.008
TOL	0.000001
XYL	0.000001
HCHO	0.00025
ALD2	0.0001
ETH	0.0001
PAN	0.00002
CO	0.08
H2O2	0.001
HNO3	0.00005
NH3	0.0001
SO2	0.0002
Particles ($\mu g/m^3$)	
CCRS	0.00000001
FCRS	0.0000001
SOA1	0.0000001
SOA2	0.0000001
SOA3	0.0000001
SOA4	0.0000001
PNH4	0.00005
PSO4	0.00015
PNA	0.0000001
PCL	0.0000001

4. MODELING RESULTS AND PERFORMANCE EVALUATION

TRACER SIMULATIONS

Inert tracer simulations were performed to evaluate the mass consistency of the model and meteorological fields and determine how long a spin-up period would be needed to remove any influence of initial conditions. The mass consistency test involved specifying a tracer with initial and boundary conditions of 1 ppm and determining the largest positive and negative deviations of the surface tracer concentrations from 1 ppm over a 1-month simulation. The persistence of initial conditions was evaluated by specifying a tracer with 1 ppm initial conditions (ICs) and zero boundary conditions (BCs) and watching the decline in tracer concentration over a 1 month simulation. Tracer simulation results for July are shown in Figure 4-1. For the mass-consistency test (Figure 4-1a), the largest positive and negative deviations were less than 0.1% throughout July (and all other months) confirming that the meteorological fields and CAMx transport algorithms are mass consistent. The IC tracer test for July showed that the IC tracer concentration was reduced by about 70% in 11 days (Figure 4-1b). The IC tracer tests for other months produced similar results suggesting that a spin-up period of about 2 to 3 weeks is needed to remove the influence of initial conditions from this modeling domain.

(a)

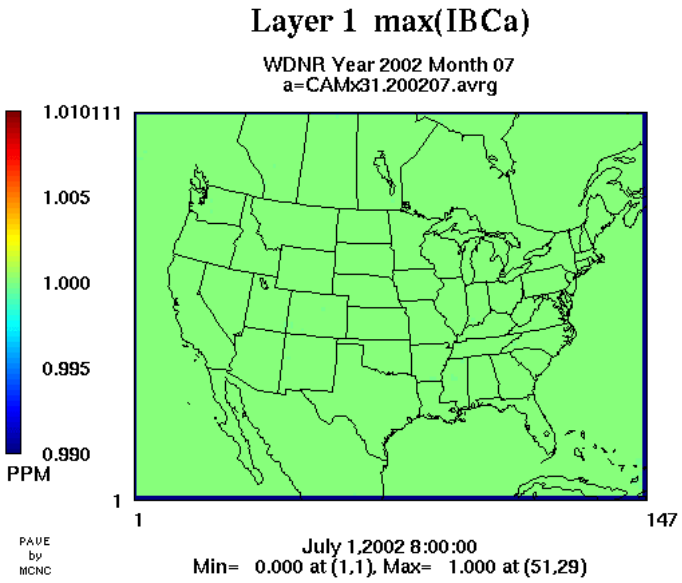

(b)

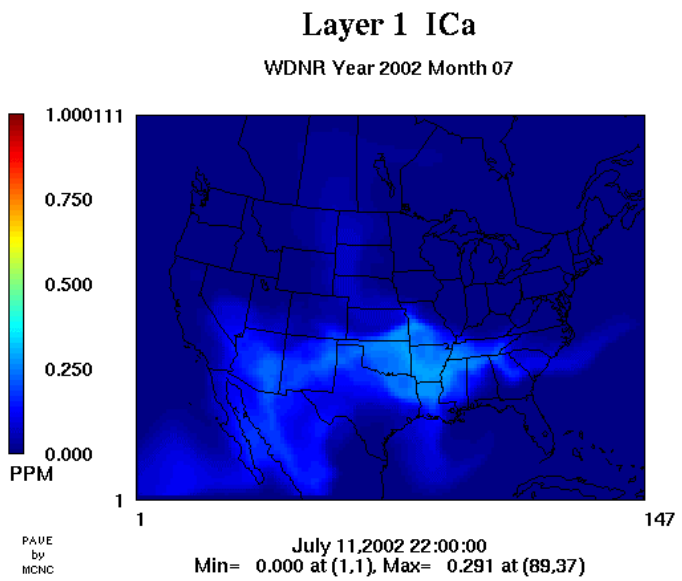

Figure 4-1. Results of inert tracer simulations for July 2002 (a) mass consistency test with a 1 PPM tracer, and (b) persistence of 1 PPM tracer from July 1 to July 11.

BASE CASE MERCURY SIMULATION

The base case mercury simulation was called "base1" and was for January 2, 2002 to December 30, 2002. An example "CAMx.in" file showing the model configuration and input file names is shown in Figure 4-2 for January 2, 2002. The model options were:

- PPM advection solver
- CMC chemistry solver
- No plume-in-grid sub-model
- Dry and wet deposition enabled

The simulation was run 1 day at a time with model restarts between days. Surface concentration and deposition information was saved hourly for all mercury species plus several ozone/PM precursors and products. The annual simulation was split into two pieces (January – June and June – December) so that the first and second parts of the year could be run simultaneously on different workstations. The complete month of June was run as a spin-up period for the second half of the year. The modeling results analyzed for June are from the end of the first part year, not the start of the second part year. Model run times were about 2 hours per simulated day on a single Athlon 2600+ processor using Red Hat Linux (7.2 and 9.0) and the Portland Group PGF77 compiler.

```
CAMx Version        |version4.0
Run Message         |WDNR Hg Modeling 2002/01/02 base1
Root output name    |/disk21/WDNR/camx/outputs/base1/CAMx4hg.2002002.base1
Start yr/mo/dy/hr   |02 01 02  0000.
End   yr/mo/dy/hr   |02 01 02  2400.
DT:max,met,ems,out  |15. 60. 60. 60.
nx,ny,nz            |147 111 14
Coordinate ID       |LAMBERT
xorg,yorg,dx,dy     |-2628.0, -1980.0, 36.0, 36.0, -97.0, 40.0, 45.0, 33.0
time zone           |5
PiG parameters      |5000. 18.
Avg output species  |16
                    |O3        PNO3      PSO4      PNH4      HG0       HG2
                    |HGP       CO        HNO3      NO        NO2       PAN
                    |NTR       H2O2      SO2       NH3
# nested grids      |0
SMOLAR,BOTT, PPM?   |PPM
Chemistry solver    |CMC
Restart             |false
Chemistry           |true
Dry dep             |true
Wet dep             |true
PiG submodel        |false
Staggered winds     |false
Treat area emiss    |true
Treat point emiss   |true
1-day emiss inputs  |true
3-D average file    |false
Probing Tool?       |false
Chemparam           |/disk41/ladco_hg/camx/preproc/CAMx4.chemparam.4_hg
Photolysis rates    |/disk41/ladco_hg/camx/preproc/tuv/outputs/tuv.ladco_hg.0201.dat.a0
Landuse             |/disk41/ladco_hg/camx/preproc/kvpatch/inputs/surf.natl.36.ld.bin.a0
Height/pressure     |/disk41/ladco_hg/camx/preproc/mm5v3_camxv4/outputs/zp.200201.bin2
Wind                |/disk41/ladco_hg/camx/preproc/mm5v3_camxv4/outputs/uv.200201.bin2
Temperature         |/disk41/ladco_hg/camx/preproc/mm5v3_camxv4/outputs/tp.200201.bin2
Water vapor         |/disk41/ladco_hg/camx/preproc/mm5v3_camxv4/outputs/qa.200201.bin2
Cloud cover         |/disk41/ladco_hg/camx/preproc/mm5v3_camxv4/outputs/cr.200201.bin2
Vertical diffsvty   |/disk41/ladco_hg/camx/preproc/kvpatch/outputs/kv.200201.bin
Initial conditions  |/disk41/ladco_hg/camx/preproc/icbc_hg/icbctc/out/ic.WDNR_hg.2002.winter.bin
Boundary conditions|/disk41/ladco_hg/camx/preproc/icbc_hg/icbctc/out/bc.WDNR_hg.2002.winter.bin
Top concentration   |/disk41/ladco_hg/camx/preproc/icbc_hg/icbctc/out/topcon.WDNR_hg.winter
Albedo/haze/ozone   |/disk41/ladco_hg/camx/preproc/ahomap/outputs/ahomap.0201.monthly.dat.a1
Point emiss         |/disk41/ladco_hg/camx/emissions.hg/final/emis.point.000114.bin.a0
Area emiss          |/disk41/ladco_hg/camx/emissions.hg/final/emis.hg_area.20000114.WDNR.bin
```

Figure 4-2. Example CAMx.in file for the base case run (base1) on January 2, 2002.

Annual mercury deposition amounts (μg/m^3) are shown in Figure 4-3 for HG2 and HGP wet and dry deposition. Note that different scales are used in each panel of Figure 4-3. HG0 deposition is not shown because it was set to zero by setting a very small Henry constant for HG0, as discussed above. HG2 deposition dominates over HGP deposition at the regional scale. The relative importance of dry and wet deposition varies with location for HG2. Generally, wet deposition of HG2 exceeds dry deposition. Dry deposition of HG2 is largest in some major urban areas and over water off the Atlantic and Gulf Coasts and the Great Lakes. The mercury deposition results are discussed in more detail in the performance evaluation that follows.

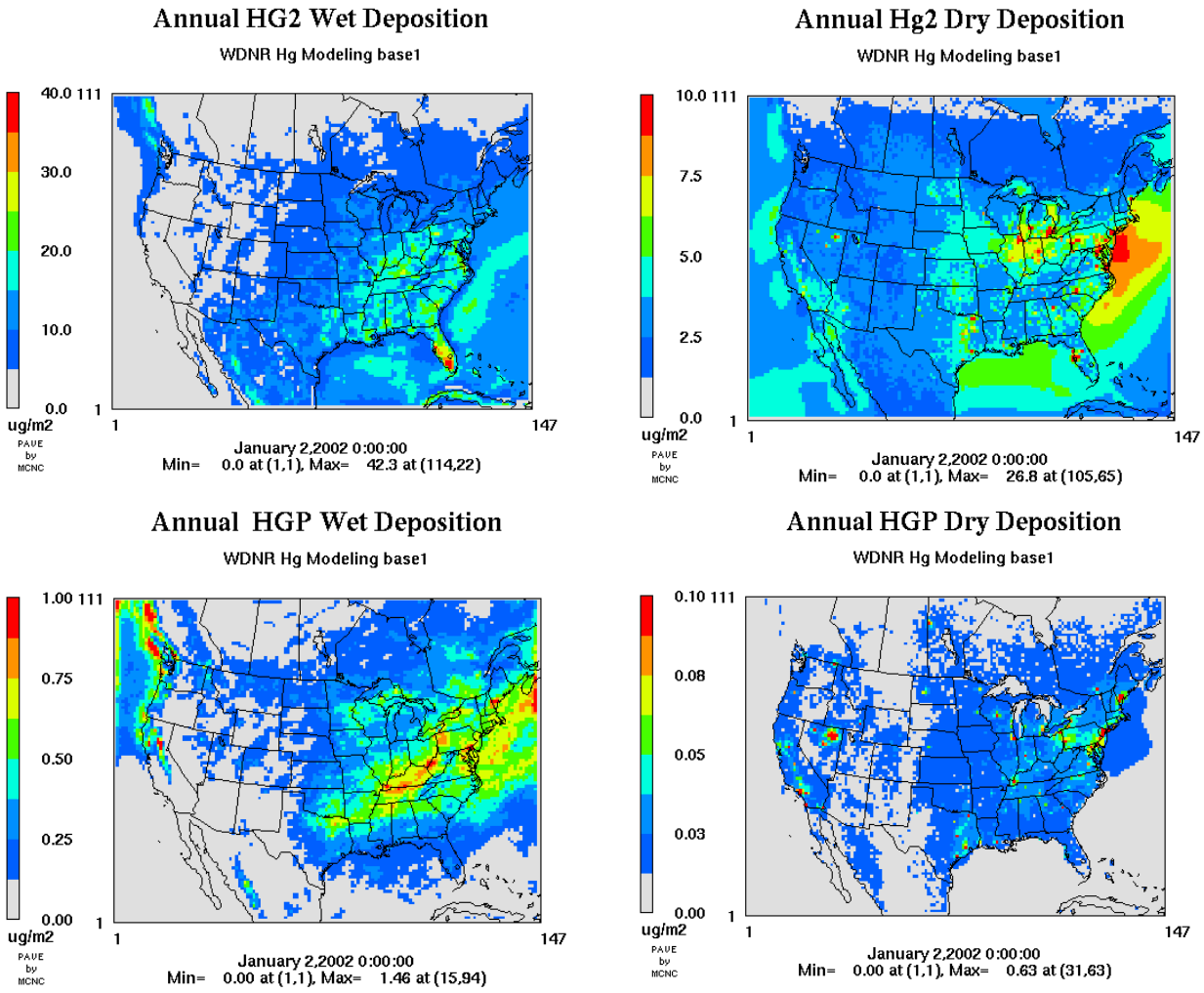

Figure 4-3. Annual mercury deposition amounts (μg/m^3) for HG2 and HGP wet and dry deposition. HG0 deposition is not shown because it was set to zero.

SENSITIVITY SIMULATIONS

Several sensitivity simulations were conducted to quantify the relative importance of different model processes for HG2 deposition. The sensitivity simulations carried out for June - July 2002 were:

1. "inert" Chemistry flag set to false in the CAMx.in file
2. "inert_noemiss" Chemistry, area and point emission flags set to false in the CAMx.in file
3. "inert_hg2top0" Chemistry, area and point emission flags set to false in the CAMx.in file and HG2 set to zero in the top concentration input file

The results of these simulations were analyzed to estimate the contributions of emissions, chemistry, boundary contributions and the top boundary contribution to HG2 wet deposition for July. The base case HG2 wet deposition for July 2002 is shown in Figure 4-4. The HG2 wet deposition amounts show a lot of spatial variation reflecting the locations of predicted rainfall.

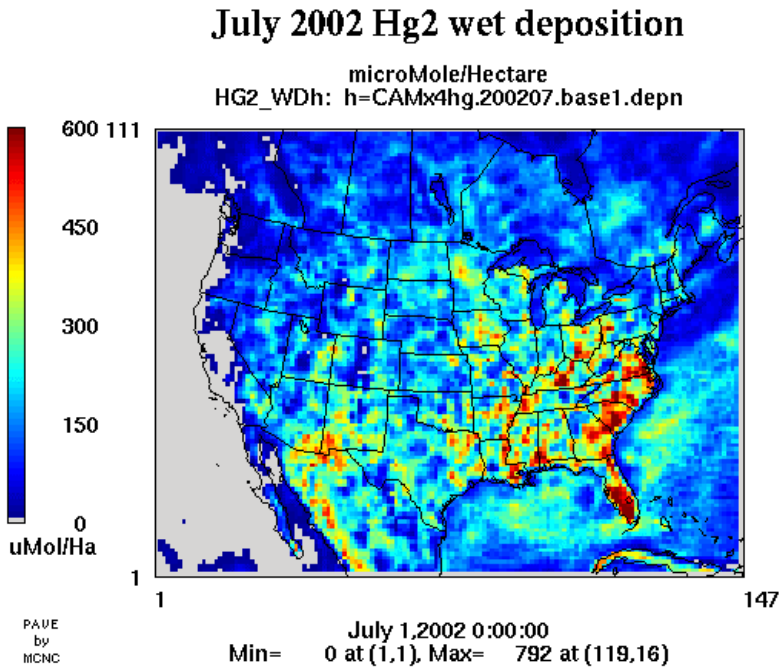

Figure 4-4. Base case wet deposition (µMole/Hectare) for HG2 for July 2002.

The relative contributions of different model processes to HG2 wet deposition were calculated using simple formulas as shown in the figure titles in Figure 4-5. In these formulas, the word delta signifies a small amount (1.0e-9) used to prevent a divide-by-zero error. Relative

contribution means the fraction of the total HG2 wet deposition attributed to the process. The following contributions were calculated:

Chemistry – HG2 that was formed in chemistry and deposited
HG2 Emissions – HG2 that was emitted as HG2 and deposited
Boundary conditions – HG2 that entered the model through BCs and was deposited
Top boundary conditions – HG2 that entered the model through top BCs and was deposited

These contributions are approximate because there are some interactions between processes (e.g., HG2 from emissions could be chemically reduced before it deposits) and because the horizontal advection scheme does not respond linearly to concentration perturbations. However, these estimated contributions do provide a very good picture of the relative importance of processes at the regional scale.

The contribution of chemistry generally is higher where oxidant concentrations are higher, namely in the south of the domain and over/downwind of the eastern US. The contribution of HG2 emissions generally is higher in the eastern US than the western US. The HG2 emissions contribution generally is smaller than the chemistry contribution. The contribution of boundary conditions is highest close to the boundaries. The contribution of the northern boundary is strong over most of Canada. The contribution of boundary conditions exceeds 50 percent over much of the western US and exceeds 25 percent over much of the eastern US. The contribution of boundary conditions to the interior of the domain was higher than expected. This is largely due to the contribution of the top boundary conditions, which approaches 50 percent over much of the western US and approaches 20 percent over much of the eastern US. High contributions from the top boundary conditions occur near areas of high terrain (e.g., the Rocky, Appalachian and Sierra Nevada mountains) and indicate resolved vertical velocities through the CAMx model top at about 7 km. Other MM5 processes besides terrain effects that could lead to vertical velocities through 7 km include frontal passages and resolved deep convection. Downward air motion at the model top will bring HG2 from the top boundary condition into the upper layers of the model where it can dissolve in precipitation and be brought down to the surface. HG2 is very soluble in water (Henry constant similar to nitric acid) and can be efficiently scavenged by precipitation.

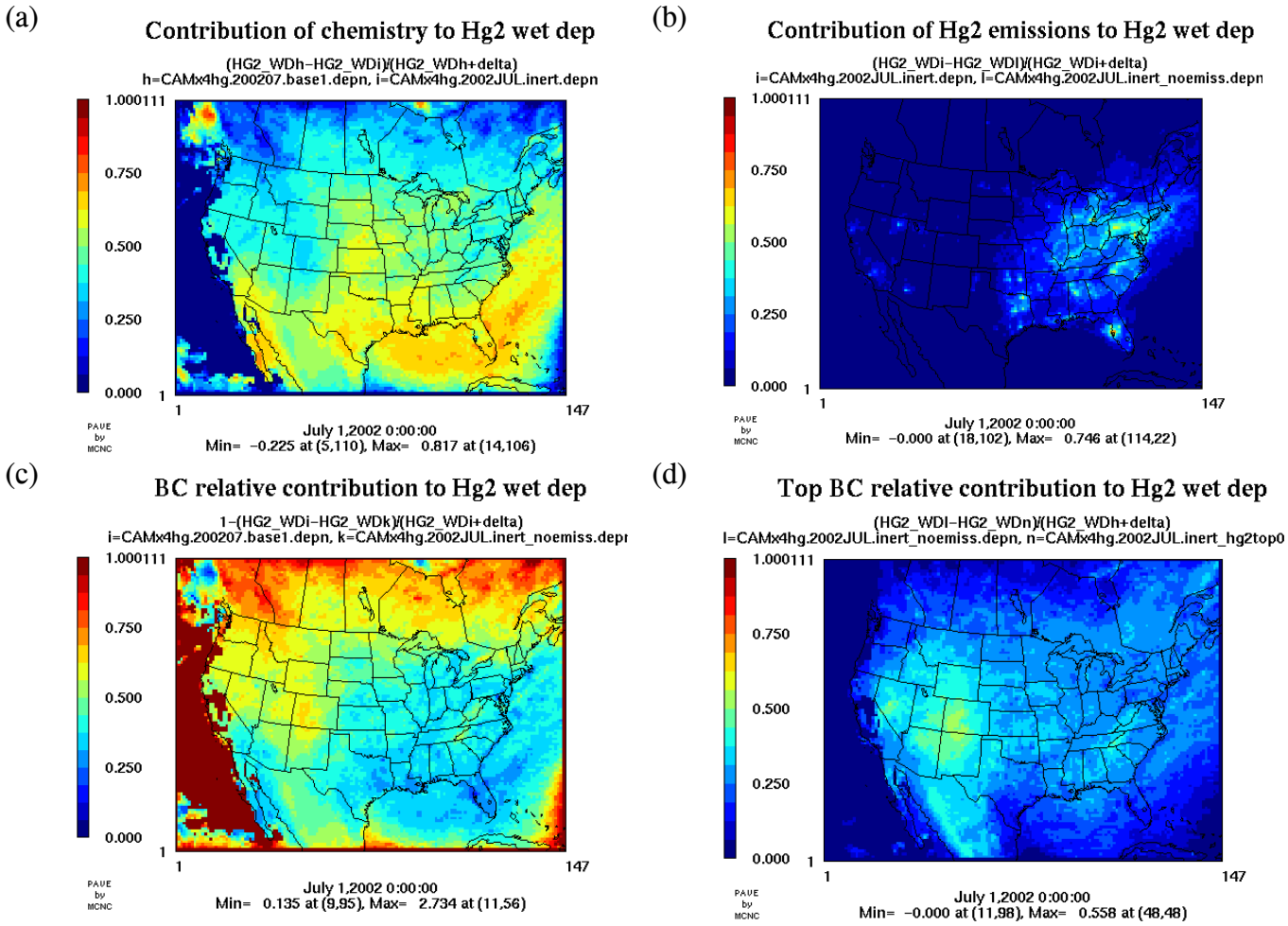

Figure 4-5. Relative contributions to July 2002 HG2 wet deposition of (a) chemistry (b) HG2 emissions (c) HG2 boundary conditions (d) HG2 top boundary conditions.

The sensitivity analysis showed an unexpected large influence of top boundary conditions on HG2 wet deposition. For comparison, the contribution of boundary conditions to nitric acid (HNO3) deposition was estimated using the same method as for HG2. Figure 4-6 shows that the contribution of HNO3 boundary conditions HNO3 wet deposition for July 2002 is small, except over the Pacific Ocean. This result shows that with an HNO3 top concentration of 50 ppt, the HNO3 wet deposition is dominated by emissions and chemistry.[1] The main source of deposited HNO3 is chemical conversion of NOx emissions to HNO3 followed by HNO3 deposition.

[1] The analysis shown in Figure 4-6 is biased toward over-stating the contribution of boundary conditions to HNO3 wet deposition because in the base simulation with chemistry on some HNO3 can deposit as particulate nitrate, whereas in the "inert_noemiss" sensitivity simulation with chemistry off HNO3 can only deposit as HNO3.

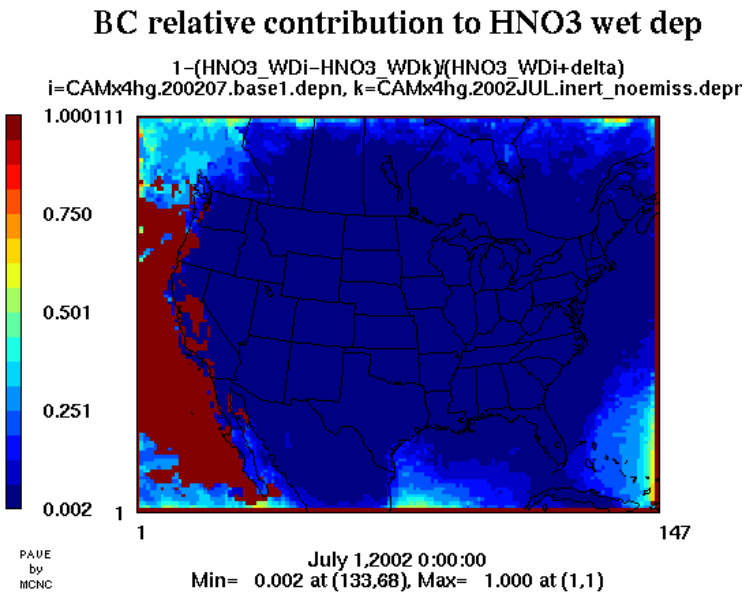

Figure 4-6. Relative contributions of HNO3 boundary conditions to July 2002 HNO3 wet deposition.

The large influence of top boundary conditions on HG2 wet deposition contrasts with the small influence on HNO3 deposition and leads to the conclusion that a higher model top is needed for modeling mercury deposition than acid deposition. A higher model top is needed for mercury because of the high solubility of HG2 in precipitation combined with an increase in HG2 mixing ratios with altitude. These attributes make HG2 different from other pollutants modeled using CAMx such as sulfate, nitrate and ozone. The HG2 mixing ratio tends to increases with height because HG2 is formed from oxidation of HG0 throughout the troposphere. In contrast, sulfate and nitrate mixing ratios decrease with altitude. Ozone has a tendency to increase in concentration in the upper troposphere, but differs from HG2 in being only slightly soluble in precipitation.

EVALUATION OF MERCURY DEPOSITION RESULTS

We compared the seasonal and annual simulated wet deposition fluxes of total mercury (Hg(0) + Hg(II) + Hg(p)) with measurements from the National Acid Deposition Program's Mercury Deposition Network (NADP/MDN). Figure 4-7a, obtained from the MDN web site (http://nadp.sws.uiuc.edu/mdn/sites.asp), shows the spatial distribution of the MDN monitoring sites in the continental United States and Canada. Note that the figure does not show the Milwaukee, WI site (WI22), which became operational on October 3, 2002. Figure 4-7b, also obtained from the MDN web site (http://nadp.sws.uiuc.edu/sites/sitemap.asp?net=MDN&state=wi) shows all the sites currently operational in Wisconsin.

There were 68 MDN sites operational in 2002. However, a few of these sites had missing or invalid data for much of the year, and data from these sites were not used for our comparisons with model results, as discussed below.

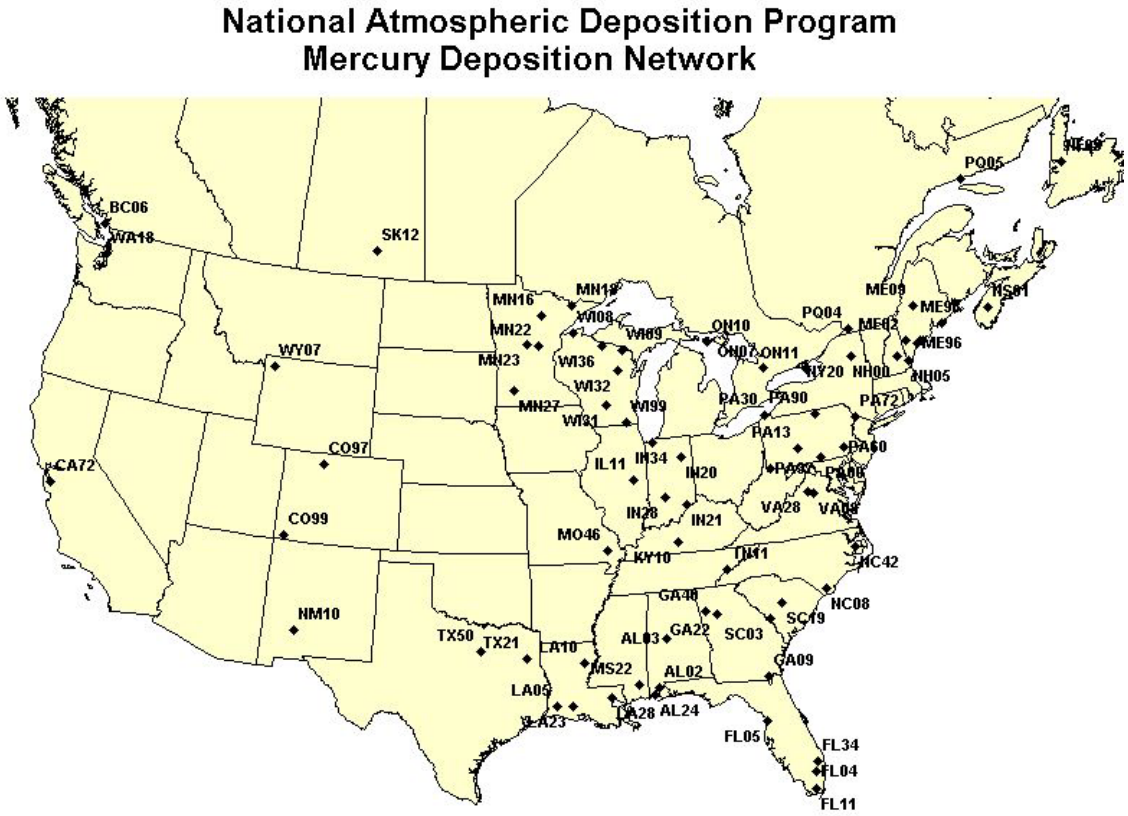

Figure 4-7a. Locations of Mercury Deposition Network (MDN) sites.

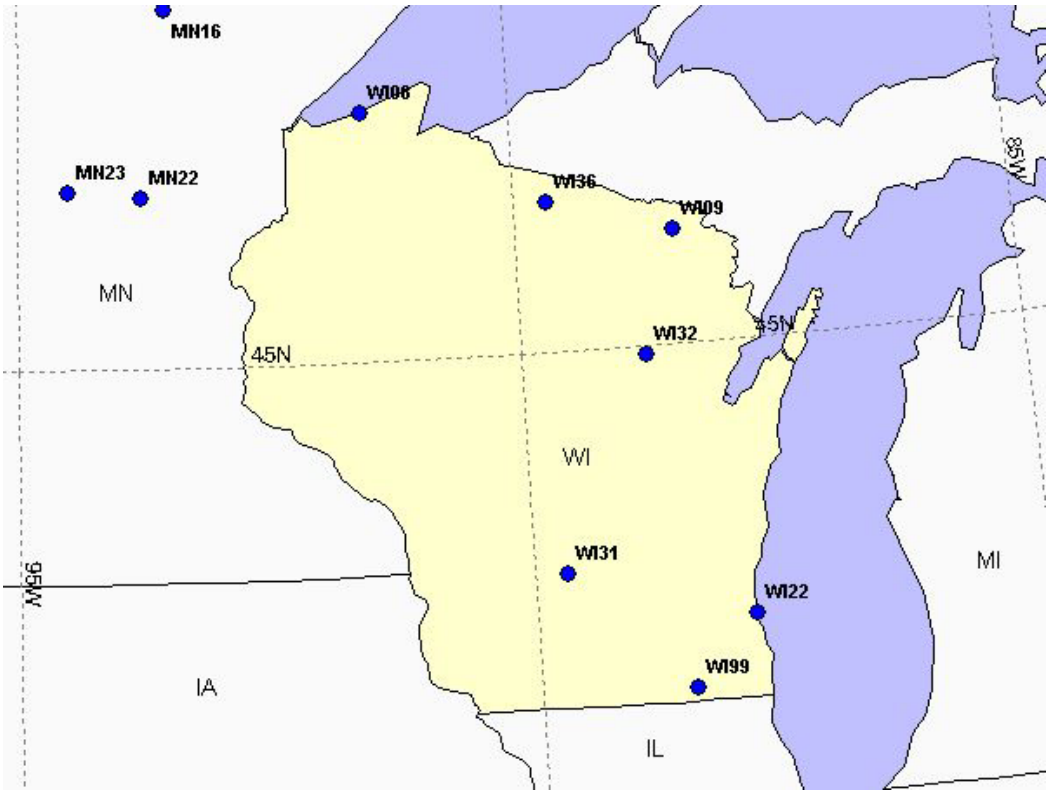

Figure 4-7b. MDN sites in Wisconsin.

We calculated total seasonal and annual wet deposition fluxes for both the model results and measurements at the MDN site locations. For the MDN observations, we first calculated monthly totals from the weekly data. Sites with less than 8 days of valid wet deposition data per month were assigned a missing value for the monthly wet deposition. For sites with 8 or more days of valid data, but less than the total number of days in the month, monthly deposition fluxes were calculated by scaling the calculated total wet deposition for the valid days using the observed precipitation data. Next, we calculated the seasonal wet deposition fluxes, discarding those sites with missing data for any month in the season (i.e., a missing value was assigned for the seasonal wet deposition at those sites). Using this approach, the number of sites reporting valid data ranged from 55 in the winter months (December, January, February) to 61 in the autumn months (September, October, November). Finally, the annual total observed wet deposition fluxes were calculated from the seasonal totals, discarding those sites with missing data for any season. This resulted in 52 sites for the comparison of annual values.

The results of our evaluation are presented both graphically and quantitatively using the model performance evaluation metrics described below. These metrics follow the EPA guideline (EPA, 1991) for ozone model performance. However, note that there are currently no regulatory guidelines for model performance for wet deposition of Hg or any other species.

Performance Evaluation Metrics

We computed the following metrics for the Hg wet deposition comparisons:

1. Normalized Bias (NB)

$$B_N = \frac{1}{N}\sum_{i=1}^{N}\left(\frac{P_i - O_i}{O_i}\right)$$

where

N - total number of measurement sites with non-missing values
P_i – Predicted value at site 'i'
O_i– Observed value at site 'i'

EPA guideline (1991) for O_3: Normalized bias $< \pm$ 5-15%
No guidelines for PM and wet deposition.

2. Fractional Bias (FB)

$$B_F = \frac{1}{N}\sum_{i=1}^{N}\left(2 \bullet \frac{P_i - O_i}{P_i + O_i}\right)$$

3. Normalized Gross Error (NGE)

$$E_N = \frac{1}{N}\sum_{i=1}^{N}\left|\frac{P_i - O_i}{O_i}\right|$$

EPA guideline (1991) for O_3: Normalized gross error $< \pm$ 30-35%
No guidelines for PM and wet deposition.

4. Fractional Gross Error (FGE)

$$E_F = \frac{1}{N}\sum_{i=1}^{N}\left|2 \bullet \frac{P_i - O_i}{P_i + O_i}\right|$$

Model Performance for Hg Wet Deposition

Figure 4-8 presents scatter-plots of the simulated and observed seasonal wet deposition fluxes at the MDN sites. The equation for the best-fit line through the origin is also shown in the scatter-plots, as is the coefficient of determination (r^2). As seen in the figure, the model overpredicts Hg wet deposition for all the seasons, by factors of 2 to 3 on average, with the largest overpredictions in the summer months.

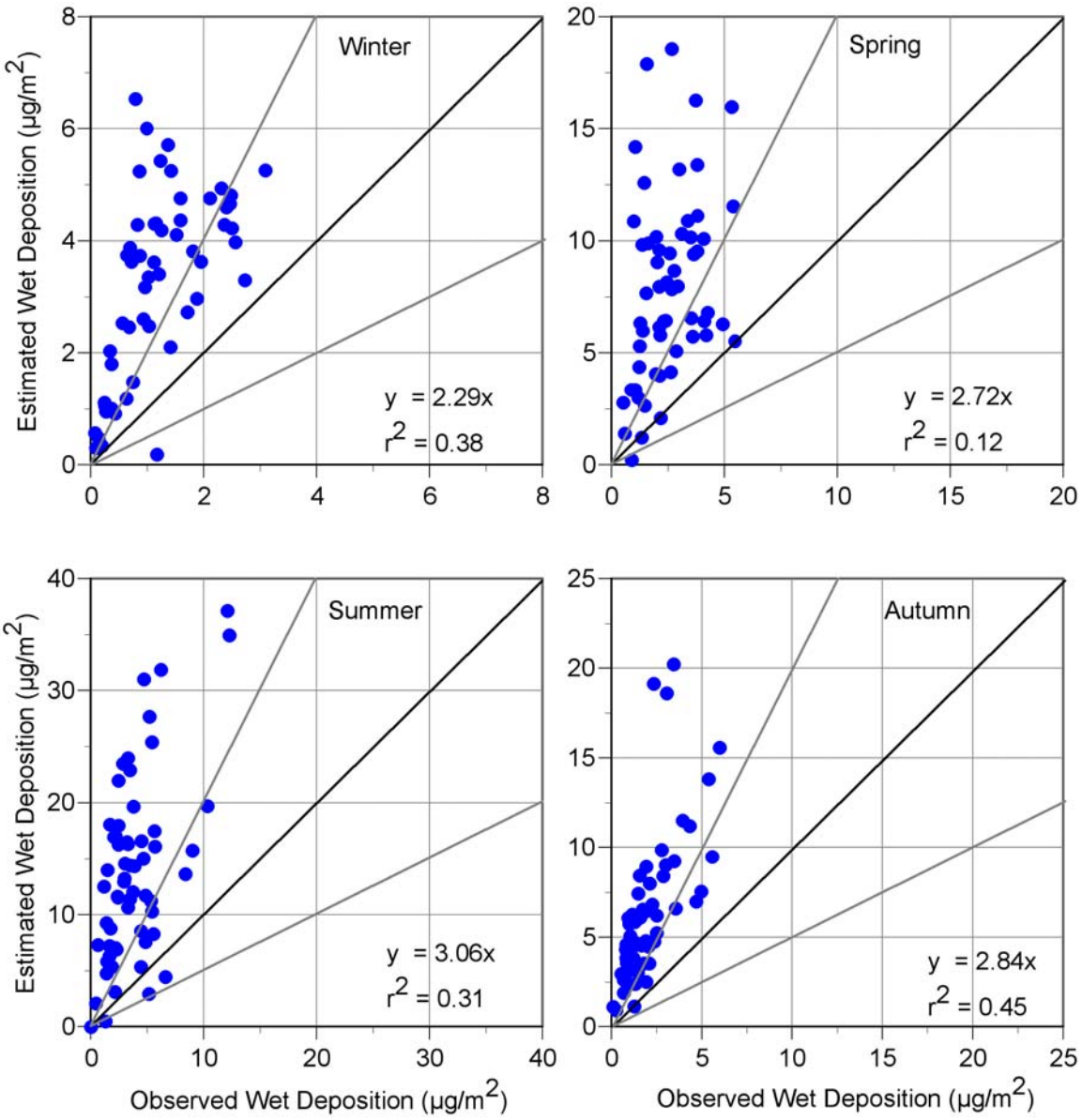

Figure 4-8. Comparison of simulated seasonal Hg wet deposition fluxes with MDN measurements; diagonal line indicates 1:1 line, lighter lines indicate 1:2 and 2:1 ratios.

To determine the possible reasons for the overpredictions, we compared the precipitation amounts used in calculating wet deposition in the model with those observed at the MDN sites. Recall that the wet deposition flux of a species is the product of its concentration in rain with the precipitation amount.

Figure 4-9 compares the model and observed precipitation amounts at the MDN sites. We see that the precipitation amounts used in the model calculations are also consistently larger than the observed values, up to a factor of 2 larger during the summer months. However, the degree of overprediction of the precipitation amounts is generally smaller than that of the deposition amounts. Nevertheless, Figure 4-9 suggests that a significant part of the

overprediction of Hg wet deposition can be attributed to errors in the precipitation amounts used in the model calculations. The modeled rainfall is discussed in more detail below.

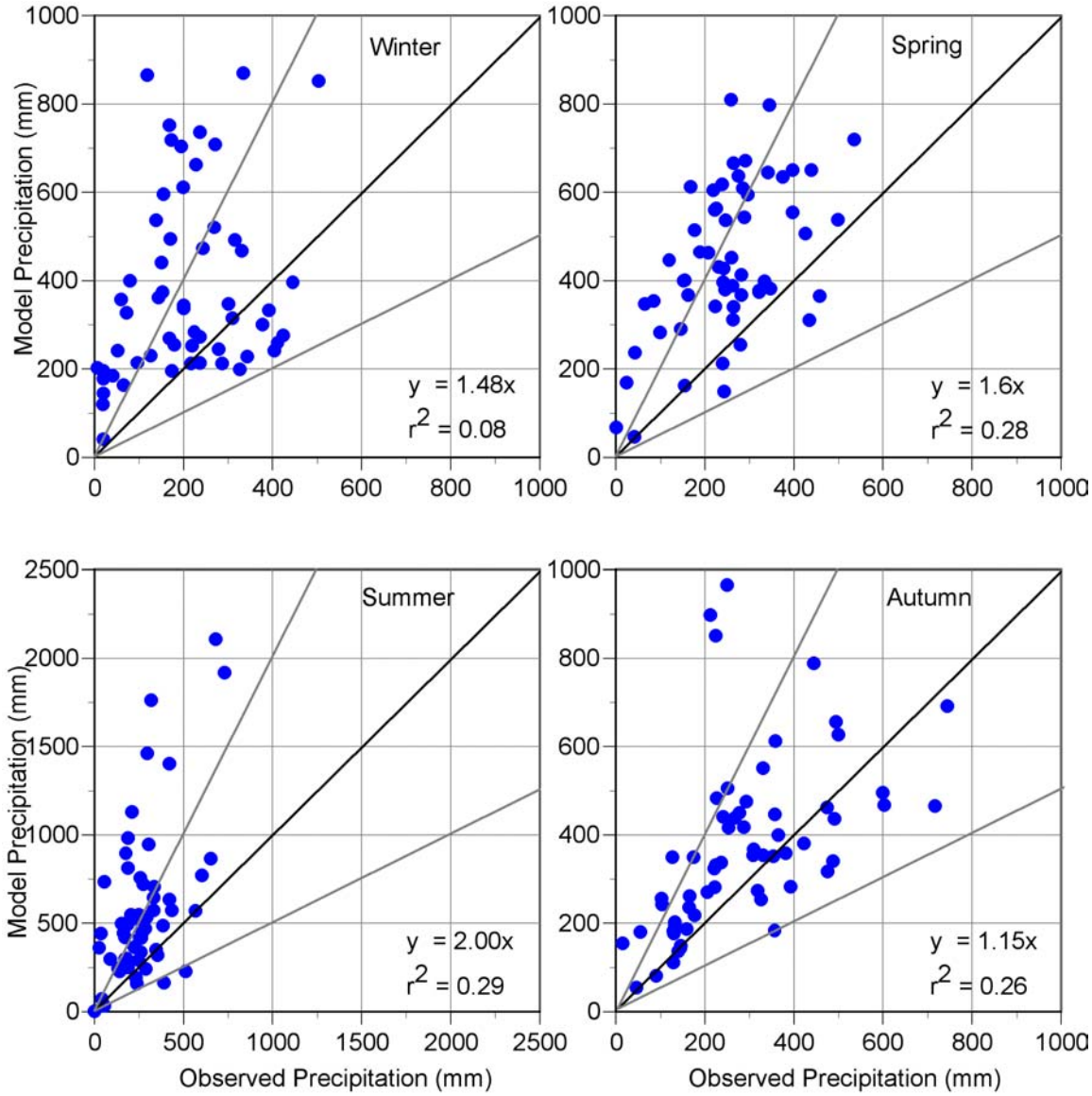

Figure 4-9. Comparison of precipitation amounts used for model wet deposition calculations with MDN measurements; diagonal line indicates 1:1 line, lighter lines indicate 1:2 and 2:1 ratios.

Since it was not possible to develop revised precipitation fields and repeat the CAMx simulations within the scope of this study, we used the model wet deposition results and the observed to model precipitation ratios to calculate what the wet deposition fluxes would be if the model precipitation amounts exactly matched the observed precipitation amounts. The simulated wet deposition value at each site was multiplied by the observed to model precipitation ratio to calculate the scaled wet deposition at that site. This calculation is an approximation since it implicitly assumes that the simulated rainwater concentrations are unchanged by changes in the precipitation field.

Figure 4-10 compares the precipitation-scaled seasonal Hg deposition values with the observed wet deposition fluxes at the MDN sites. We see that using the observed precipitation amounts reduces the overprediction of Hg wet deposition, with the largest improvements for the summer season. As expected, the correlations between the estimated and observed wet deposition fluxes are larger, primarily because of the common factor (precipitation amounts) in the two quantities.

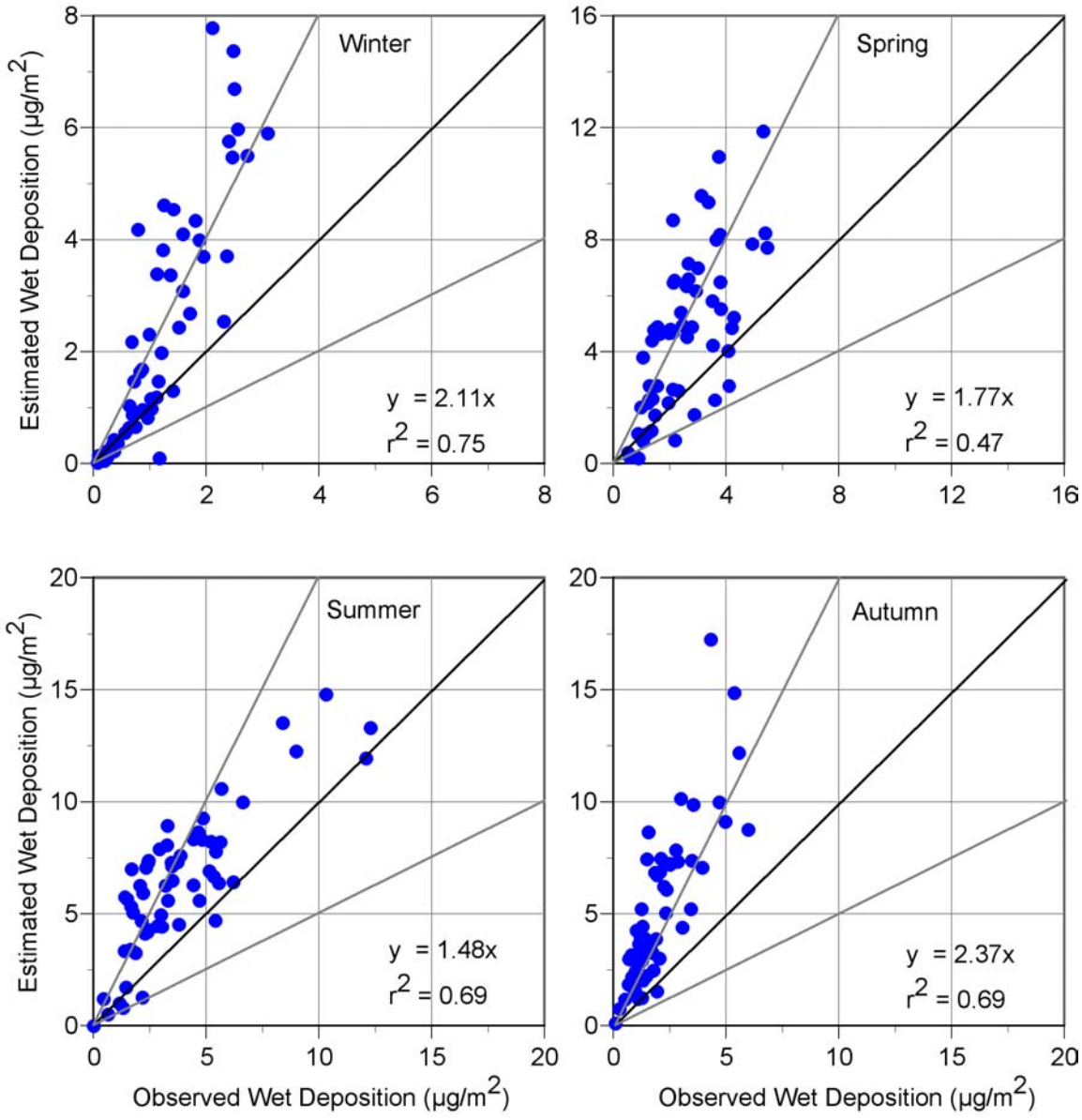

Figure 4-10. Comparison of precipitation-scaled simulated seasonal Hg wet deposition fluxes with MDN measurements; diagonal line indicates 1:1 line, lighter lines indicate 1:2 and 2:1 ratios.

Table 4-1 shows the seasonal model performance statistics for Hg wet deposition, while Table 4-2 shows the comparison statistics for the precipitation amounts. These statistics provide a quantitative measure of the over-estimation of both the wet depositions and the precipitation

amounts. Table 4-3 shows the corresponding statistics for the precipitation-scaled Hg wet deposition, calculated as discussed above.

Table 4-1. Model performance statistics for seasonal Hg wet deposition fluxes (μg/m^2).

Performance Measure	Spring	Summer	Autumn	Winter
Average observation	2.54	3.80	2.00	1.19
Average prediction	7.88	13.85	6.35	3.22
Normalized bias	264%	339%	266%	231%
Fractional bias	0.92	1.04	1.03	0.92
Normalized error	267%	343%	266%	234%
Fractional error	0.97	1.10	1.03	0.97
r^2	0.12	0.31	0.45	0.38

Table 4-2. Comparison statistics for observed and model seasonal precipitation amounts (mm).

Performance Measure	Spring	Summer	Autumn	Winter
Average observation	251.8	268.8	283.1	205.9
Average model value	445.3	584.0	371.9	379.4
Normalized bias	499%	175%	62%	230%
Fractional bias	0.59	0.65	0.29	0.64
Normalized error	503%	183%	72%	240%
Fractional error	0.63	0.75	0.41	0.75
r^2	0.28	0.29	0.26	0.08

Table 4-3. Model performance statistics for seasonal precipitation-scaled[a] Hg wet deposition fluxes (μg/m^2).

Performance Measure	Spring	Summer	Autumn	Winter
Average observation	2.54	3.8	2.00	1.19
Average prediction	4.65	6.4	4.96	2.38
Normalized bias	85%	89%	158%	70%
Fractional bias	0.44	0.51	0.8	0.3
Normalized error	98%	93%	158%	90%
Fractional error	0.62	0.56	0.8	0.59
r^2	0.47	0.69	0.69	0.75

[a] Scaled deposition is calculated as: modeled deposition *x* observed precipitation / model precipitation.

Since the precipitation-scaling showed that the largest improvements were obtained for the summer season, we performed a site-by-site comparison of the observed and estimated values for summer. Figures 4-11a and 4-11b show these comparisons for the 59 MDN sites with valid measurements during the summer season. For many of the MDN sites, such as most of the Florida sites, as well as sites in Colorado, British Columbia, New Mexico, Texas, Washington, and Wyoming, the precipitation-scaling results in good agreement between the estimated and observed Hg wet deposition values (in other words, the simulated and observed rainwater concentrations are comparable at these sites). For some sites, the precipitation-scaling results in lower estimated Hg wet deposition fluxes but they are still significantly higher than the observed values. For example, we see that, at most of the Pennsylvania sites, the estimated Hg deposition amounts are more than a factor of 2 higher than the observations,

even after scaling. For 5 sites (AL24 – Bay Road, Alabama; GA40 – Yorkville, Georgia; NB02 – St. Andrews, New Brunswick; PQ05 – Mingan, Quebec; and WI08 – Brule River, Wisconsin), the scaling results in larger discrepancies between the estimated and measured values. However, for the most part, it is clear that reducing the errors in precipitation amounts can result in significant improvements in model performance for wet deposition.

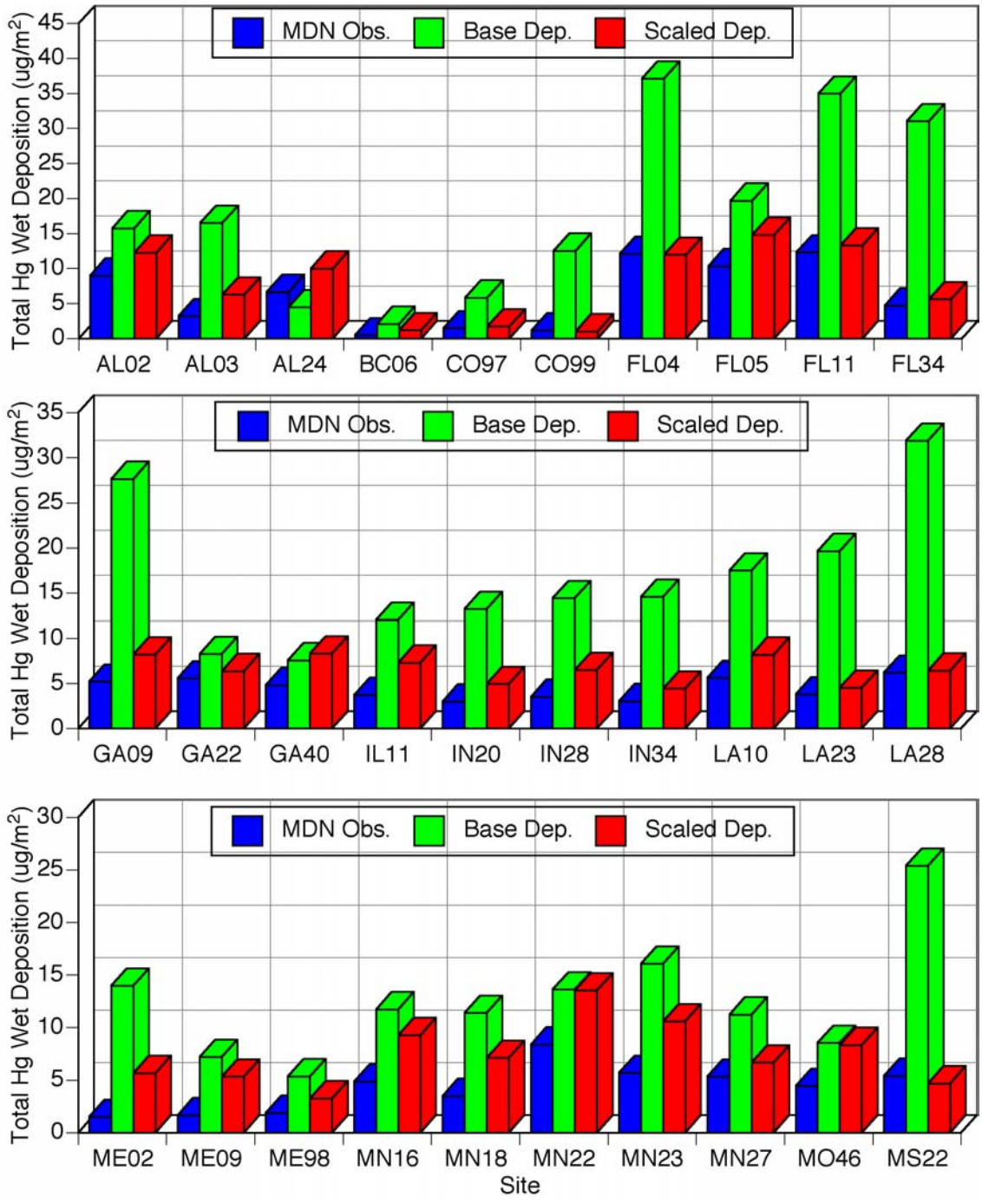

Figure 4-11a. Site-by-site comparison of observed, simulated, and precipitation-scaled simulated Hg wet deposition fluxes for summer 2002 at MDN site locations.

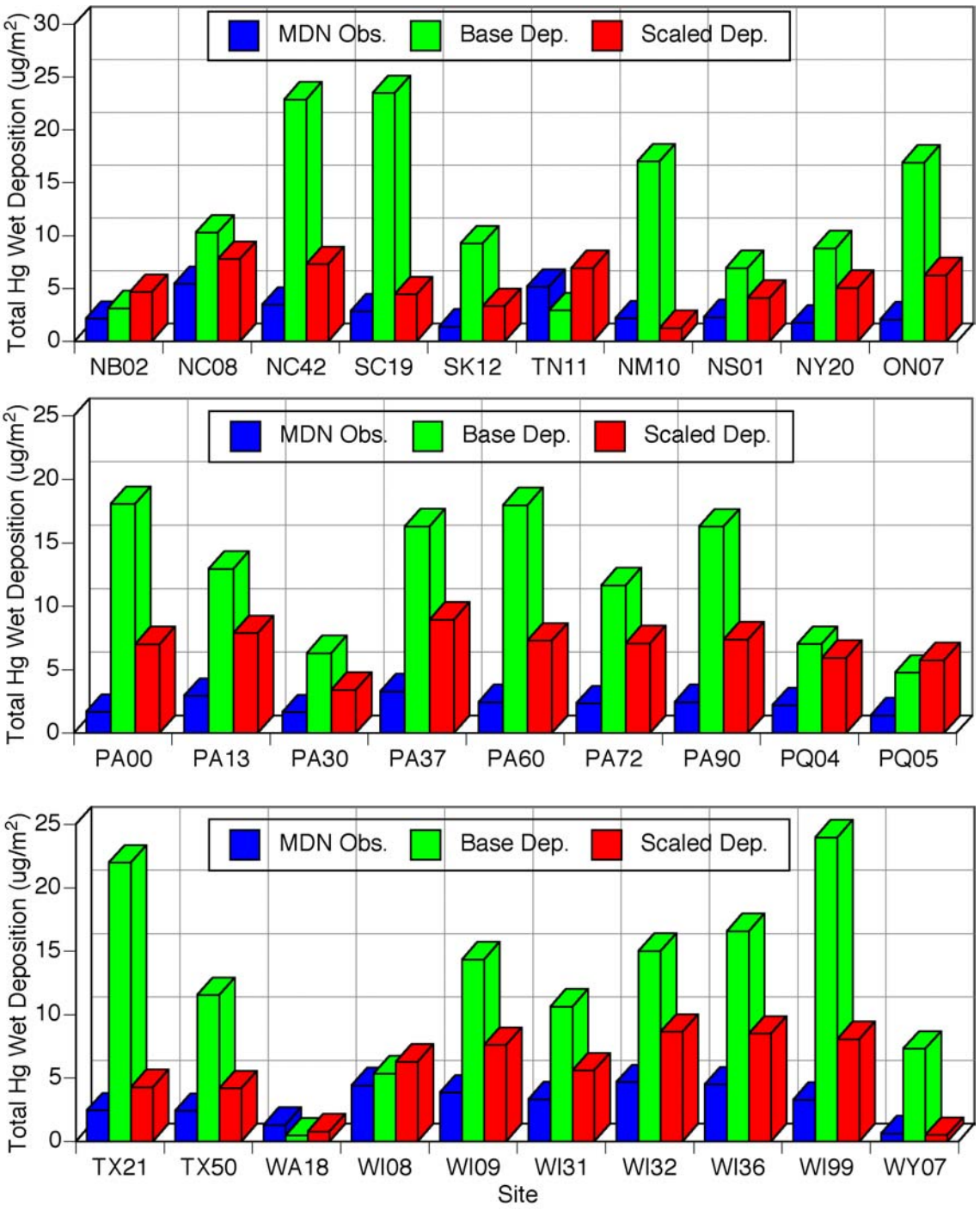

Figure 4-11b. Site-by-site comparison of observed, simulated, and scaled precipitation-scaled simulated Hg wet deposition fluxes for summer 2002 at MDN site locations.

The annual comparisons are shown in Figure 4-12. Figure 4-12a compares the simulated and observed annual Hg wet deposition fluxes at the MDN sites, while Figure 4-12b compares the annual precipitation amounts. Figure 4-12c shows the comparison between observed Hg wet deposition and the precipitation-scaled model estimates. The annual results are qualitatively similar to the seasonal results – the model overpredicts annual Hg wet deposition by about a factor of 3 on average, but the overprediction decreases to less than a factor of 2 when the

simulated wet deposition fluxes are corrected using the observed precipitation amounts. The annual model performance statistics are shown in Table 4-4.

Table 4-4. Model performance statistics for annual Hg wet deposition fluxes (μg/m^2) and precipitation amounts (mm).

Performance Measure	Hg Wet Deposition	Precipitation	Scaled Hg Wet Deposition
Average observation	9.56	995.6	9.56
Average prediction	32.21	1792.7	18.32
Normalized bias	256%	105%	92%
Fractional bias	1.04	0.57	0.58
Normalized error	256%	106%	93%
Fractional error	1.04	0.59	0.59
r^2	0.48	0.27	0.74

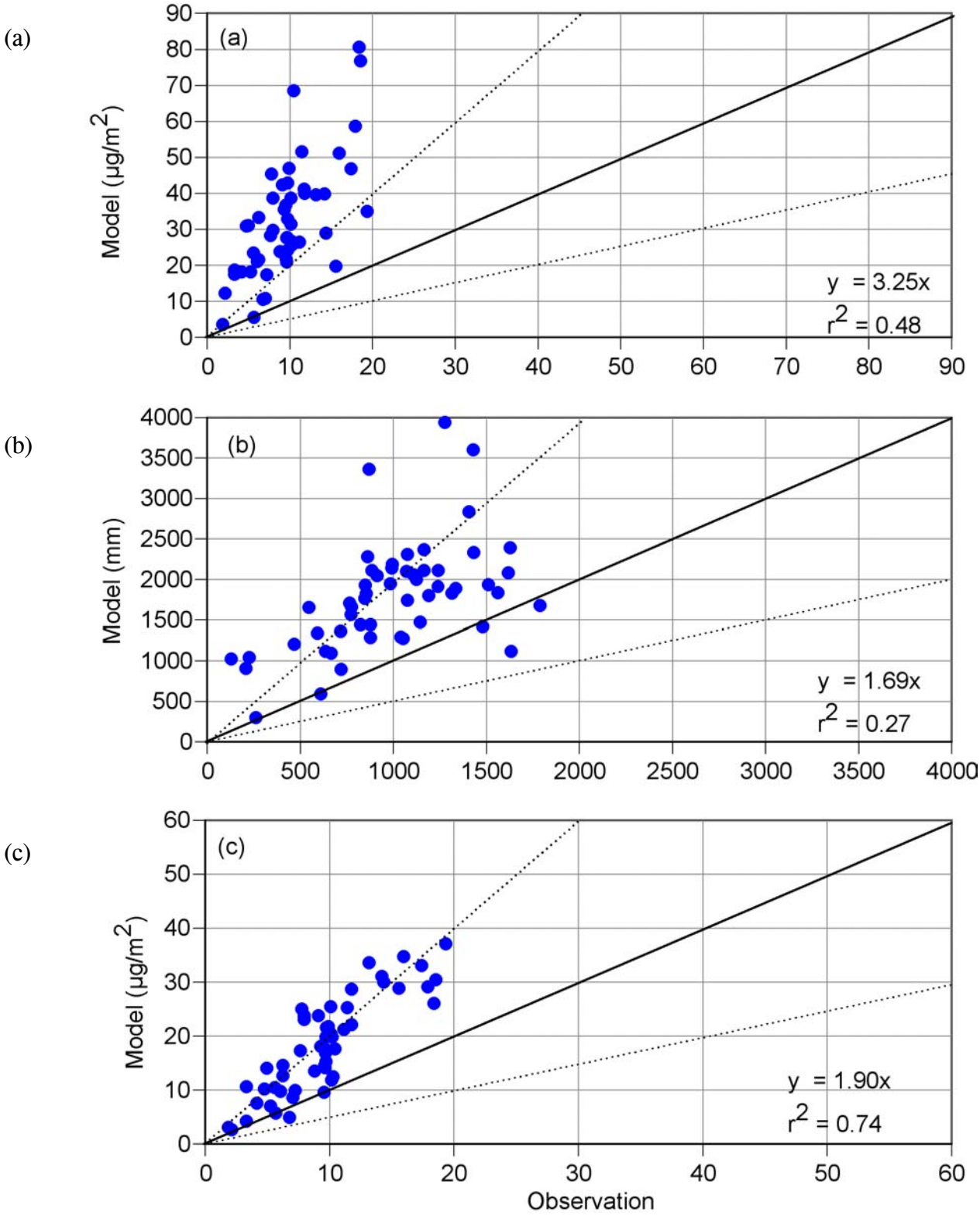

Figure 4-12. Comparison of annual (a) simulated Hg wet deposition fluxes, (b) model precipitation amounts, and (c) precipitation-scaled simulated Hg wet deposition fluxes, with MDN measurements.

Site-by-Site Analysis of Sensitivity Studies

As discussed in the previous section, discrepancies between the observed precipitation amounts and those used in the simulation could not explain all the discrepancies between the observed and estimated Hg wet deposition fluxes. Thus, we conducted a number of sensitivity studies for July 2002 after performing our preliminary evaluation of model performance. These studies were described above and were designed to determine the role of the various processes contributing to the simulated mercury wet deposition.

As in the evaluation of the summer period results above, we performed a site-by-site analysis at the MDN sites reporting valid measurements in July 2002. The results are shown in Figures 4-13a and 4-13b for selected sites from different states (the results for other sites in the same state are qualitatively similar). The figures show the contributions of chemistry, direct emissions of Hg(II), and top and lateral boundary conditions to the Hg wet deposition. In general, chemistry plays an important role in influencing mercury deposition at all the sites. For the Andytown, Florida site (FL04), the contribution of chemistry is larger than the combined contributions of direct Hg(II) emissions and the top and lateral boundary conditions. However, there are many sites (e.g., CO99 – Mesa Verde National Park; IL11 – Bondville, Illinois; MN16 – Marcell Experimental Forest, Minnesota; WI09 – Popple River) for which the combined contributions of the top and lateral boundary conditions are comparable to or larger than the chemistry contributions. At many of these sites, the top boundary condition appears to play a more important role than the lateral boundary conditions.

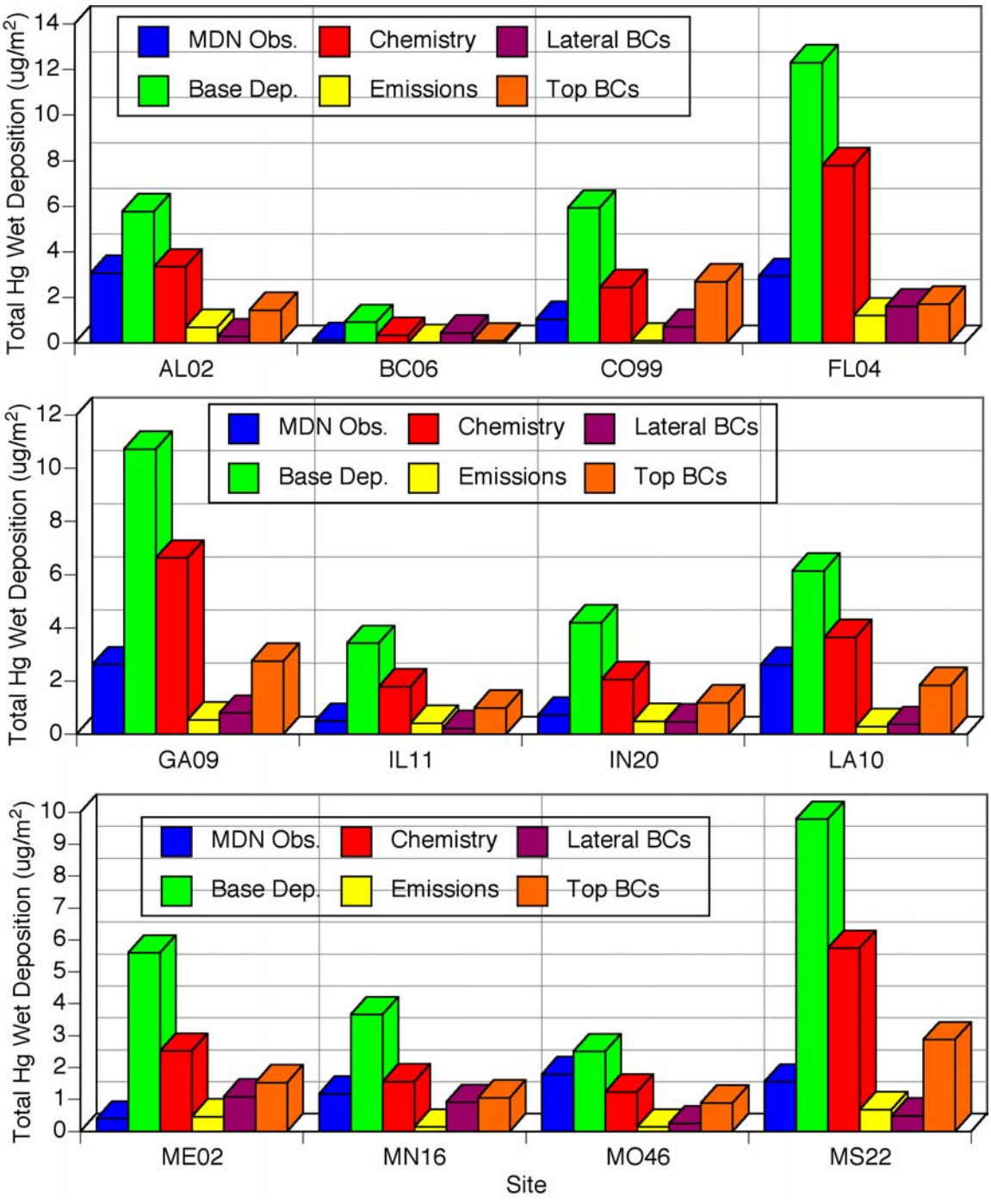

Figure 4-13a. Site-by-site comparison of observed, simulated, and process contributions to simulated Hg wet deposition fluxes for July 2002 at selected MDN site locations.

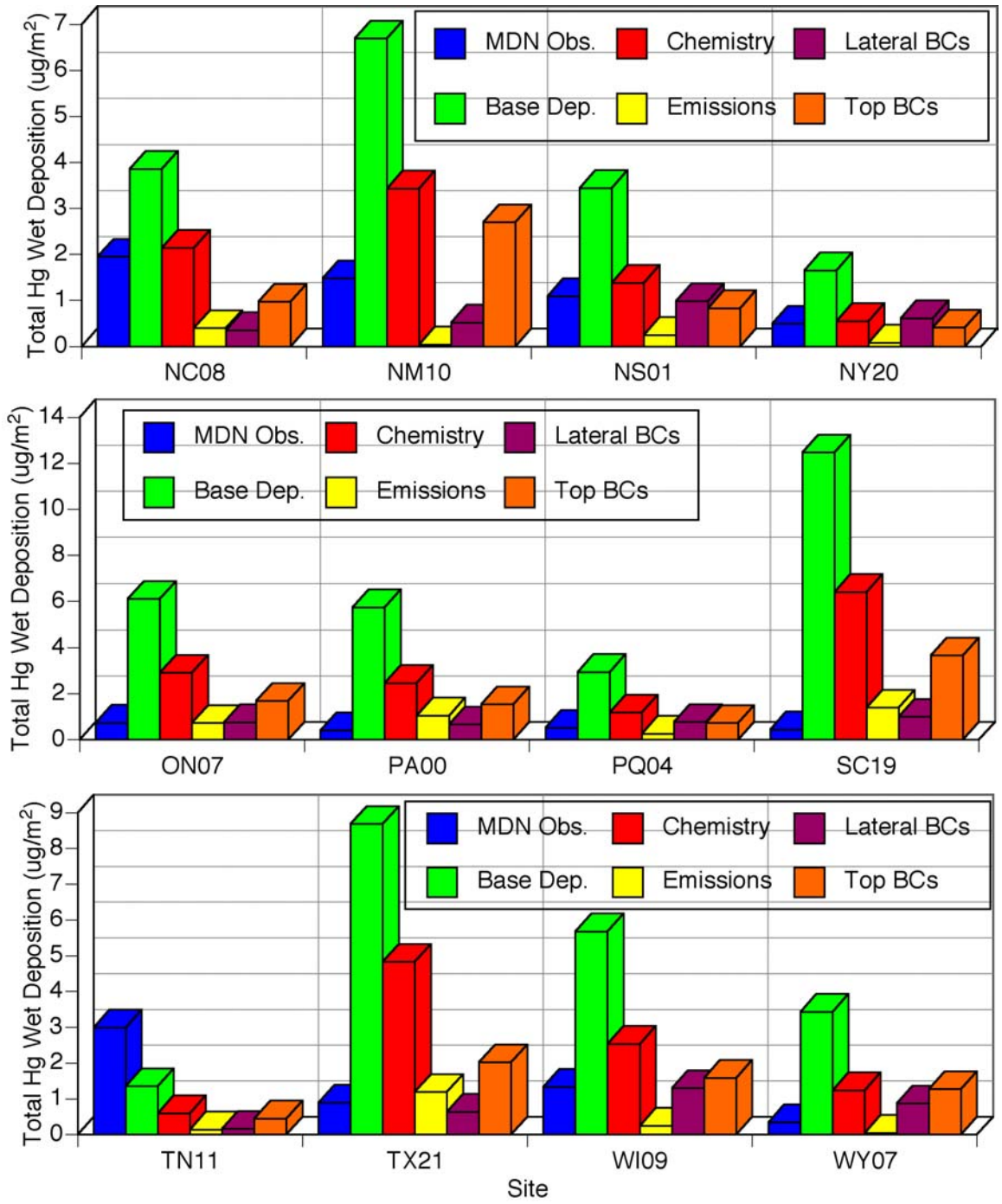

Figure 4-13b. Site-by-site comparison of observed, simulated, and process contributions to simulated Hg wet deposition fluxes for July 2002 at selected MDN site locations.

The large sensitivity to the top boundary conditions suggests that it may be necessary to examine these values carefully as well as the role of vertical processes in transporting pollutants from above the modeling domain. It is possible that a large part of the remaining discrepancies (after precipitation-scaling, discussed in the previous section) between the simulated and measured Hg wet deposition fluxes at the MDN sites can be attributed to inaccuracies in the specification or treatment of the top boundary conditions.

As discussed in Section 2, current treatments of Hg chemistry (including the treatment implemented in CAMx) do not account for the apparent reduction of Hg(II) to Hg(0) in power plant plumes that has been inferred from various experimental studies. This may account for some of the overpredictions at sites directly downwind of power plants, such as the MDN sites in Pennsylvania. Similar results have been obtained in previous regional mercury modeling studies (e.g., Seigneur et al., 2003e).

MODELED RAINFALL

Comparison of predicted and observed rainfall at the MDN sites showed that the modeled rainfall was over-predicted and that this caused a large positive bias in the modeled mercury deposition. Precipitation data are output by the MM5 in two forms: (1) 3-dimensional instantaneous precipitation content (g/m^3), and (2) surface accumulated precipitation rate (mm/hr) in liquid water equivalent. The MM5 surface precipitation has the advantage of comparability to observations since it directly provides the surface precipitation rate and includes both resolved and sub-grid scale precipitation. However, the surface accumulated precipitation provides no information on the vertical extent profile of precipitation rate as needed for the wet deposition calculation in a 3-D model. The MM5 3-D instantaneous precipitation amount has the advantages of providing 3-D information and consistency between the 3-D distributions of precipitation and clouds. However, the 3-D MM5 output provides precipitation amount (g/m^3) rather than precipitation rate (mm/hr) and does not include sub-grid scale precipitation.

The wet deposition scheme implemented in CAMx version 4 was designed to preserve consistency with the 3-D location of clouds and precipitation between CAMx and the meteorological model (MM5). This is done by using the 3-D instantaneous precipitation (and cloud water) content output by MM5 rather than the surface accumulated rainfall amount. Consequently, the liquid precipitation rate must be diagnosed from the precipitation content via droplet diameters and fall speeds. The mean raindrop diameter and fall speed are derived from the empirical relationships of Scott (1978) as described in the CAMx User's Guide (ENVIRON, 2003). Because the precipitation rate is diagnosed in CAMx from the precipitation amount, the surface precipitation rate in CAMx may not be the same as in the 2-D surface output from MM5.

The MM5 surface precipitation and the CAMx diagnosed surface precipitation are compared in Figures 4-14 and 4-15 for the first and third quarters of 2002, respectively. The MM5 surface precipitation figures were prepared by WDNR directly from the MM5 2-D surface output. The CAMx surface precipitation figures were prepared from the surface layer of the MM5 3-D precipitation amount using the diagnostic equations implemented in CAMx. There is good agreement in the spatial distributions of rainfall in both winter and summer. The largest differences occur in winter in the north of the modeling domain (e.g., British Columbia, Ontario and Quebec) and at high elevations (e.g., the Cascades, Rockies and Sierra Nevada mountains) where precipitation is frequently frozen. The CAMx equations for diagnosing liquid precipitation rate from precipitation amount are overestimating when the precipitation is frozen because snow falls more slowly than rain. The CAMx equations for diagnosing precipitation rate also overestimate the precipitation in the summer for areas with very high rainfall (e.g., Florida and the Gulf of Mexico). The MM5 output and CAMx

diagnosed precipitation are in much better agreement for areas with moderate precipitation in the summer and in the southern part of the domain in winter. These patterns suggest that the CAMx equations for diagnosing precipitation rate work reasonably well for moderate rainfall events but over- predict precipitation for intense rainfall and when precipitation is frozen.

(a)

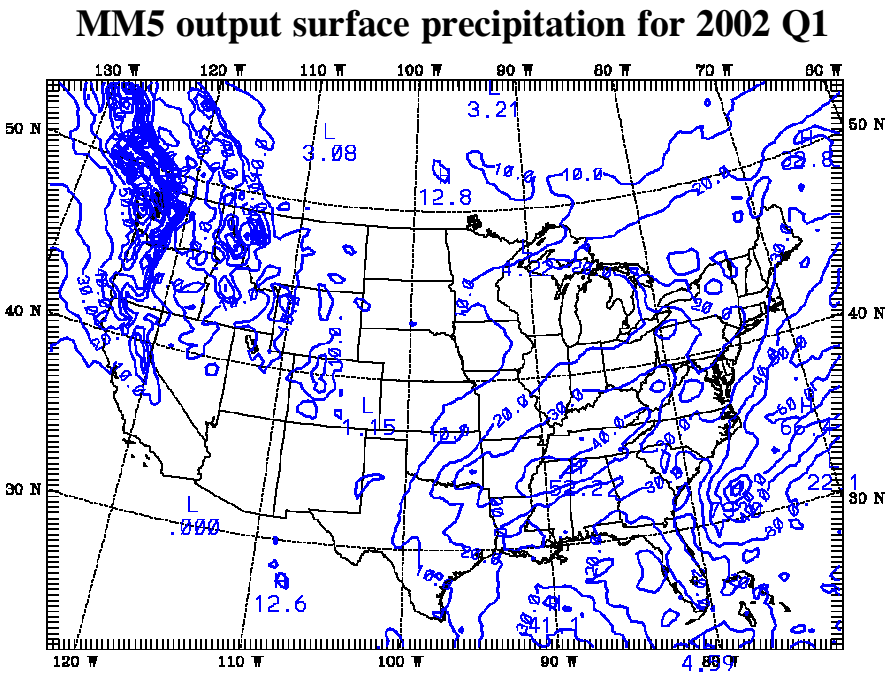

(b)

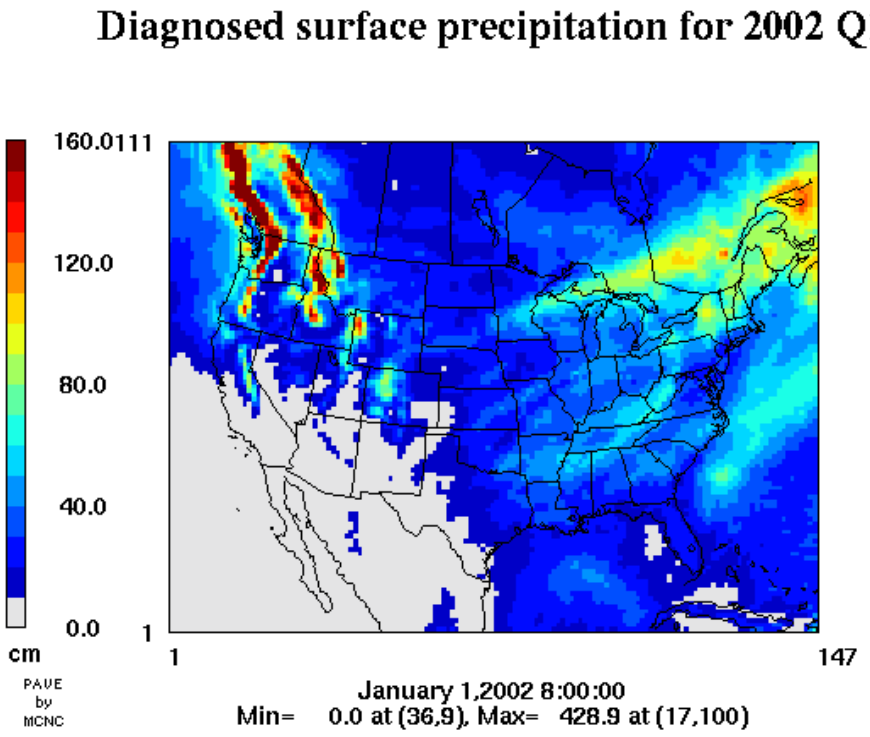

Figure 4-14. Comparison of modeled cumulative precipitation (cm) for 2002 Q1 (January – March) (a) MM5 surface 2-D output and (b) surface precipitation diagnosed from MM5 3-D output.

(a)

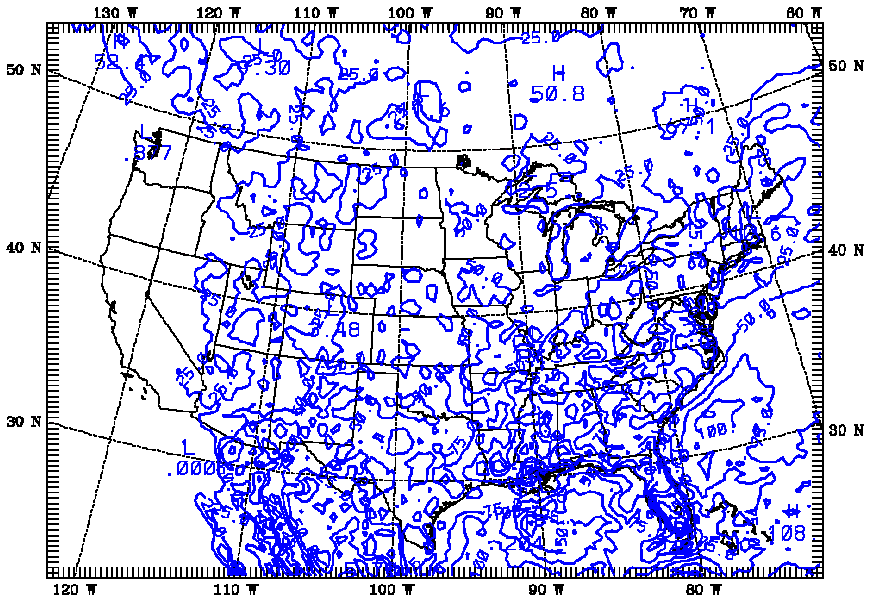

(b)

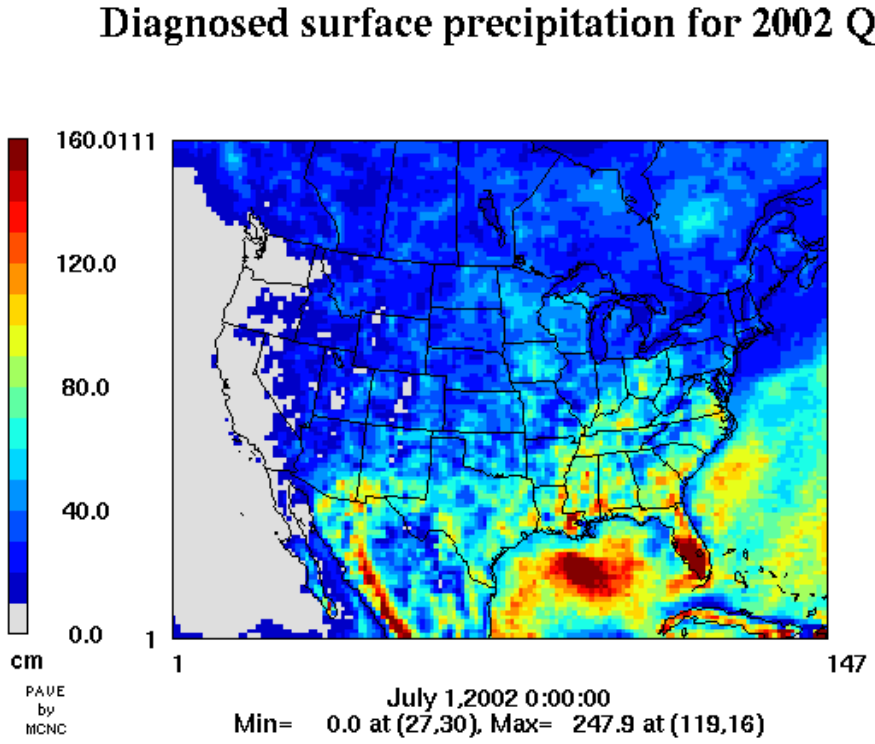

Figure 4-15. Comparison of modeled cumulative precipitation (cm) for 2002 Q3 (June – August) (a) MM5 surface 2-D output and (b) surface precipitation diagnosed from MM5 3-D output.

The CAMx wet deposition algorithm does not model wet deposition in frozen precipitation, but the cut point for frozen precipitation was set at 268 K to allow for super-cooling. Distinguishing between the fraction of liquid and frozen precipitation from MM5 is not possible with the "simple ice" scheme because only the total precipitation is reported. Many studies use the "simple ice" scheme in MM5 for air quality purposes because it is much faster than alternative MM5 options with full microphysics. When liquid and frozen precipitation must be distinguished based on temperature it probably would be better to use a threshold of 273k to avoid counting snowfall as rain.

The over-predicted surface precipitation is related to several factors. The major factor is the approach that was used to derive the CAMx liquid precipitation rate from the MM5 output data. A related factor is the difficulty in distinguishing between liquid and frozen precipitation from MM5 when the MM5 "simple ice" scheme is used that reports only the total precipitation as liquid. Less important in this study, but still a significant issue, is the level of spatial and temporal agreement between the predicted and observed precipitation.

The recommended approach to improving the calculation of mercury wet deposition is to provide a simpler wet deposition approach in CAMx so that calculations can be based on the predicted surface rainfall rate or interpolated surface observations. A simpler surface precipitation-driven wet scavenging algorithm is likely to improve the wet deposition amounts but will lead to less consistency between the locations of clouds and rain than in the current scheme. The surface precipitation-driven wet scavenging algorithm could be implemented as an option alongside the existing algorithm. Separately, the diagnosis of precipitation rate from precipitation amount should be refined for the current CAMx wet deposition algorithm to better account for frozen precipitation and intense rain.

OZONE COMPARISON FOR JUNE 2002

The chemical mechanism for mercury implemented in CAMx depends upon the levels of several atmospheric oxidants for calculating the rate of oxidation of HG0 to HG2. We performed a qualitative comparison of modeled ozone levels for June 2002 to evaluate whether the modeled oxidant levels over the continental US were reasonable for summer conditions. For observed ozone, we used the maps of interpolated ozone levels prepared by EPA for the "Air Now" web site (http://www.epa.gov/airnow/). We selected EPA's maps of interpolated daily maximum 1-hour ozone, rather than 8-hour ozone, because a quantitative ozone scale is provided only for the 1-hour maps. The WDNR plotted the CAMx predicted daily maximum 1-hour ozone levels for every day in June 2002 using a color scale that matched the Air Now maps. The modeled and observed ozone levels are compared in Figure 4-16 for days at the beginning, middle and end of June 2002. The modeled and observed maximum ozone levels show reasonable agreement on the spatial distributions of moderately high ozone levels (above 60 ppb). There is less good agreement for higher ozone levels (above 100 ppb) that are more localized. The model performance for ozone was limited by having seasonal emission inventories that are less representative than the day specific inventories normally used for ozone modeling. Overall, the agreement for ozone was reasonable and is suitable for supporting mercury deposition modeling.

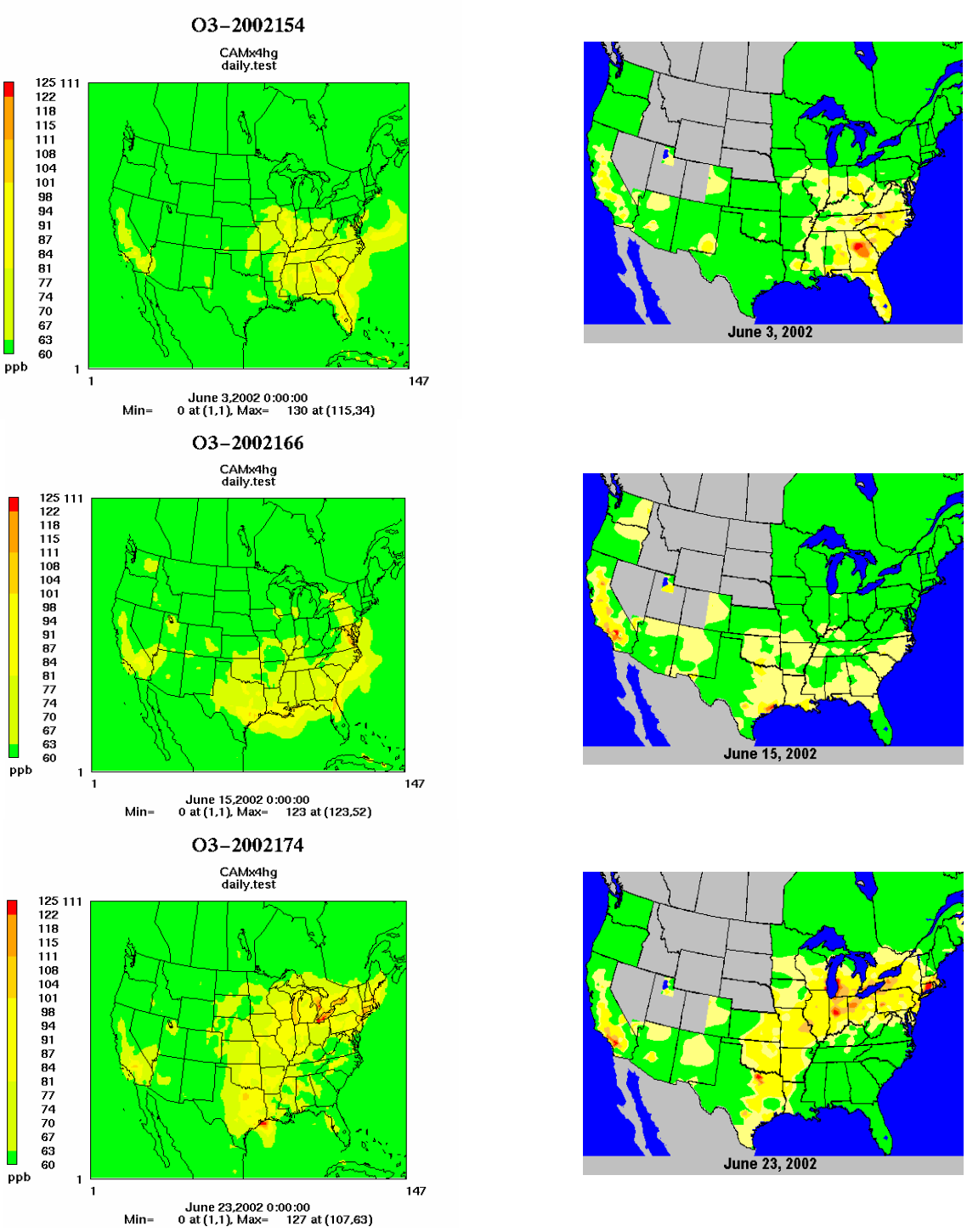

Figure 4-16. Comparison of modeled (left) and interpolated observations (right) daily maximum 1-hour ozone for June 3, June 15 and June 23, 2002.

PARTICULATE MATTER DEPOSITION

A qualitative evaluation of deposition for several particulate matter (PM) species was performed to support the mercury deposition evaluation. Annual wet deposition maps for sulfate, nitrate and ammonium are prepared by the National Acid Deposition Program (NADP) and made available at http://nadp.sws.uiuc.edu/. In order to reveal seasonal variations in wet deposition, we prepared similar maps using the NADP seasonal data for 2002 (NADP/NTN, 2003). The maps of observed wet deposition were prepared by spatially interpolating the observed data using the Kriging algorithm in the Golden Software Surfer program, version 7. ENVIRON developed the methodology for preparing the seasonal observed wet deposition maps and then the WDNR prepared the maps shown in this report. The WDNR also prepared corresponding deposition maps for the model results. The observed and predicted wet depositions for sulfate, nitrate and ammonium are shown for spring, fall, summer and winter in Figures 4-17 – 4-28.

The observed and modeled sulfate wet deposition maps (Figures 4-17 – 4-20) generally show higher values in the eastern US and lower values in the western US over all seasons. In the spring, sulfate deposition is highest through the Ohio River valley to western New England. The modeled distribution is similar, but the deposition amounts are generally lower. In the summer, sulfate deposition is high in the upper Ohio River valley to western New England as well as FL and near New Orleans. The modeled distribution does not show the same high values and is consistently lower than the observed sulfate deposition. In the fall, the observed sulfate deposition maximums are lower than in either the spring or summer, but in contrast, the modeled maximum is highest in the fall. Apart from this modeled fall maximum in KY/TN, the modeled sulfate deposition tends to be lower than the observed values and has a fairly similar distribution. In the winter, sulfate deposition is highest from TX through the Ohio River valley to western New England. The modeled maximums are displaced to the east and are lower. Both the observations and model results show some locally elevated sulfate deposition along the Pacific Northwest coast in winter. Overall, the modeled sulfate deposition tends to be lower than observed.

The observed and modeled nitrate wet deposition maps (Figures 4-21 – 4-24) generally show higher values in the eastern US and lower values in the western US over all seasons. In the spring, the observed nitrate deposition has several local maximums through the Ohio River valley and PA to western New England. The modeled distribution is generally similar but has higher values over a wider area and has too high a peak in the Ohio River valley. In the summer, the observed nitrate deposition is highest in MN/WI, FL, the New Orleans area and western PA. The modeled nitrate deposition has highs in these areas, but also has highs in TX, the plains, the lower Midwest and the Northeast seaboard that are much higher than the observed values. In the fall, the highest nitrate deposition is observed in PA and NY and there are several smaller highs across the eastern US. The modeled fall nitrate deposition is generally higher than observed across most of the eastern US. In the winter, nitrate deposition is highest near the lower Ohio River valley, the Great Lakes and Salt Lake City. The model results under predict some of these high values but generally over predict winter nitrate deposition across the eastern US. The model results for winter show elevated nitrate deposition in the Pacific Northwest and Northern CA that was not observed. Overall, the modeled nitrate deposition tends to be higher than observed.

The observed ammonium wet deposition maps (Figures 4-25 – 4-28) generally show higher values in spring and summer and lower values in fall and winter. The modeled deposition shows less seasonal variation and is generally is much lower than observed. The highest regional ammonium deposition levels occur in MN/WI in the summer and the model results show a similar feature but with much lower levels. Overall, the modeled ammonium deposition tends to be much lower than observed.

In summary, the seasonal deposition results for sulfate/nitrate/ammonium show only limited agreement with the observations for 2002. The overall trends are over prediction of nitrate, under prediction of sulfate and large under prediction of ammonium wet deposition. The over prediction tendency for nitrate is in the same direction as for mercury, discussed above, and over predicting the precipitation may be a factor for nitrate as well as mercury. It was shown above that boundary conditions were not important to the modeled nitrate deposition. The under prediction tendencies for sulfate and ammonium are in the opposite direction to mercury suggesting sources of bias other than precipitation for sulfate and ammonium deposition. Uncertainties in the ammonia inventory will influence ammonium deposition and, to a lesser extent, the sulfate and nitrate deposition. The ammonia inventory for this study had only limited seasonal variation because spring and fall were estimated as the average of summer and winter.

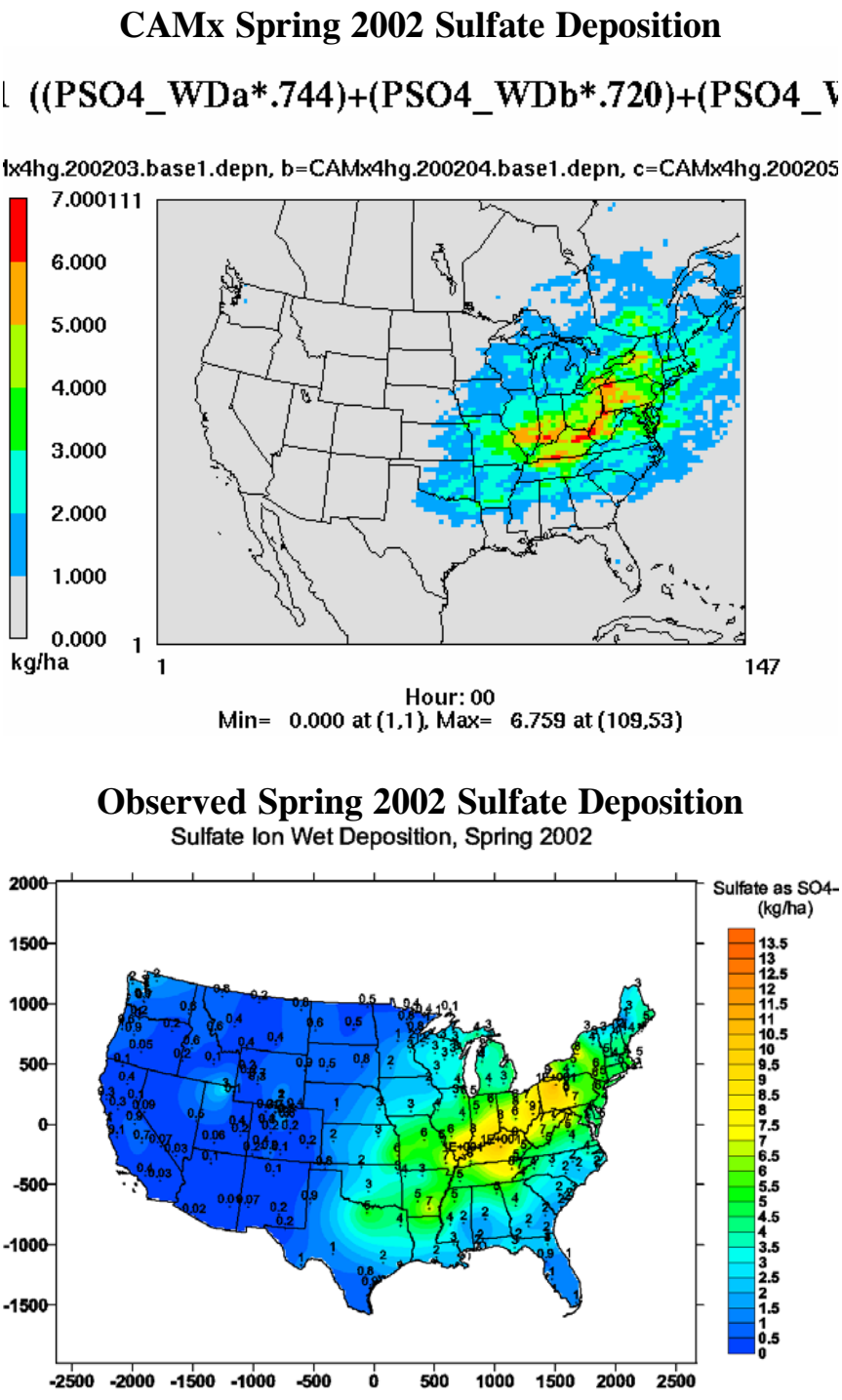

Figure 4-17. Observed and predicted sulfate wet deposition (kg/hectare) for spring 2002.

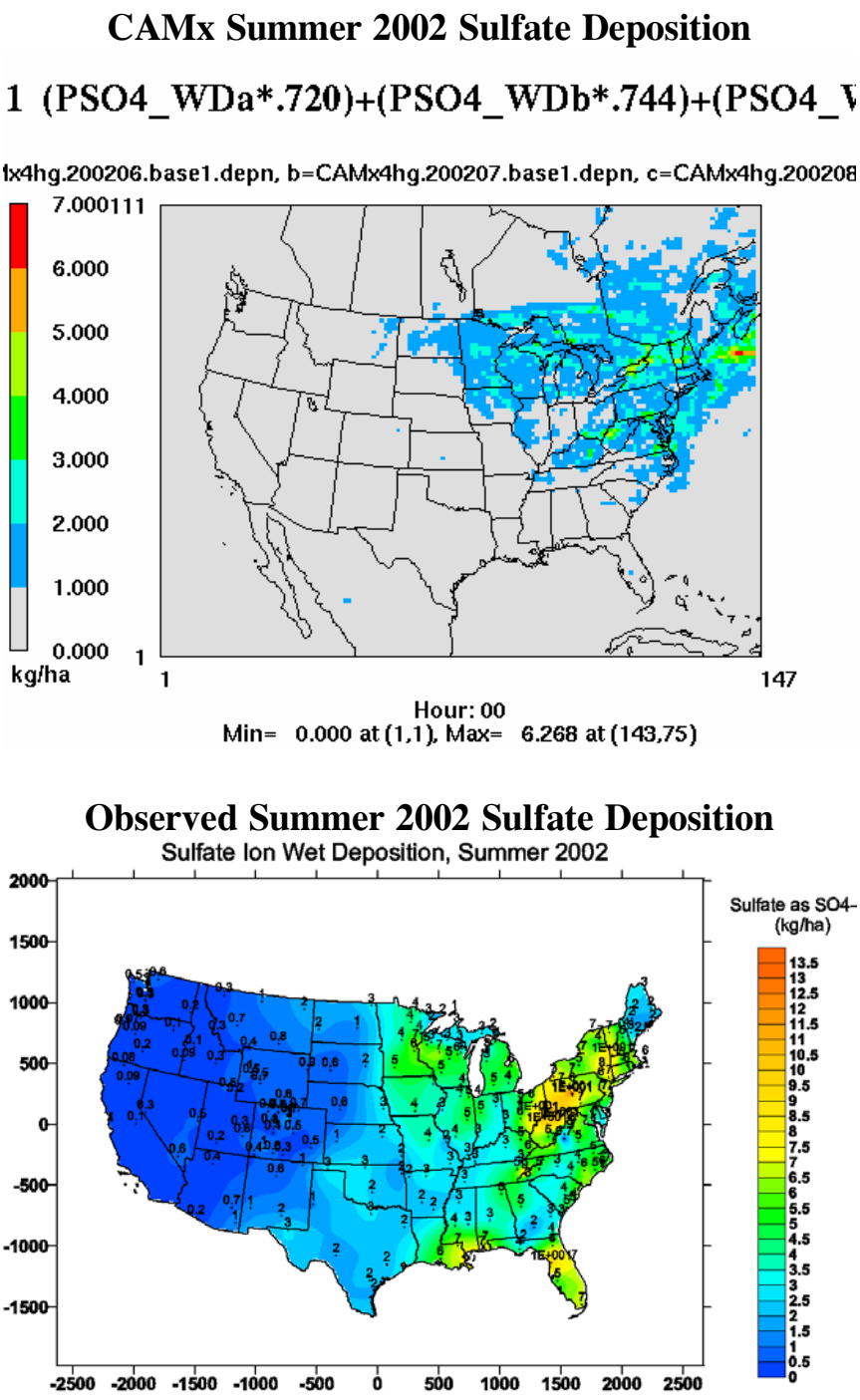

Figure 4-18. Observed and predicted sulfate wet deposition (kg/hectare) for summer 2002.

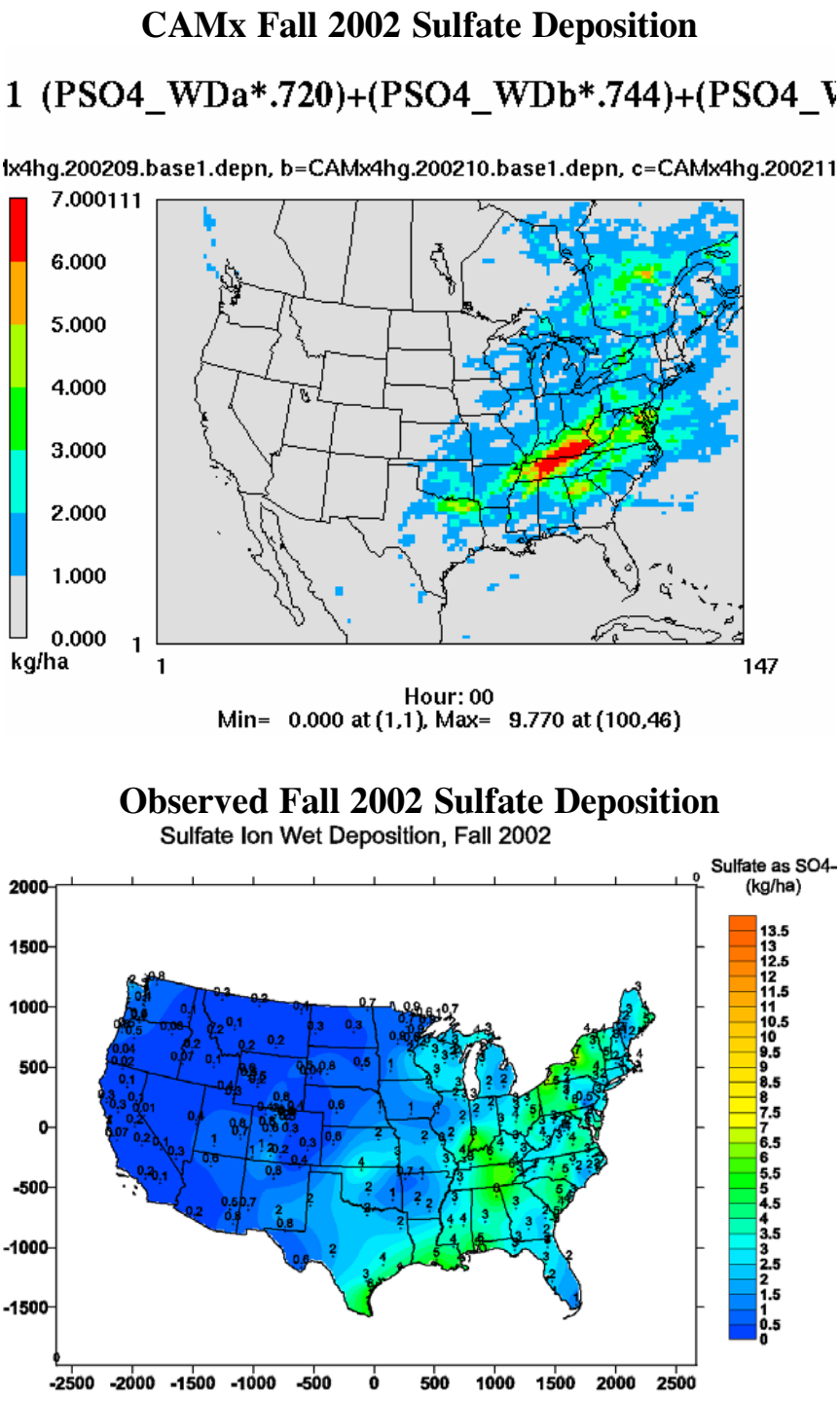

Figure 4-19. Observed and predicted sulfate wet deposition (kg/hectare) for fall 2002.

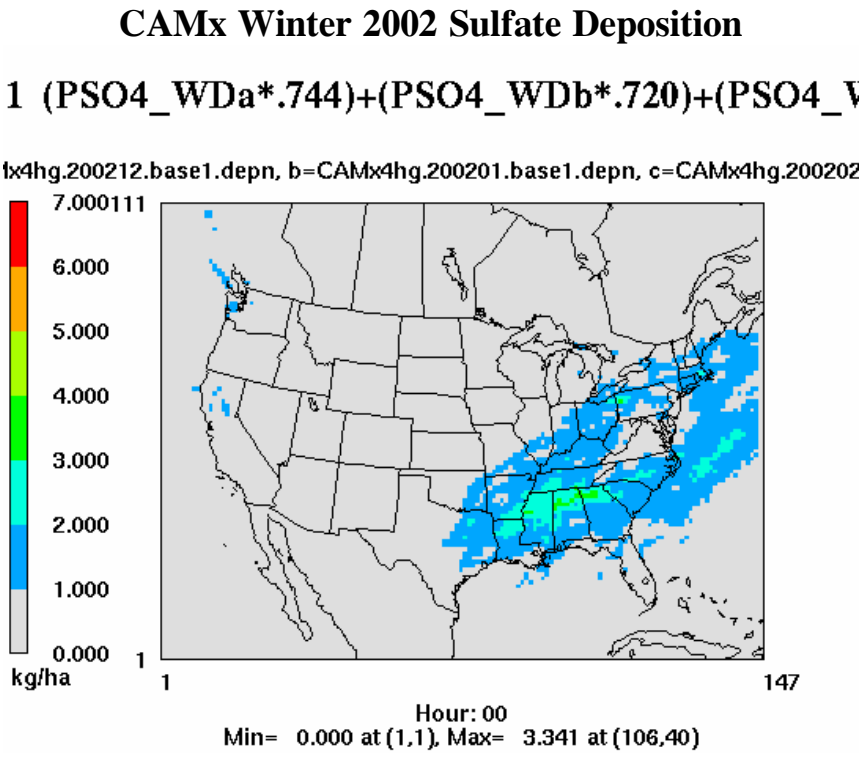

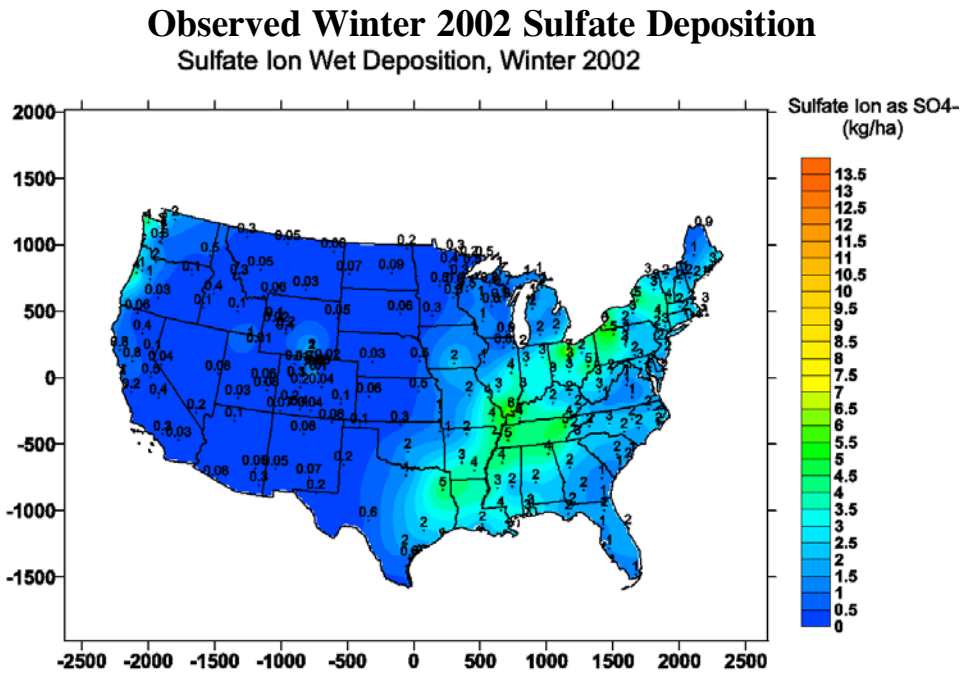

Figure 4-20. Observed and predicted sulfate wet deposition (kg/hectare) for winter 2002.

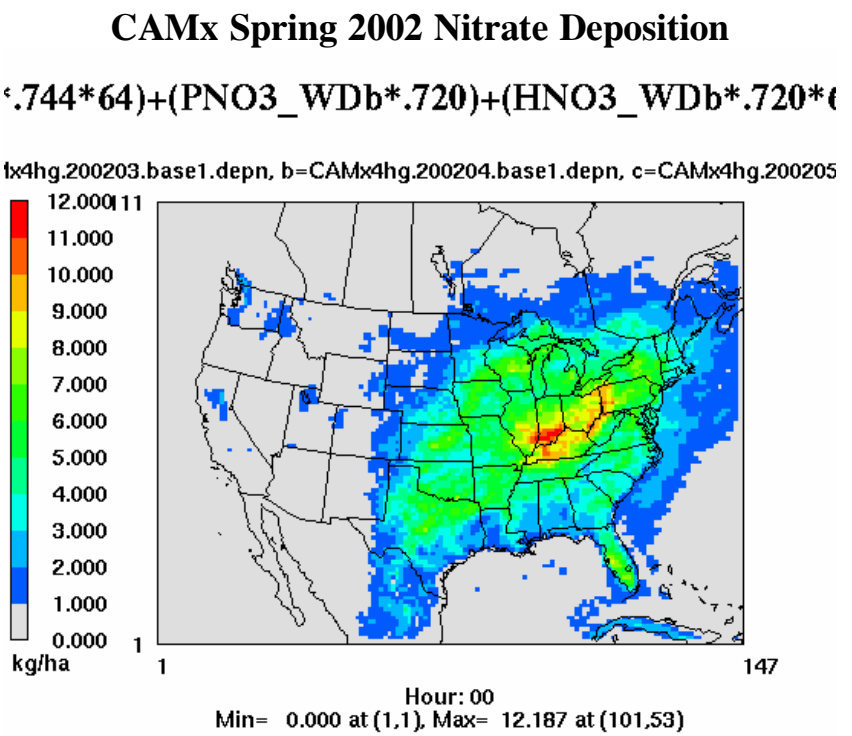

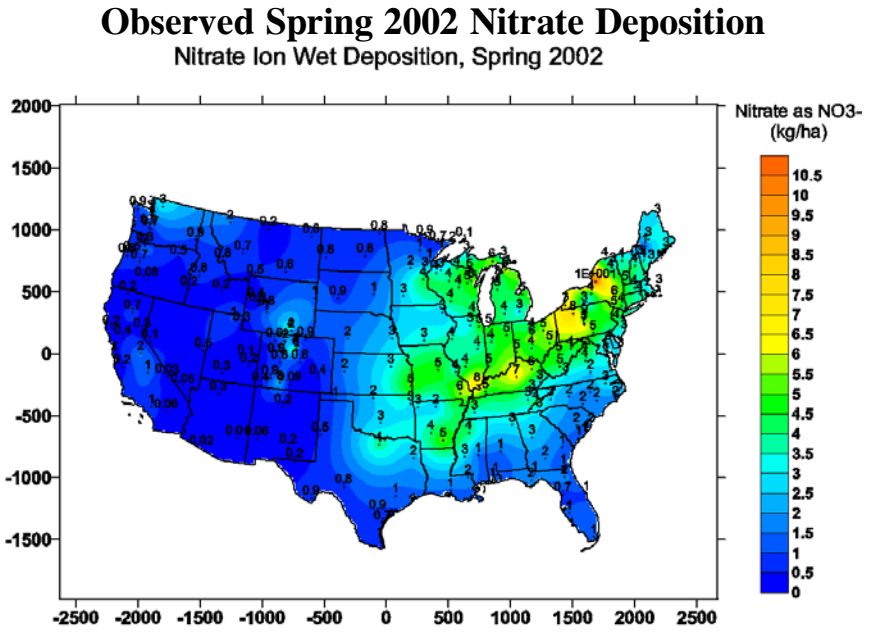

Figure 4-21. Observed and predicted nitrate wet deposition (kg/hectare) for spring 2002.

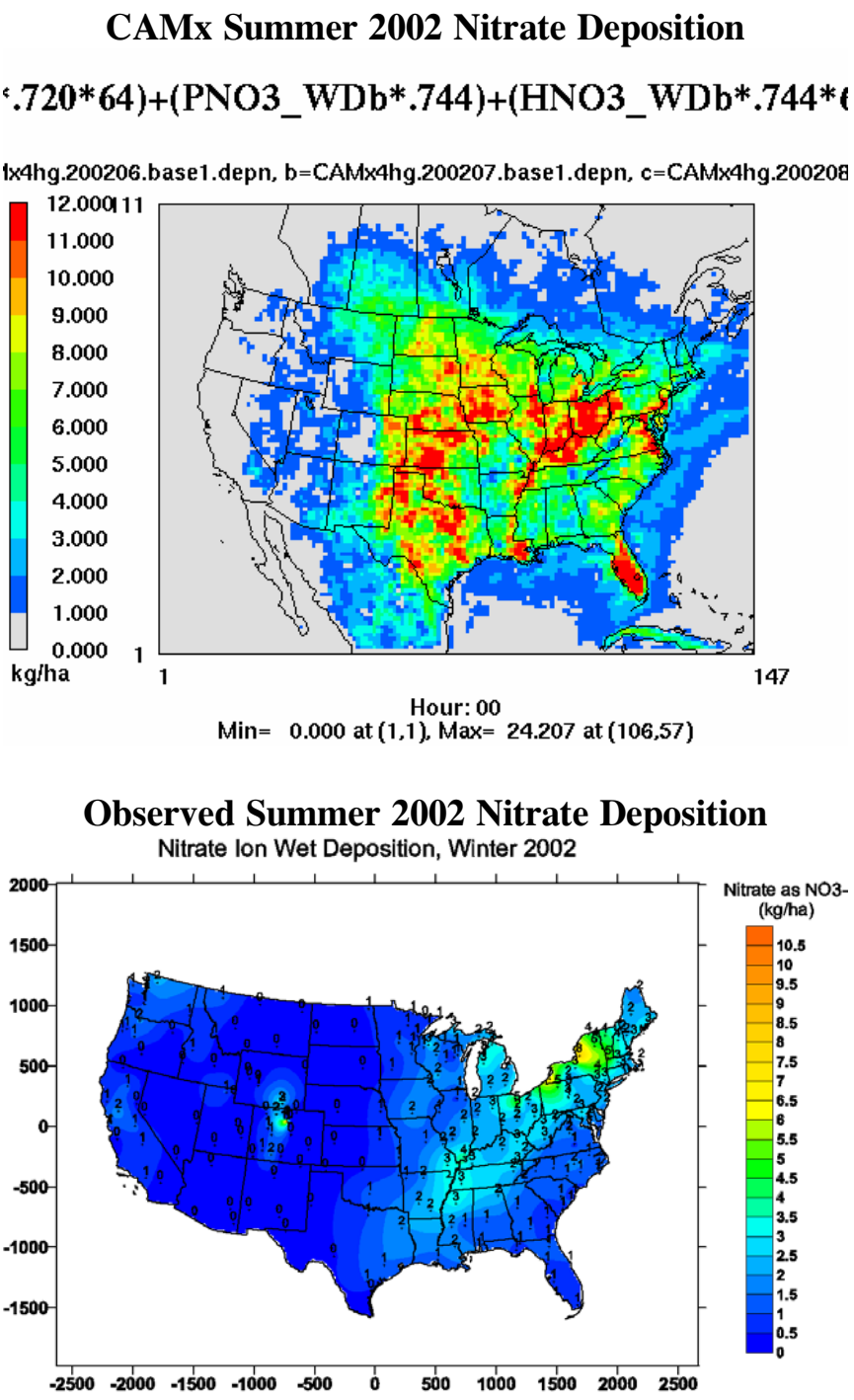

Figure 4-22. Observed and predicted nitrate wet deposition (kg/hectare) for summer 2002.

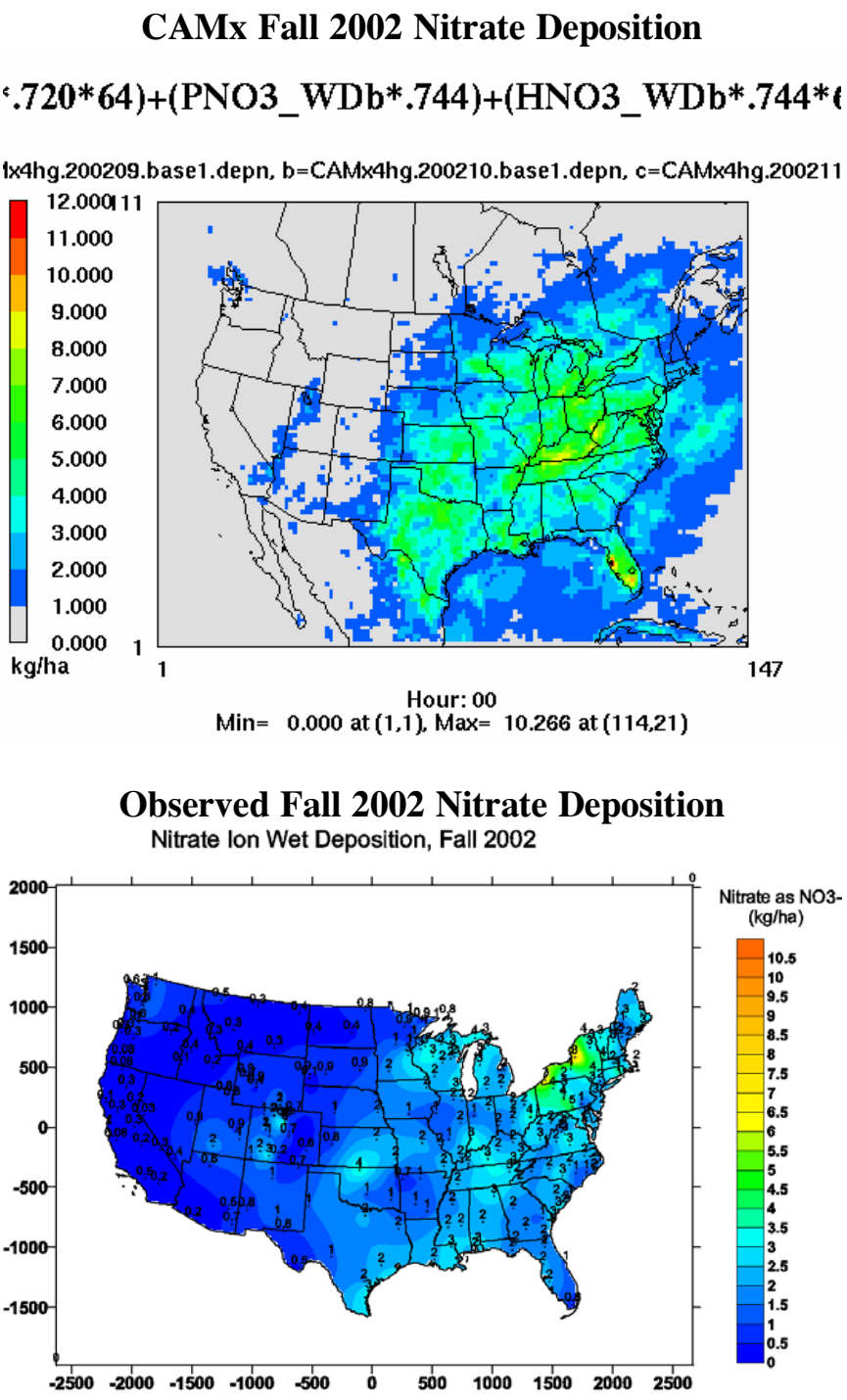

Figure 4-23. Observed and predicted nitrate wet deposition (kg/hectare) for fall 2002.

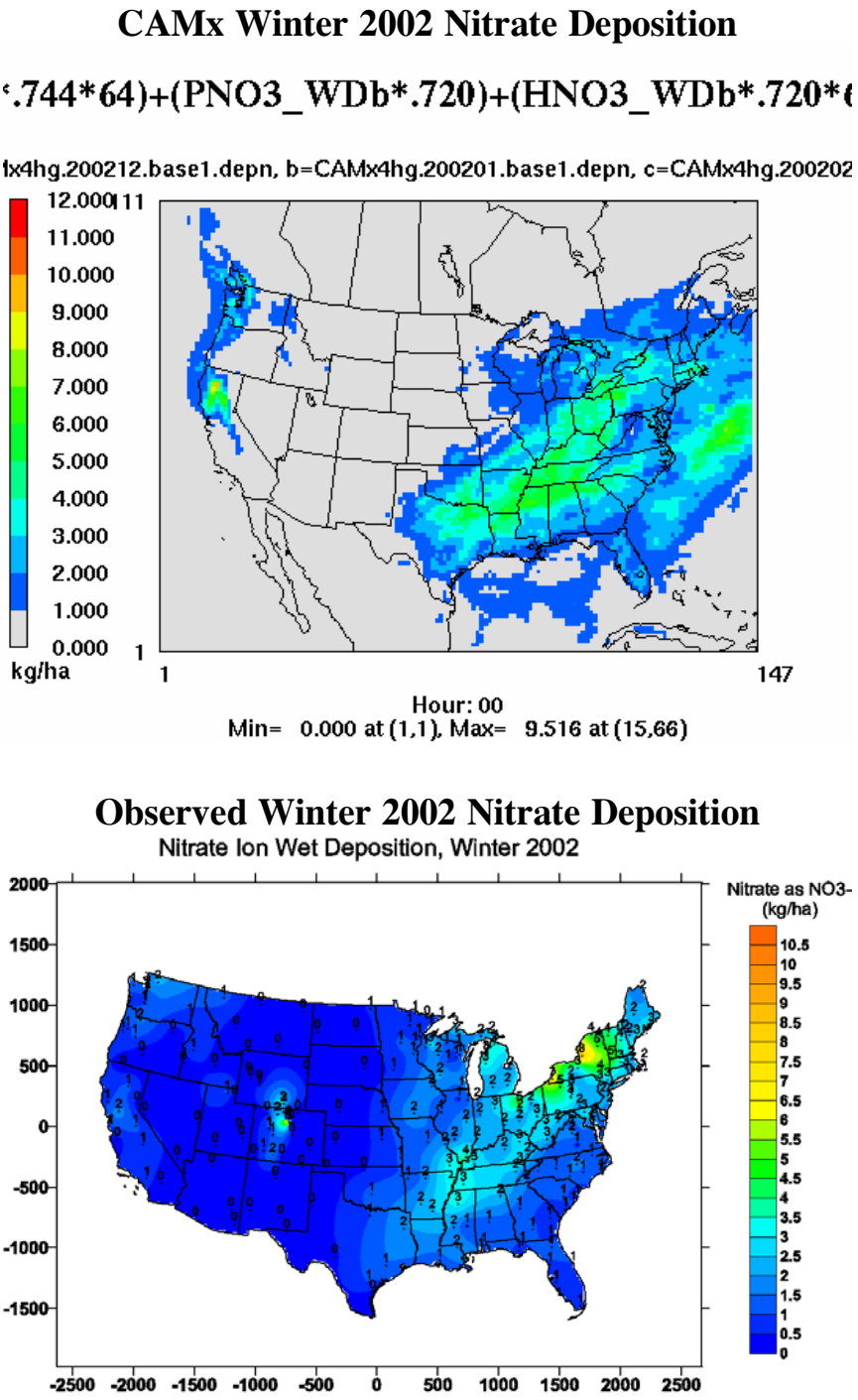

Figure 4-24. Observed and predicted nitrate wet deposition (kg/hectare) for winter 2002.

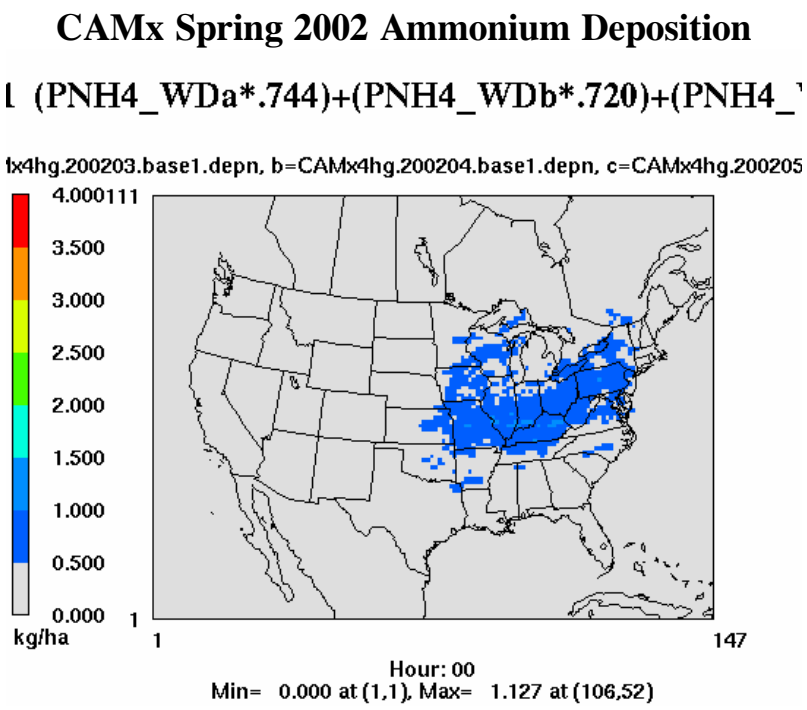

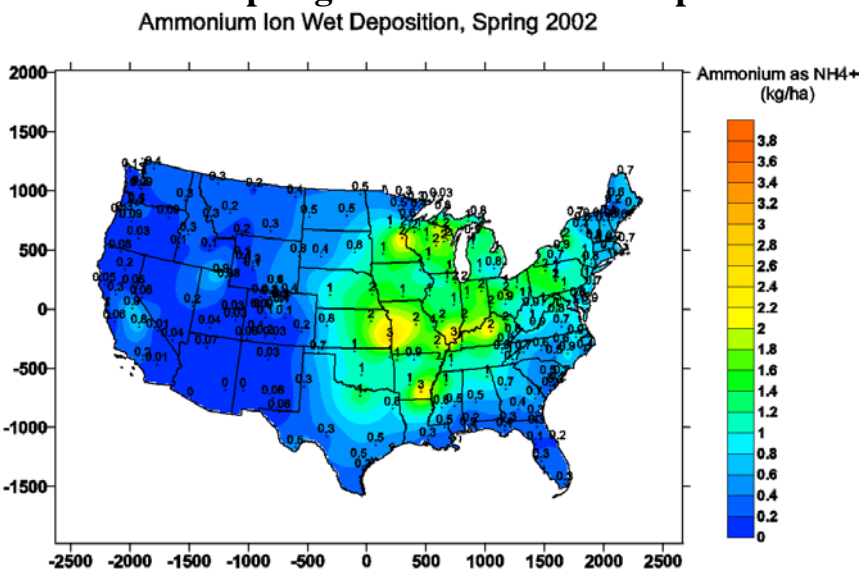

Figure 4-25. Observed and predicted ammonium wet deposition (kg/hectare) for spring 2002.

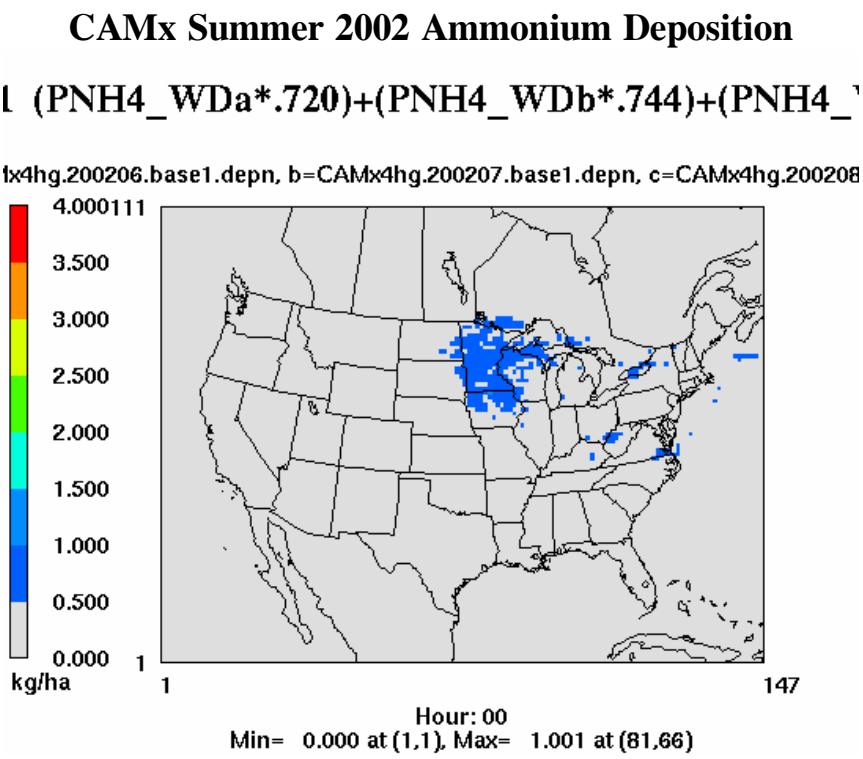

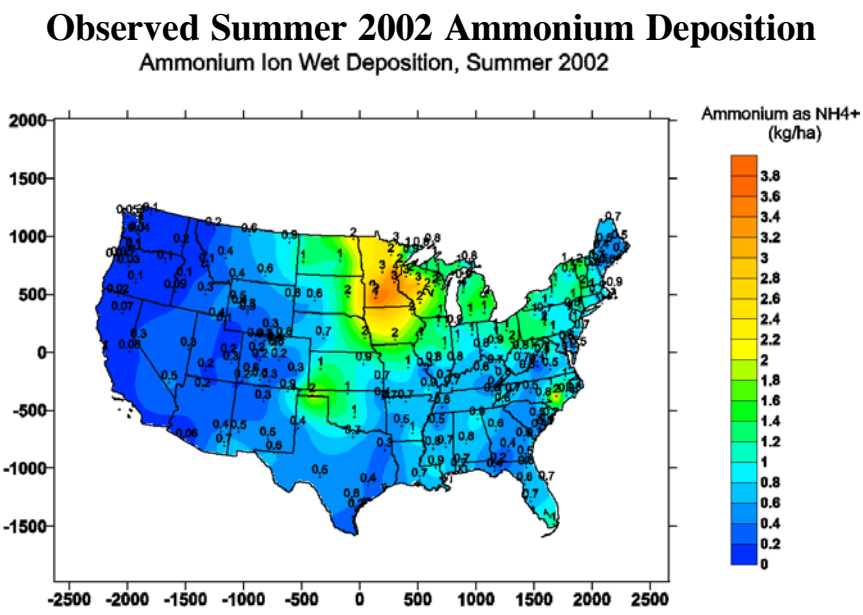

Figure 4-26. Observed and predicted ammonium wet deposition (kg/hectare) for summer 2002.

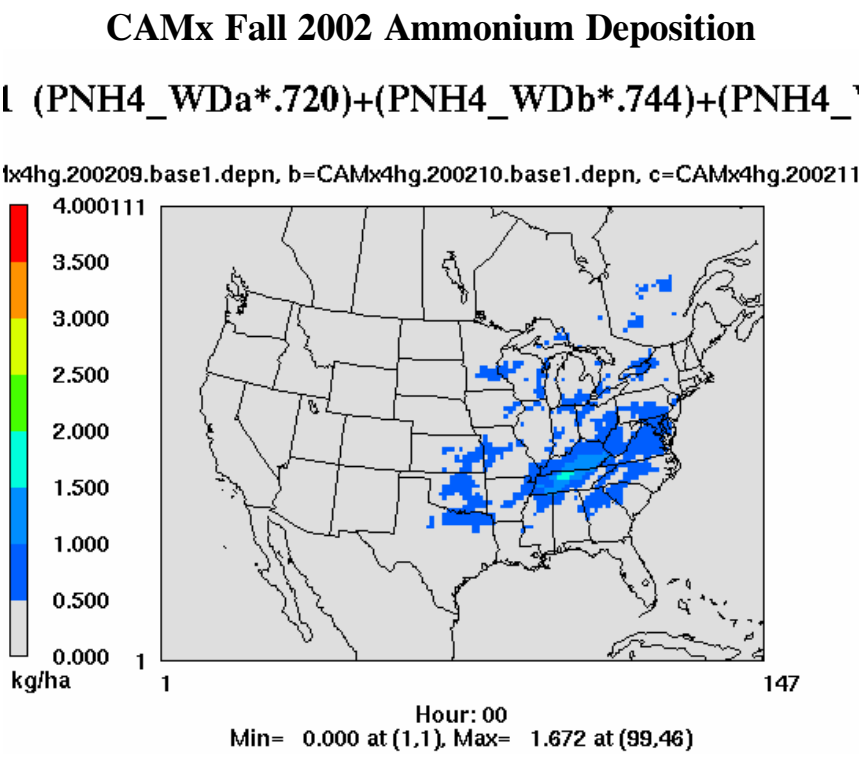

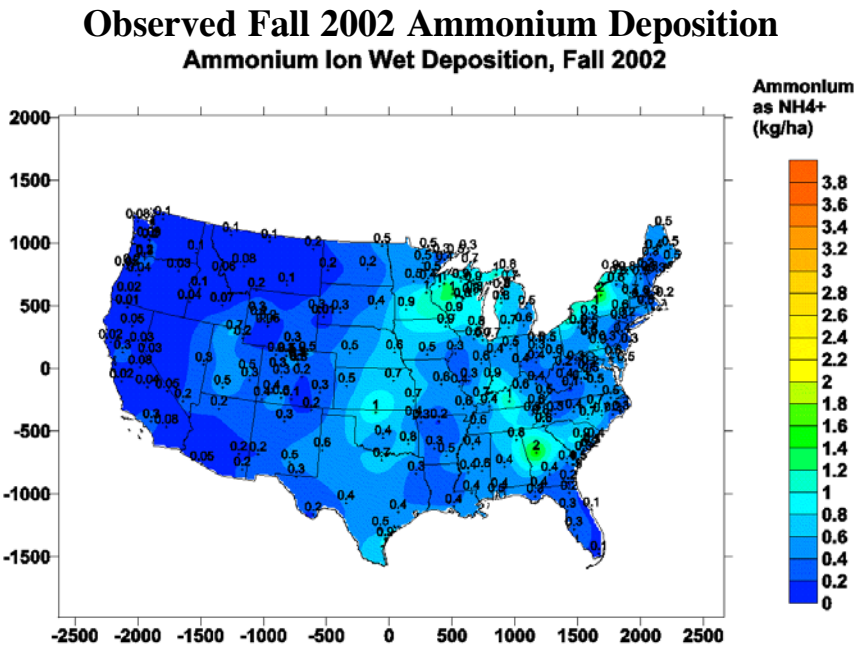

Figure 4-27. Observed and predicted ammonium wet deposition (kg/hectare) for fall 2002.

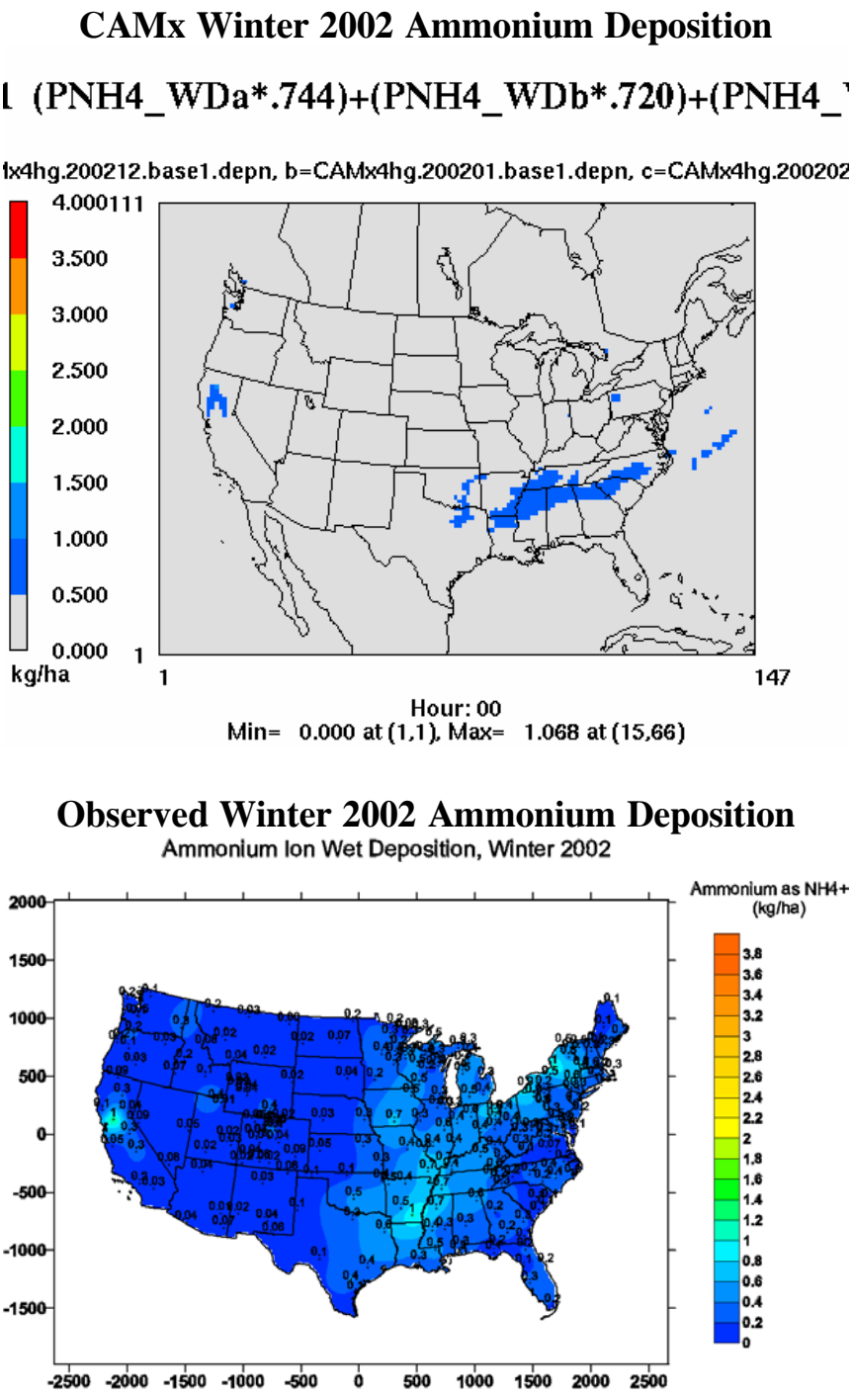

Figure 4-28. Observed and predicted ammonium wet deposition (kg/hectare) for winter 2002.

5. CONCLUSIONS

The objectives of this study were to modify CAMx to treat atmospheric process for mercury (Hg) and test the model for an application suitable for investigating Hg deposition in Wisconsin. The starting point for model development was the publicly released version 4.02 of the Comprehensive Air quality Model with extensions (CAMx4) which is described in ENVIRON (2003). The major modification to CAMx was the addition of a new chemistry module to treat the gas and aqueous-phase chemistry of Hg species. The mercury chemistry module was developed by AER and has been previously used in global and regional scale modeling as described by Seigneur et al. (2001a; 2003b). The Hg chemistry module treats chemical conversions between elemental mercury, Hg(0), and oxidized mercury, Hg(II). The oxidized form of mercury is sometimes referred to as reactive gaseous mercury (RGM). CAMx also treats primary particulate mercury, Hg(P), as a chemically inert species. Other modifications to CAMx included improvements to the dry deposition module to better resolve differences between seasons and the effects of snow cover. The modifications to CAMx for modeling Hg species will be included in a future public release of the model.

An annual 2002 modeling database was developed to test and evaluate the CAMx mercury model. The modeling domain was the 36 km resolution "National RPO grid" covering the entire continental United States and parts of Canada and Mexico. The Regional Planning Organizations (RPOs) developed this modeling grid to promote consistency in regional particulate matter (PM) and visibility modeling. Modeling an entire year is important to capture seasonal cycles in mercury deposition and modeling a continental-scale domain is preferable to maximize the influence of mercury emissions over boundary conditions. However, even with a continental-scale modeling domain the lateral boundary conditions are more important for mercury than for other pollutants (e.g., PM or ozone) because the long atmospheric lifetime of Hg(0) leads to global scale mercury transport. To account for the global mercury background, this study followed the multiscale approach of Seigneur et al. (2001a) of specifying the continental scale boundary conditions for Hg species from a global model. Study participants developed the model inputs for the annual 2002 CAMx simulation as follows. The Wisconsin Department of Natural Resources (WDNR) conducted annual meteorological modeling to develop the 2002 meteorology. The WDNR also developed the mercury emissions inventory. The Lake Michigan Air Directors Consortium developed the emission inventory for non-mercury species for Midwest RPO modeling studies. AER developed the mercury boundary conditions from global model simulations. ENVIRON developed other model inputs including the boundary conditions for non-mercury species. The model simulations were performed by ENVIRON.

Model Performance for Hg Wet Deposition

The CAMx mercury modeling results were evaluated against wet deposition data collected during 2002 at all Mercury Deposition Network (MDN) sites. The simulated mercury wet deposition was dominated by Hg(II), because of its high solubility. The evaluation showed that the modeled mercury wet deposition was consistently higher than the observed values. On average, the simulated wet deposition fluxes were greater than measured values by factors of 2 to 3. The largest overpredictions occurred in the summer months. An examination of the

precipitation amounts used in the model wet deposition calculations showed that they were consistently higher than those observed at the MDN sites, up to about a factor of 2 on average during the summer months. When the simulated wet deposition fluxes were scaled by the ratio of observed precipitation to those used in the model, there was better agreement between the simulated and observed wet deposition fluxes, although the simulated values were still higher than the observations.

A model sensitivity analysis was conducted for July 2002 to determine what factors influenced the wet deposition of mercury. This analysis identified two main causes for the overprediction of mercury wet deposition: (1) The modeling showed an unexpectedly large influence of the top boundary condition for Hg(II) on mercury wet deposition, and; (2) The modeled precipitation amounts were consistently higher than the observed precipitation at the MDN sites, as discussed above. These issues are discussed in more detail below and approaches to improving model performance are recommended.

The CAMx modeling domain for this study had a model top at about 7 km or about 450 mb. A 7 km deep modeling domain has been sufficient for regional PM and ozone modeling with CAMx but is apparently too low for mercury modeling with CAMx. Wet deposition efficiently removed Hg(II) from upper model layers because Hg(II) is very water-soluble. The Hg(II) removed from upper model layers by wet deposition was replenished from top boundary conditions via vertical motions through the model top. These factors produced an unreasonably large influence of the model top boundary concentration for Hg(II) on wet deposition and contributed to the overprediction of Hg(II) deposition. This problem can be addressed by setting the model top higher in the top of the troposphere or lower stratosphere.

The over-predicted surface precipitation is related to several factors. The major factor is the approach that was used to derive the CAMx precipitation rate from the MM5 output data. A related factor is the difficulty in distinguishing between liquid and frozen precipitation from MM5 when the MM5 "simple ice" scheme is used that reports only the total precipitation as liquid. A third factor is the level of spatial and temporal agreement between the predicted and observed precipitation.

Precipitation data are output by the MM5 in two forms: (1) 3-dimensional instantaneous precipitation content (g/m^3), and (2) surface accumulated precipitation rate (mm/hr). The MM5 surface precipitation has the advantage of comparability to observations since it directly provides the surface precipitation rate and includes both resolved and sub-grid scale precipitation. However, the surface accumulated precipitation provides no information on the vertical extent profile of precipitation rate as needed for the wet deposition calculation in a 3-D model. The MM5 3-D instantaneous precipitation amount has the advantages of providing 3-D information and consistency between the 3-D distributions of precipitation and clouds. However, the 3-D MM5 output provides precipitation amount (g/m^3) rather than precipitation rate (mm/hr) and does not include sub-grid scale precipitation. ENVIRON investigated using the MM5 surface output to specify the surface precipitation rate and the 3-D output to specify vertical profiles of precipitation rate. This approach was unsuccessful because frequently the 3-D files showed no precipitations in locations where precipitation had accumulated at the surface. There are at least two potential reasons for this: (1) Especially in fine grids, fast moving clouds leave a precipitation track in the accumulated surface precipitation output whereas the 3-D instantaneous output sees only discreet "snap-shots" of the cloud location. (2)

The surface output includes sub-grid scale precipitation whereas the 3-D output does not. When we diagnosed 3-D precipitation and cloud fields that were consistent with the surface precipitation, we found the result was over estimating the amount of cloudiness. Updating the meteorology more frequently (e.g., every 15 minutes rather than hourly) could reduce problems resulting from the "snap-shot" nature of the 3-D instantaneous MM5 output and is feasible for episodic modeling.

The wet deposition scheme implemented in CAMx4 was designed to preserve consistency with the 3-D location of clouds and precipitation between CAMx and the meteorological model (MM5). This is done by using the 3-D instantaneous precipitation (and cloud water) content output by MM5 rather than the surface accumulated rainfall amount. Consequently, the precipitation rate must be diagnosed from the precipitation content via droplet diameters and fall speeds. The mean raindrop diameter and fall speed are derived from the empirical relationships of Scott (1978) as described in the CAMx User's Guide (ENVIRON, 2003). The results of this study show that these relationships are overestimating the precipitation rate when precipitation is frozen and during intense rain events. The overestimation is most severe when the precipitation is frozen because snow tends to fall more slowly than rain. The CAMx wet deposition algorithm does not model wet deposition in frozen precipitation, but the cut point for frozen precipitation was set at 268 K to allow for super-cooling. This cut point is too low because a lot of predicted snow falling above 268 K is being treated as rain, which significantly over predicted the precipitation rate in winter. Distinguishing between liquid and frozen precipitation from MM5 is difficult with the "simple ice" scheme because only the total precipitation is reported. Many studies use the "simple ice" scheme in MM5 for air quality purposes because it is much faster than alternative options with full microphysics.

The recommended approach to improving the calculation of mercury wet deposition is to go back to a simpler wet deposition approach in CAMx that can be based on the predicted surface rainfall rate or interpolated observations. A simpler, surface precipitation driven wet scavenging algorithm is likely to improve the wet deposition amounts but will lead to less consistency between the locations of clouds and rain than in the current scheme. The surface precipitation driven wet scavenging algorithm could be implemented as an option alongside the existing algorithm. Separately, the diagnosis of precipitation rate from precipitation amount should be refined in the current CAMx wet deposition algorithm to better account for frozen precipitation and intense rain.

Model Performance for Other Species

The evaluation of mercury deposition against MDN data showed that an over prediction of the precipitation rate in combination with the model top being too low caused the deposition of Hg(II) to be over predicted. Uncertainties in the mercury emission inventory also may have contributed to errors in the predicted mercury deposition. A qualitative evaluation of deposition for several particulate matter (PM) species was performed to support the mercury deposition evaluation. The overall trends found were over prediction of nitrate, under prediction of sulfate and larger under prediction of ammonium wet deposition. The over prediction tendency for nitrate is in the same direction as for mercury, discussed above, and over predicting the precipitation may be a factor for nitrate as well as mercury. Sensitivity tests showed that boundary conditions were not important to the modeled nitrate deposition.

The under prediction tendencies for sulfate and ammonium are in the opposite direction to mercury suggesting sources of bias other than precipitation for sulfate and ammonium deposition. Uncertainties in the ammonia inventory will influence ammonium deposition and, to a lesser extent, the sulfate and nitrate deposition. The ammonia inventory for this study had only limited seasonal variation because spring and fall were estimated as the average of summer and winter.

We also performed a qualitative comparison of modeled ozone levels for June 2002 to evaluate whether the modeled oxidant levels over the continental US were reasonable for summer conditions. Atmospheric oxidants determine the rate of oxidation of HG0 to HG2. The modeled and observed maximum ozone levels showed reasonable agreement on the spatial distributions of higher and lower ozone levels. The model performance for ozone was limited by having seasonal emission inventories that are less representative than the day specific inventories normally used for ozone modeling. Overall, the agreement for ozone was reasonable and is suitable for supporting mercury deposition modeling.

Recommendations

The two major recommendations from this study are for improvements to the modeling to correct biases that over predict the amount of Hg(II) wet deposition.

Model top and top boundary conditions: For mercury modeling, the CAMx modeling domain should be extended to include the entire troposphere and perhaps the lower stratosphere. We recommend a model top above 10 km.

Wet deposition: An alternate wet deposition option should be added that would be driven by surface precipitation data. Advantages with this approach are the ability to use surface rainfall amount predicted by the MM5 or interpolated observations of surface rainfall. Separately, the diagnosis of precipitation rate from precipitation amount should be refined in the current CAMx wet deposition algorithm.

The improved model should be reevaluated using the 2002 annual simulation and the observed mercury deposition data from the MDN.

REFERENCES

Ariya, P.A., A. Khalizov and A. Gidas. 2002. Reactions of gaseous mercury with atomic and molecular halogens: kinetics, product studies, and atmospheric implications, *J. Phys. Chem.*, **106**, 7310-7320.

Clever, H., S.A. Johnson and E.M. Derrick. 1985. The solubility of mercury and some sparingly soluble mercury salts in water and aqueous solutions, *J. Phys. Chem. Ref. Data*, **14**, 631-680.

Edgerton, E.S., B.E. Hartsell and J.J. Jansen. 2001. Atmospheric mercury measurements at a rural and urban site near Atlanta, GA, USA. *6th International Conference on Mercury as a Global Pollutant*, 15-19 October 2001, Minamata, Japan.

ENVIRON. 2003. "User's Guide to the Comprehensive Air Quality Model with extensions, version 4." June 2003. Available from http://www.camx.com.

EPA. 1991. *Guidelines for the Regulatory Application of the Urban Airshed Model*, U.S. Environmental Protection Agency, Research Triangle Park, NC.

Gardfeldt, K. and M. Johnson. 2003. Is bimolecular reduction of Hg(II)-complexes possible in aqueous systems of environmental importance?, *J. Phys. Chem.*, in press.

Hall, B. 1995. The gas-phase oxidation of elemental mercury by ozone, *Water Air Soil Pollut.*, **80**, 301-315.

Hall, B. and N. Bloom. 1993. Report to EPRI, Palo Alto, CA.

IDNR. 2003. "Meteorological Modeling Protocol IDNR 2003 Annual Modeling Application." http//www.state.ia.us/epd/air/prof/progdev/RegionModel.htm, accessed October 20, 2003

Jacob, D.J. 2000. Heterogeneous chemistry and tropospheric ozone, *Atmos. Environ.*, **34**, 2131-2159.

Jaegle, L., D.J. Jacob, W.H. Brune and P.O. Wennberg. 2001. Chemistry of HO_x radicals in the upper troposphere, *Atmos. Environ.*, **35**, 469-489.

LADCO. 2003. "How Was the Base D inventory Constructed." Available at http//64.27.125.175/tech/emis/BaseD/BaseD_Build.htm, accessed October 20, 2003.

Landis, M.S. and G. Keeler. 2002. Atmospheric mercury deposition to Lake Michigan during the Lake Michigan Mass Balance Study, *Environ. Sci. Technol.,* 36, 4518-4524.

Lin, C.J. and S.O. Pehkonen. 1997. Aqueous-free radical chemistry of mercury in the presence of iron oxides and ambient aerosol, *Atmos. Environ.*, **31**, 4125-4137.

Lin, C.J. and S.O. Pehkonen. 1998. Oxidation of elemental mercury by aqueous chlorine (HOCl/OCl$^-$): Implications for tropospheric mercury chemistry, *J. Geophys. Res.*, **103**, 28093-28102.

Lindqvist, O. and H. Rodhe. 1985. Atmospheric mercury - a review, *Tellus*, **37B**, 136-159.

van Loon, L., E. Mader and S.L. Scott. 2000. Reduction of the aqueous mercuric ion by sulfite: UV spectrum of $HgSO_3$ and its intramolecular redox reactions, *J. Phys. Chem.*, **104**, 1621-1626.

van Loon, L.L., E.A. Mader and S.L. Scott. 2001. Sulfite stabilization and reduction of the aqueous mercuric ion: kinetic determination of sequential formation constants, *J. Phys. Chem.*, **105**, 3190-3195.

Munthe, J. 1992. The aqueous oxidation of elemental mercury by ozone, *Atmos. Environ., Part A*, **26**, 1461-1468.

National Atmospheric Wet deposition Program (NRSP-3)/National Trends Network. 2003. NADP Program Office, Illinois State Water Survey, 2204 Griffith Drive, Champaign, IL 61820.

Pehkonen, S.O. and C.J. Lin. 1998. Aqueous photochemistry of divalent mercury with organic acids, *J. Air Waste Manage. Assoc.*, **48**, 144-150.

Ryaboshapko, A., R. Bullock, R. Ebinghaus, I. Ilyin, K. Lohman, J. Munthe, G. Petersen, C. Seigneur and I. Wängberg. 2002. Comparison of mercury chemistry models, *Atmos. Environ.*, **36**, 3881-3898.

Sanemasa, I. 1975. The solubility of elemental mercury vapor in water, *Bull. Chem. Soc. Jpn.*, **48**, 1795-1798.

Schroeder, W.H. and J. Munthe. 1998. Atmospheric mercury – An overview, *Atmos. Environ.*, **32**, 809-822.

Scott, B.C. 1978. Parameterization of sulfate removal by precipitation. *J. Appl. Meteor.*, 17, 1375-1389.

Seigneur, C., H. Abeck, G. Chia, M. Reinhard, N.S. Bloom, E. Prestbo and P. Saxena. 1998. Mercury adsorption to elemental carbon (soot) particles and atmospheric particulate matter, *Atmos. Environ.*, **32**, 2649-2657.

Seigneur, C., P. Karamchandani, K. Lohman, K. Vijayaraghavan and R.-L. Shia. 2001a. Multiscale modeling of the atmospheric fate and transport of mercury, *J. Geophys. Res.*, **106**, 27795-27809.

Seigneur, C., P. Karamchandani, K. Lohman and J. Jansen. 2001b. Modeling of mercury in power plant plumes, *6th International Conference on Mercury as a Global Pollutant*, 15-19 October 2001, Minamata, Japan.

Seigneur, C., K. Lohman, K. Vijayaraghavan And R-L. Shia. 2003a. Contributions Of Global And Regional Sources To Mercury Deposition In New York State, *Environ. Pollut.*, 123, 365-373.

Seigneur, C., K. Vijayaraghavan, K. Lohman and P. Karamchandani. 2003b. Modeling the atmospheric fate and transport of mercury over North America, *Fuel Processing Technol.*, in press.

Seigneur, C., K. Vijayaraghavan, K. Lohman, P. Karamchandani and C. Scott. 2003c. Global source attribution for mercury deposition in the United States, *Environ. Sci. Technol.*, submitted.

Seigneur, C., P. Karamchandani, K. Vijayaraghavan, K. Lohman and G. Yelluru. 2003d. *Scoping Study for Mercury Deposition in the Upper Midwest*, AER Report CP149-03-01a, prepared for the Midwest Regional Planning Organization, Des Plaines, IL.

Seigneur, C., P. Karamchandani, K. Vijayaraghavan, K. Lohman, R.-L. Shia and L. Levin. 2003e. On the effect of spatial resolution on atmospheric mercury modeling, Sci. Total Environ. 304, 73-81.

Shia, R.L., C. Seigneur, P. Pai, M. Ko and N.D. Sze. 1999. Global simulation of atmospheric mercury concentrations and deposition fluxes, *J. Geophys. Res.*, **104**, 23747-23760.

Sillen, G.L. and A.E. Martell, (Eds.). 1964. Stability constants of metal ion complexes, *Spec. Publ. Chem. Soc.*, **17**, 754.

Sommar, J., K. Gårdfeldt, D. Strömberg and X. Feng. 2001. A kinetic study of the gas-phase reaction between the hydroxyl radical and atomic mercury, *Atmos. Environ.*, **35**, 3049-3054.

Tokos, J.J.S., B. Hall, J.A. Calhoun and E.M. Prestbo. 1998. Homogeneous gas-phase reaction of Hg^0 with H_2O_2, O_3, CH_3I, and $(CH_3)_2S$: Implications for atmospheric Hg cycling, *Atmos. Environ.*, **32**, 823-827.

Vijayaraghavan, K., C. Seigneur, K. Lohman, P. Karamchandani, L. Levin and J. Jansen. 2003. Simulation of mercury deposition over the eastern United States with a fine spatial resolution, *Air Quality IV*, 22-24 September 2003, Arlington, VA.

WDNR. 2003. "Mercury in the Environment." http://www.dnr.state.wi.us/org/caer/ce/mercury/